ISSN 2587-1366

TUJE

TURKISH JOURNAL OF ENGINEERING

VOLUME 4 ISSUE 3 JULY 2020

Dr. Ghazi DROUBI
Robert Gordon University Engineering Faculty
Scotland, UK

JOURNAL SECRETARY

Nida DEMİRTAŞ
nidademirtas@mersin.edu.tr

TURKISH JOURNAL OF ENGINEERING (TUJE)

Turkish Journal of Engineering (TUJE) is a multi-disciplinary journal. The Turkish Journal of Engineering (TUJE) publishes the articles in English and is being published 4 times (January, April, July and October) a year. The Journal is a multidisciplinary journal and covers all fields of basic science and engineering. It is the main purpose of the Journal that to convey the latest development on the science and technology towards the related scientists and to the readers. The Journal is also involved in both experimental and theoretical studies on the subject area of basic science and engineering. Submission of an article implies that the work described has not been published previously and it is not under consideration for publication elsewhere. The copyright release form must be signed by the corresponding author on behalf of all authors. All the responsibilities for the article belongs to the authors. The publications of papers are selected through double peer reviewed to ensure originality, relevance and readability.

AIM AND SCOPE

The Journal publishes both experimental and theoretical studies which are reviewed by at least two scientists and researchers for the subject area of basic science and engineering in the fields listed below:

Aerospace Engineering
Environmental Engineering
Civil Engineering
Geomatic Engineering
Mechanical Engineering
Geology Science and Engineering
Mining Engineering
Chemical Engineering
Metallurgical and Materials Engineering
Electrical and Electronics Engineering
Mathematical Applications in Engineering
Computer Engineering
Food Engineering

PEER REVIEW PROCESS

All submissions will be scanned by iThenticate® to prevent plagiarism. Author(s) of the present study and the article about the ethical responsibilities that fit PUBLICATION ETHICS agree. Each author is responsible for the content of the article. Articles submitted for publication are priorly controlled via iThenticate ® (Professional Plagiarism Prevention) program. If articles that are controlled by iThenticate® program identified as plagiarism or self-plagiarism with more than 25% manuscript will return to the author for appropriate citation and correction. All submitted manuscripts are read by the editorial staff. To save time for authors and peer-reviewers, only those papers that seem most likely to meet our editorial criteria are sent for formal review. Reviewer selection is critical to the publication process, and we base our choice on many factors, including expertise, reputation, specific recommendations and our own previous experience of a reviewer's characteristics. For instance, we avoid using people who are slow, careless or do not provide reasoning for their views, whether harsh or lenient. All submissions will be double blind peer reviewed. All papers are expected to have original content. They should not have been previously published and it should not be under review. Prior to the sending out to referees, editors check that the paper aim and scope of the journal. The journal seeks minimum three independent referees. All submissions are subject to a double blind peer review; if two of referees gives a negative feedback on a paper, the paper is being rejected. If two of referees gives a positive feedback on a paper and one referee negative, the editor can decide whether accept or reject. All submitted papers and referee reports are archived by journal Submissions whether they are published or not are not returned. Authors who want to give up publishing their paper in TUJE after the submission have to apply to the editorial board in written. Authors are responsible from the writing quality of their papers. TUJE journal will not pay any copyright fee to authors. A signed Copyright Assignment Form has to be submitted together with the paper.

PUBLICATION ETHICS

Our publication ethics and publication malpractice statement is mainly based on the Code of Conduct and Best-Practice Guidelines for Journal Editors. Committee on Publication Ethics (COPE). (2011, March 7). Code of Conduct and Best-Practice Guidelines for Journal Editors. Retrieved from http://publicationethics.org/files/Code%20of%20Conduct_2.pdf

PUBLICATION FREQUENCY

The TUJE accepts the articles in English and is being published 4 times (January, April, July and October) a year.

CORRESPONDENCE ADDRESS

Journal Contact: tuje@mersin.edu.tr

CONTENTS

Volume 4 – Issue 3

ARTICLES

Turkish Journal of Engineering

Turkish Journal of Engineering (TUJE)
Vol. 4, Issue 3, pp. 104-112, July 2020
ISSN 2587-1366, Turkey
DOI: 10.31127/tuje.637050
Research Article

IMPORTANCE OF UNMANNED AERIAL VEHICLES (UAVs) IN THE DOCUMENTATION OF CULTURAL HERITAGE

Ali Ulvi *[1]

[1] Selcuk University, Hadim Vocational High School, Konya, Turkey
ORCID ID 0000-0003-3005-8011
aliulvi@selcuk.edu.tr

* Corresponding Author
Received: 23/10/2019 Accepted: 27/11/2019

ABSTRACT
Cultural heritage is the most important resource providing communication between the past and future. The societies utilizing this resource in the best way, have had an inventory of cultural heritage and contributed to world culture. The efforts made for being able to the accurate and healthy data in the documentation of cultural heritage led the new techniques to emerge other than documentation and, together with the developing technology, documentation with traditional method replaced with modern documentation techniques using new technological devices. One of these documentation techniques is the use of Unmanned Aerial Vehicles (UAVs) in the documentation studies. In this study, the usability of unmanned aerial vehicles in the studies of cultural heritage was studied.

Keywords: *Cultural Heritage, UAV, Documentation*

1. INTRODUCTION

Cultural heritage is one of the most important bridges between the past and future of the people. It has an important place in the individual and social development of human being. Originally leaving these heritages to the next generations is an important issue on the name of humanity.

Historical artifacts that stand as cultural heritage are buildings that connect the past and future of the world(Şasi &Yakar,2018).

Many international organizations such as UNESCO (United Nations Educational, Scientific and Cultural Organization), ICOMOS (International Council for Monuments and Sites), ISPRS (International Society for Photogrammetry &Remote Sensing), ICOM (International Council for Museums), ICCROM (International Centre for the Conservation and Restoration of Monuments) and UIA (International Union of Architects) have undertaken some missions to conserve world cultural heritages (Callegari , 2003) .

Besides producing information regarding the various physical, social, economic, cultural, and historical aspects of cultural heritage in the various quality and scale, processing much amount of information produced and transforming it into the usable information is an indispensable requirement in terms of conserving (URL-1, 2007).

1.1. Cultural Heritage and Conservation

Just as cultural entities can be divided as movable and immovable entities, they are also classified as the intangible and tangible entities. While the tangible monumental ruins and archeological antiques used to be included in the scope of cultural heritage, today, the scope of this term enlarged and has begun to cover intangible ethnographic, industrial, and intellectual heritage (e.g. language, beliefs, traditions) (Can, 2009).

Cultural heritages are the history of the nations, and history forms the identities of the nations. Therefore, protection of cultural heritages means protection of the history and identity of the nations(Yakar&Doğan,2018).

Cultural heritages due to have their different natural characteristics, different sizes, and complicated structure they require more sophisticated measurement tools and techniques to documentation (Ulvi & Toprak, 2016)

Among the values UNESCO includes in tangible cultural heritage, the historical cities are also cultural landscapes, natural and holy sites, underwater cultural heritages, and museums. Cultural heritage revealing itself as historical spaces of a city is the most valuable part of social welfare. Therefore, “adopting conservation of heritage not only provides the possibility of healthy life for a city but also it helps recognition of cultural identity of that city” (Tweed & Shutherland,2007).

1.2. The importance of documenting Cultural Heritage

Documenting a structure covers the studies carried out on the purpose of measuring it as well as identifying its quality and variation process (Kuban , 2000).

Nowadays, with the development of data acquisition technologies, digital works of architectural works are documented and restoration projects are being used in many fields (Ulvi et al.,2020).

The importance of documenting cultural heritage has been more recognized in the recent years, and an increasing pressure about conserving and documenting this heritage has formed. The existing technologies and methodologies related to this issue give 2D and 3D results, in order to be used with the archeological, digital conservation, restoration, and conservation purposes and many purposes such as VR applications, catalogues, web, geographical systems, and visualization (Remondino, F. & Rizzi, A. 2009).

In addition, in documenting cultural heritage, the accuracy of relievo should also compatible with the scale of the project to be carried out (English Heritage, 2003).

Table 1.The relationship between project scale and error margin (English Heritage.,2003).

Scale	Acceptable Error Margin
1/10	**+/- 5 mm**
1/20	**+/- 6 mm**
1/50	**+/- 15 mm**
1/100	**+/- 30 mm**
1/200	**+/- 60 mm**
1/500	**+/- 150 mm**

In documenting our cultural heritage, the efforts made to be able to obtain the accurate and healthy data led new techniques to emerge in the documentation area and, together with developing technology, documentation with traditional method has replaced with modern documentation techniques, and this enabled contemporary documentation techniques to rapidly improve. The current technology enables the historical works and structures to be conserved to any longer to be documented more rapidly and transferred to the next generations (Korumaz., Dülgerler & Yakar .2011).

One of modern documentation techniques is also documentation with unmanned aerial vehicles (UAVs).

2. UAV OVERVIEW

According to the international definition of UVs (Unmanned Vehicle System), an unmanned aerial vehicle (UAV) is a generic aircraft design that does not accommodate humans in it. (URL-25).

The use of UAVs has become a recently adopted method in acquiring needed spatial data(Ulvi,2018).

“UAVs should be understood as uninhabited and reusable motorized air vehicles.” states van Blyenburgh, 1999 (Van Blyenburgh,1999). These vehicles are remote-controlled, semi-autonomous, autonomous or have some combination of these capabilities.

When comparing the UAV to human aircraft, it is clear that the main difference between the two systems is that no pilot in the UAV is physically present in the aircraft. This does not necessarily mean that a UAV flies autonomously by itself. In many cases, the crew responsible for the UAV (operator, backup pilot, etc.) Is larger than a conventional aircraft (Everaerts, 2008).

The term UAV is commonly used in Computer

Science, Robotics, and artificial intelligence, as well as in the photogrammetry and Remote Sensing communities.

Additionally, synonyms such as remote-controlled vehicle (RPV), remote-controlled Air Transport (ROA) or remote-controlled Air Transport (RPA) and Unmanned Vehicle Systems (UVS) can also be rarely found in the literature.

RPV is a term used to describe a robotic aircraft flown by the pilot using a ground control station. The first use of the term may have been directed at the United States (U.S.) Department of Defense in the 1970s and 1980s. The terms ROA and RPA have been used by the National Aeronautics and Space Administration (NASA) and Federal Aviation Administration (FAA) in the United States instead of the UAV. The term Unmanned Aircraft System (UAS) is also used. (Colomina et al., 2008).

The FAA adopted the general class UAS, originally introduced by the U.S. Navy. The common understanding is that UAS terminology represents the entire system, including unmanned aerial vehicle (UA) and Ground Control Station (GCS). (Eisenbeiss, Stempfhuber & Kolb. 2009).

2.1. Classification of UAVs

When the literature is examined, Unmanned Aerial Vehicles are classified in various ways. However, it is much more accurate to divide the UAVs into two classes as fixed-wing and rotary-wing UAVs. In addition, kite, balloon and zeppelins were used in the study of cultural heritage under the name of UAV.

2.1.1. Rotary -Wing UAV Systems

4-wing Quadrotor, 6-wing Hexacopter and 8-wing Octocopter systems are included in this group. These systems have the features such as balanced flight feature by means of pilot even if complete manual flights; return feature with GPS, altitude fixing, carefree (orientation freedom) feature, routing flight through map, and full autonomous flight. This system is seen n in Fig. 1.

Fig. 1. Autonomous Routing Flight through Map (URL-2).

2.1.2. Fixed Wing UAV Systems

Fixed wing UAVs have more flight time compared to rotary wings. In addition, they have some advantages from the aspect of durability and flight height. Fixed wing systems, with the properties of high attitude they have and long durability, are ideal for photogrammetric and remote control applications. Also in these systems, flight routing can be defined. Entering column values to the system, autonomous flight can be realized. The disadvantage of fixed wing systems compared to rotary wing systems is that they cannot be hung in the air. In figure 2, a fixed wing UAV is seen.

Fig. 2. Ebee UAV(URL-3)

2.1.3. Kite, Balloon and Zeppelin

-Kites

Kite was used in the various scientific studies based on aerial photography in 1997. It was used in discovering fossil bed in a forest (Bigras. 1997) and in documentation of mapping archeological site in Russia (Gawronski & Boyarsky. 1997). There are some sorts of the kites used in kite systems used as photogrammetric-aimed. These are:

****Delta Kite**

Fig. 3. Delta Kite (URL-22)

**** Fled Kite**

Fig. 4. Fled Kite (URL-22)

**** Soft Kite**

Fig. 5. Soft Kite (URL-22)

- Balloon

Today, zeppelins are divided into two as motorized and

non-motorized. Non-motorized zeppelins are driven by means of ground –controlled ropes the same as balloons. Zeppelins include helium gas according to carrying capacity. If the load you will carry is heavy, you have to use bigger zeppelin and, thus, there is need for more helium gas. This certainly increases cost. In addition, motorized systems have generally two wings and carry 2-3 electric motors.

Fig. 6. General Appearance of Zeppelin (URL-24).

2.2. The Platforms Used

There are also photo taking platforms, mounted to kite systems as photographic –aimed and operated by remote control, Photos taking platforms are shown in Fig. 7 and Fig. 8.

Fig. 7. Photos Taking Platforms (URL-22)

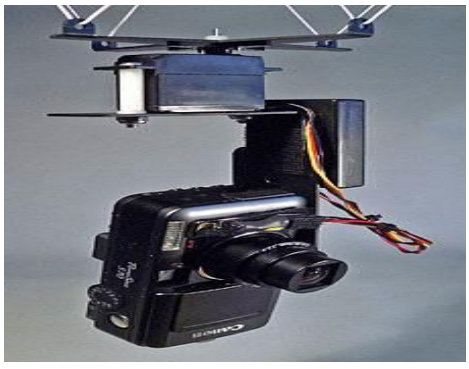

Fig. 8. Photos Taking Platforms (URL-22)

Fig. 9. Kite Aerial photography can be used to obtain more analyses and data. It is a low cost and effective method that is suitable for working in small regions (URL-23).

Fig. 10. General Appearance of Zeppelin (URL-24)

2.3. Its Benefits

The biggest advantages of UAV against manned flight systems: UAV is used in risky states, unreachable regions, low attitudes, and places, in which flight profile is near the object and manned flight system cannot be used, without jeopardizing human life.In these regions, for example, in the sites of natural disasters, mountainous and volcanic areas, flood plains, earthquake areas and deserts, accident scenes, regions that is difficult to going into, and in the places, in which airplane can be used as unmanned or flight permission is not given, the only option is sometimes UAV. In addition, cloudy and drizzling weather conditions, it is possible to collect by means of UAV

2.4. UAV Applications

Some UAVs civilian applications are mentioned in (Nıranjan, Gupta, Sharma, Mangal & Sıngh 2007) while(Everaerts, 2007) reports on UAV projects, regulations, classifications and application in the mapping domain. The application fields where UAVs images and photogrammetrically derived DSM or orthoimages are generally employed include: Agriculture, Forestry, Archaeology and architecture, Environment, cadastral mapping, thermal analyses, excavation volume computation, volcano monitoring or natural resources documentations for geological analyses are also feasible, Emergency management, Traffic monitoring: surveillance, travel time estimation, trajectories, lane occupancies and incidence response are the most required information.

3. UAV PHOTOGRAMMETRY

Terminology UAV photogrammetry (Eisenbeiss. 2008c) defines a photogrammetric measurement platform, which operates remote controllably and is semi- independent or independent, and in which there is not any pilot. Platform was equipped by photogrammetric measurement systems. This also includes small or medium sized fixed video or video camera, thermic or infrared camera systems, and aerial LIDAR systems. The existent standard UAV enables to monitor the record and position and the direction of sensors applied in a local or local coordinate system. Hence, UAV photogrammetry can be understood as a technique that makes photogrammetric measurements with the help of an unmanned aerial vehicle.

UAV photogrammetry, combining aerial and terrestrial photogrammetry, leads to the new applications in close distance effective area but also it introduces traditional aerial photogrammetry with the new (close) real time applications and low cost options..

4. STUDIES WITH UAV

4.1. UAVs for The Documentatıon of Archaeologıcal Excavatıons

This study made by M. Sauerbier and H. Eisenbeiss.

In this study, Sauerbier and Eisenbeis, the deployment of drones for the certification of such sites, or 3D digital Surface models, Ortho images provide a basis for further processing and the derivation of different products such as high quality offers 3 different case studies that are caused in the image data.

The second is the documentation of a Maya site in Copán, Honduras, and the second is the quick and simple documentation of an excavation site in Palpa, Peru. Different types of UAVs were used in these projects: in Honduras and Peru we worked with Surveycopter 1B (Aeroscout, Switzerland) driven by a two-stroke engine, in Bhutan we used a quadrocopter MD 4-100 supplied by Microdrones. by the company omnisight (Switzerland). The experiences gathered by the projects described above and the test site surveys allowed them to come to different conclusions regarding the actual state of the UAVs, especially in terms of their applicability in photogrammetric projects for the cultural heritage site. Compared to the Falcon 8 and MD4-200 systems, the positional accuracy of Copter 1B (1m) is quite high compared to 2-5m for multi-rotor systems (Sauerbier & Eisenbeiss.2010).

4.2. Uav Platforms For Cultural Heritage Survey: First Results

This study made by M. Lo Brutto, A. Garraffa,P. Meli.

In this study, the two systems were tested in two different regions: the site of the Temple of Isis at the temples Valley Archaeological Park in Agrigento was examined by the md4-200 microdron, the site of the "Gibellina Cretto Cretto". "Near the town of Trapani with Swinglet glass. The first is one of the least-known areas of the entire archaeological park, followed by being released by tourists. The temple is located only in a partially excavated area and is formed with a podium and triportico identifying a square.

This study shows the potential of the UAV survey in the area of Cultural Heritage. Although it requires earlier and more detailed research, some initial results can already be deduced. In particular, initial tests on orientation phases do not highlight any reduction in the increments of CPS using more stable block configurations. 2000-4000 points per image and the percentage of overlap of the images, respectively, due to the number of binding points for each image High, A lot of measurements (on average, at every point there is at least 8-10 ledge) , may make unnecessary the use of photogrammetric blocks with a more stable configuration.

The final products (3D models and Ortho-images) show a very high level of detail, allowing you to do very accurate work and analysis. Due to the high level of automation achieved through the software used, the processes followed were very fast.

In the assessment of 3D point clouds, the vertical residues obtained both for all the data sets of the Temple of Isis and for two of the three data sets of "Cretto of Gibellina" appear to be quite high. Apart from the distribution of residues, 3D models show some slight deformations. In order to better understand the reasons for these latest results, certainly more extensive testing needs to be done (Eisenbeiss. 2008c)

4.3. Balloon photogrammetry for cultural heritage

Altan *et al*. (2004) took aerial photographs in Patara antique city by means of Helium gas balloon system. Balloon is in 25 m of diameter and filled with 8 m^3 of Helium gas. This system consists of flight unit and ground control unit. Flight unit consist of helium balloon, camera platform, and Olympus Camedia C-40404 Camera of Mega-Pixel. Ground control unit consists of monitor remote control for camera, and control ropes.

Fig. 11. Camera platform, camera, and balancing ropes under balloon (Altan.2004)

Fig. 12. Ground control unit with monitor (Altan.2004)

4.4. Studying the usability of non-metric digital camera, mounted to kite platform, in archeological documentation studies

This study was conducted by Ali Ulvi in Uzuncaburç Diocaesarea Antique Theater, located in Silifke district of Mersin province. in the scope of doctorate study.

Fig. 13. Digital Camera and its carrying platform

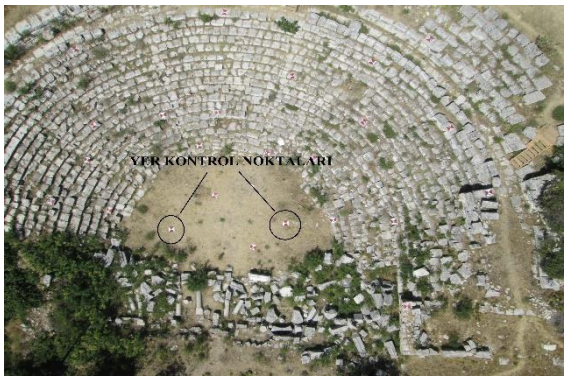

Fig. 14. Ground Control Points used in aerial photographs

Fig. 15. Mounting the camera and platform to a kite

Fig. 16. Operation of taking aerial photos with kite

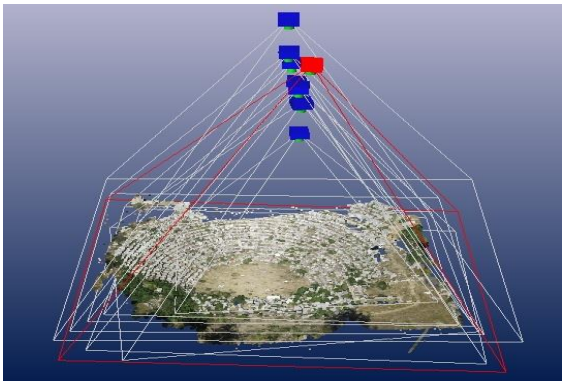

Fig. 17. Appearance of the stations of taking photos

After this stage, accuracy study of archeological documentation application, carried out by means of UAV kite by using photogrammetric techniques, was carried out. 30 pieces of ground control points were used for this study. The coordinates of ground control points were measured by total station device and were accepted as definite coordinates in accurate study. After this operation, coordinate values of ground control points were identified through archeological documentation carried out by using photogrammetric techniques

Table 2. Average position error

	Vy (cm)	Vx (cm)	Vz (cm)
m	±3.1	±3.1	±2.9
m_{yxz}	±5.3		

In the light of these data, in the accuracy study of archeological documentation carried out by means of UAV kite, the average position error in y, x, and z coordinates was found ± 5.3 cm. According to the results calculated, using photogrammetric techniques, archeological documentations carried out by UAV provides sufficient position accuracy.

In this way, excavation work in the production of litter, modeling before and after excavation, monitoring the development of the excavation phases, has the qualities that can be used in the study area determination and restoration projects.

4.5. Neptune Temple in the Archeolojical area in Italy

An example of such a practice is given in Figure 18, where the Temple of Neptune at the archaeological site of Paestum (Italy) is shown. Given the shape, complexity and dimensions of the monument, a combination of terrestrial and UAV (vertical and oblique) images was used to guarantee the integrity of the 3D surveying work. The UAV used is a 4-rotor MD4-1000 Microdrone system. It is entirely carbon fiber, capable of carrying instruments up to 1.0 kg with a duration of more than 45 minutes. For rare images. The UAV mounted an Olympus E-P1 camera (12 megapixels - 4.3 pm pixels in size) with a focal length of 17 mm, while an Olympus XZ-I (10 megapixels) with a focal length of 6 mm for oblique images. 2 pm pixel size) was used.

The average GSD of images on both flights is about 3 cm. The Autopilot system allowed it to perform two full flights in autonomous mode, but the stored coordinates of the projection centers were not sufficient for direct georeferencing. Therefore, a number of reliable GCP (measured by the total station measured by the corners and total features of the temple) was required to achieve scaled and geographically referenced 3D results. The orientation procedure processed terrestrial and UAV images (ca 190) simultaneously to bring all data in the same coordinate system. After the recovery of camera poses, a DSM was produced for the purpose of documentation and visualization (Fiorillo et al., 2015).

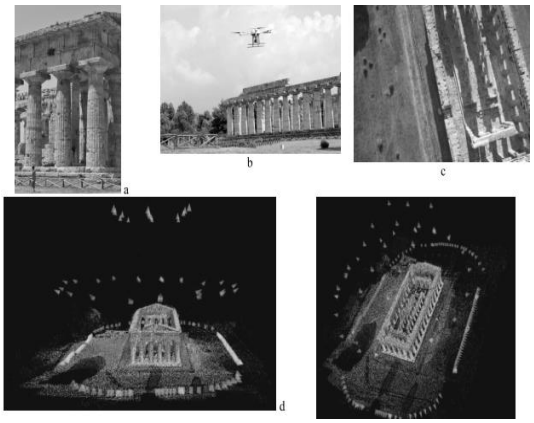

Fig. 18. Orientation results of an aerial block over a flat area of ca 10km(a). The derived camera poses are shown in red/green, while color dots are the 3D object points on the ground. The absence of ground constraint (b) can led to a wrong solution of the computed 3D shape (i.e. ground deformation). The more rigorous approach based on GCPs used as observations in the bundle solution (c),deliver the correct 3D shape of the surveyed scene, i.e. a flat terrain

4.6. Archaeological area of Pave

A second specimen was reported in Figure 19, showing the archaeological site of Pave (ca 60 x 50 m) surveyed annually at the beginning and end of the excavation period to monitor the progress of the work, calculate the volume of the flare, and produce lots. - Temporary orthographic images of the area. Flights (35 m altitude) were made with the Microdrone MD4-200 in 2010 and 2011. The Heritage site was quite windy, so the electrified platform was probably not the optimal one. For each session, a reliable set of images (ca 40), averaging one cm of GSD, were obtained using multiple shots for each waypoint. To assess the quality of the image triangulation procedure, some circular targets measured by a total station are used as Ground Control (GCP) and others as control points (CK). After the orientation step, the RMSE on the CK resulted in 0.037 m in planimetry and 0.023 in height. The resulting DSMs (figure 19b, c) were used to produce vector layers in Pava's GIS, onho images (figure 19d), and to control advances in excavation or excavation volumes (figure 19e).

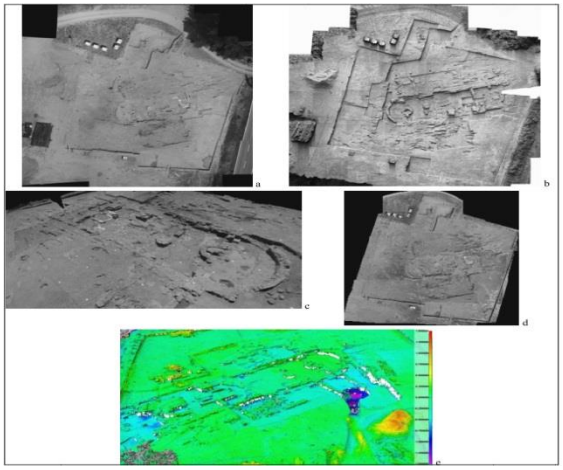

Fig. 19. A mosaic view of the excavation area in Pava (Siena, Italy) surveyed with UAV images for volume excavation computation and GIS applications(a).The derived DSM shown as shaded (b) and textured mode (c) and the produced ortho-image (d) (75). If multi-temporal images are available, DSM differences can be computed for volume exaction estimation

5. CONCLUSION

Unmanned Aerial Vehicles (UAVs) have found place for themselves in every area of life in these days. Antique cities and antique roads taking place in the areas having archeological quality and reaching today have a great importance in terms of cultural heritage. Due to the fact that unmanned aerial vehicles produce (UAVs) 3D data and ortophotos in low cost and high accuracy, they present serious advantages to measure archeological areas (Tercan.2017) .

UAV provides advantages for user in documentation of cultural works as both speed and cost and accuracy and technology in the documentation of historical and cultural works.

Thanks to UAV, it is possible to obtain orthophotos, 3D point clouds and high quality 3D models.

It is also possible to observe cultural heritage, measure, and analyze cultural heritage.

It has a great importance since it reduces the risk of time and budgetary loss and provides usability of the outputs.

Results are presented of photogrammetric projects after his drone archaeological research contexts can be evaluated as highly effective in the field, and excavation of archaeological features and structures in relation to the needs thanks to the versatility of the process.

Unmanned Aerial vehicle can be considered as a quick documentation tool for low-cost mapping.

In the meantime, 3D models will become a convenient database for placing / collecting / accumulating other reading data in a geospatial perspective, such as findings from digging activities and stratigraphic information, and for performing comparative analyses.

Today, thanks to the tilted camera contribution, which studies applications and optimizations in current geography research, 3D models achieve high descriptive performance in terms of geometric surfaces and radiometry, both on the tops and on the vertical facades of steep walls.

In complex and dense areas it can be extremely effective at both detecting details and comparing them.

REFERENCES

Altan, M. O., Celikoyan, T. M., Kemper, G. & Toz, G.(2004). Balloon photogrammetry for cultural heritage In: International Archives of the Photogrammetry, Remote Sensing and Spatial Information Sciences, XX ISPRS Congress, Istanbul, Turkey, XXXV-B5, 964-968.

Berni, J.A.J.; Zarco-Tejada, P.J.; Suárez, L.; Fereres, E.(2009). Thermal and Narrowband Multispectral Remote Sensing for Vegetation Monitoring From an Unmanned Aerial Vehicle. Transactions on Geoscience and Remote Sensing, 2009, Vol. 47, pp. 722-738.

Bigras, C. (1997). Kite aerial photography of the Axel Heiberg Island fossil forest, In: American Society of Photogrammetry and Remote Sensing, First North American Symposium on Small Format Aerial Photography, University of Minnesota, USA, 147-153

Callegari, F. (2003). Sustainable development prospects for Italian coastal cultural heritage: a Ligurian case study, Journal of Cultural Heritage, pp. 49–56

Can, M. (2009). Kültürel Miras ve Müzecilik; Çalışma Raporu. Erişim: 12 Eylül 2009. http://www.kultur.gov.tr/teftis/Genel/BelgeGoster.aspx?F6E10F-8892433CFF530CECBE8DDD19208B89614C9154F631

Chiabrandoa F., D'Andriab F., Sammartanoa G. & Spanòa A.(2016). Uav Photogrammetry For Archaeologıcal Sıte Survey. 3d Models At The Hıerapolıs In Phrygıa (Turkey),Virtual Archaeology Review, 9(18): 28-43, 2018 http://dx.doi.org/10.4995/var.2018.5958 © UPV, SEAV, 2015 Received: June 16, 2016 Accepted: August 4, 2017, Filiberto Chiabrandoa

Colomina, I., Blázquez, M., Molina, P., Parés, M. E. & Wis, M. (2008). Towards A New Paradigm for High-Resolution Low-Cost Photogrammetryand Remote Sensing, In: The International Archives of the Photogrammetry, Remote Sensing and Spatial Information Sciences, ISPRS Congress, Beijing, China, XXXVII. Part B1, 1201-1206.

Eisenbeiss, H., 2008c. UAV photogrammetry in plant sciences and geology, In: 6th ARIDA Workshop on "Innovations in 3D Measurement, Modeling and Visualization, Povo (Trento), Italy.

Eisenbeiss, H., (2009). Stempfhuber, W. & Kolb, M., 2009.

English Heritage. (2003). Metric Survey for Heritage Documentation, Documentation for Conservation:A Manual for Teaching Metric Survey Skills.

Everaerts, J. (2007).The Use of Unmanned Aerial Vehicles (UAVS) for Remote Sensing and Mapping. In: Int. Archives of Photogrammetry, Remote Sensing and Spatial Information Sciences, Beijing, China, 2008; Vol. 37 (B1), pp. 1187-1192.

Everaerts, J. (2008). The Use of Unmanned Aerial Vehicles (UAVS) for Remote Sensing and Mapping, In: The International Archives of the Photogrammetry, Remote Sensing and Spatial

Information Sciences, ISPRS Congress, Beijing, China, XXXVII. Part B1, 1187-1192

Fiorillo F, Jimenez F.-Palacios B, Remondino F, Barba S, 2012. 3D Surveying and modeling of the archaeological area of Paestum, Italy. In: Proc. 3rd Inter. Conference Arquelogica 2.0, 2012, Sevilla, Spain.

Gawronski, J. H. G. & Boyarsky, P. V., (1997). Northbound with Barents: Russian-Dutch integrated archaeologic research on the Archipelago Novaya Zemlya, Uitgeverij Jan Mets, Amsterdam, p. 255.

Korumaz, A.G., Dülgerler O.N. & Yakar M. (2011). Digital Techniques in Cultural Heritage Documentation, Selçuk Üniversitesi Mühendislik-Bilim ve Teknoloji Dergisi.

Kuban, D. (2000). Tarihi çevre Koruma ve Onarımın Mimarlık Boyutu Kuram ve Uygulama, Yapı Endüstri Merkezi Yayınları, İstanbul.

Manyoky, M.; Theiler, P.; Steudler, D.; Eisenbeiss, H.(2011). Unmanned aerial vehicle in cadastral applications. In: Int. Archives of Photogrammetry, Remote Sensing and Spatial Information Sciences, Zurich, Switzerland, 2011; Vol. 38 (1/C22).

Niranjan, S., Gupta, G. Sharma N.,Mangal, M. & Singh, V.(2007). Initial efforts toward mission-specific imaging surveys from aerial exploring platforms: UAV. In: Map World Forum, Hyderabad, India, 2007; on CD-ROM.

Remondino, F. & Rizzi, A. (2009). "Reality-Based 3D Documentation of World Heritage Sites:Methodologies, Problems and Examples", 22nd CIPA Symposium, Kyoto, Japan, October 11-15 2009.

Sauerbier M. , Eisenbeiss H.,2010. Uavs for the documentatıon of archaeologıcal excavatıons,

International Archives of Photogrammetry, Remote Sensing and Spatial Information Sciences, Vol. XXXVIII, Part 5 Commission V Symposium, Newcastle upon Tyne, UK. 2010

Şasi A., Yakar M.(2018). Photogrammetric modelling of hasbey dar'ülhuffaz (masjid) Using an unmanned aerial vehicle, International Journal of Engineering and Geosciences (IJEG),Vol; 3; , Issue; 1, pp. 006-011, February, 2018, ISSN 2548-0960, Turkey
DOI: 10.26833/ijeg.328919

Tercan E.(2017). İnsansız Hava Aracı Kullanılarak Antık Kent Ve Tarıhı Kervan Yolunun Fotogrametrık Belgelenmesı: Sarıhacılar Örneği,Journal of Engineering Sciences and Design DOI: 10.21923/jesd.315232

Tweed, C., & Shutherland, M.(2007). Built cultural heritage and sustainable urban development. Landscape and Urban Planing, 83, 62-69.

Ulvi A., Yakar M., Yiğit A.Y., Kaya Y.(2020), İHA ve Yersel Fotogrametrik Teknikler Kullanarak Aksaray Kızıl Kilise'nin 3 Boyutlu Nokta Bulutu ve Modelinin Üretilmesi, Geomatik Dergisi Journal of Geomatics Araştırma Makelesi DOI: 10.29128/geomatik.560179 2020; 5(1);22-30

Ulvi A.,(2018). Analysis of the utility of the Unmanned Aerial Vehicle(uav) in volume calculation by using photogrammetric techniques, International Journal of Engineering and Geosciences (IJEG),Vol; 3; , Issue; 2, pp. 043-049, June, 2018

Ulvi, A., Toprak, A. 2016. Investigation of threedimensional modelling availability taken photograph of the unmanned aerial vehicle; sample of kanlidivane church. International Journal of Engineering and Geosciences, 1 (1), 1-7. DOI: 10.26833/ijeg.285216

Van Blyenburgh, P. (1999). UAVs: and Overview, In: Air & Space Europe, I, 5/6, 43-47

Yakar M., Doğan Y.,(2018). Gis and three-dimensional modeling for cultural heritages, International Journal of Engineering and Geosciences (IJEG), Vol; 3; Issue; 2, pp. 050-055, June, 2018, ISSN 2548-0960, Turkey, DOI: 10.26833/ijeg.378257

URL-1, 2007, ODTÜ Mimarlık Fakültesi Araştırma, Tasarım, Planlama Ve Uygulama Merkezi http://matpum.arch.metu.edu.tr/index.php?option=com_content&task=view&id=31&Itemid=6
URL-2, http://www.robonik.com.tr
URL-3, http://www.sensefly.com/drones/ebee.html
URL-22, http://www.brooxes.com
URL-23, http://www.birdseye.nl
URL-24, http://www.rc-zeppelin.com
URL-25,http://www.uvs-international.org/(last accessed: December, 2012).

Turkish Journal of Engineering

Turkish Journal of Engineering (TUJE)
Vol. 4, Issue 3, pp. 113-122, July 2020
ISSN 2587-1366, Turkey
DOI: 10.31127/tuje.641501
Research Article

AUTOMATIC GROUND EXTRACTION FOR URBAN AREAS FROM AIRBORNE LIDAR DATA

Sibel Canaz Sevgen *[1] and Fevzi Karsli [2]

[1] Ankara University, Faculty of Applied Sciences, Department of Real Estate Development and Management, Ankara, Turkey
ORCID ID 0000-0001-5552-6067
ssevgen@ankara.edu.tr

[2] Karadeniz Technical University, Engineering Faculty, Geomatics Engineering Department, Trabzon, Turkey
ORCID ID 0000-0002-0411-3315
fkarsli@ktu.edu.tr

* Corresponding Author
Received: 01/11/2019 Accepted: 19/12/2019

ABSTRACT
Terrain models play a key role in many applications, such as hydrological modeling, volume calculation, wire and pipeline route planning as well as many engineering applications. While terrain models can be generated from traditional data sources, an advanced and recently popular geospatial technology, Light Detection and Ranging (LiDAR) data, is also a source for generating high-density terrain models in the last decades. The main advantage of LiDAR technology over traditional data sources is that it generates 3D point clouds directly so that the representation of the surfaces is obtained fast. On the other hand, before terrain modeling, ground points need to be extracted by point labeling in the 3D point cloud. In this study, a new algorithm is proposed for automatic ground point extraction from airborne LiDAR data for urban areas. The proposed algorithm is mainly based on height information of the points in the dataset and labels ground points comparing height differences in local windows. The algorithm does not require any user input threshold and a neighborhood definition. The proposed ground extraction algorithm was tested with three different urban area LiDAR data. The quality control basically performed qualitatively by visual inspection and quantitatively by calculation of overall accuracy, which is conduct by comparing the proposed algorithm results with data provider's ground classification and Cloth Simulation Filtering (CSF) algorithm's results. The overall accuracy of the proposed algorithm is found between 95%-98%. The experimental results showed that the algorithm promises reliable results to extract ground points from airborne LiDAR data for urban areas.

Keywords: *Ground Extraction, LiDAR, Ground Modeling, Urban Area, Remote Sensing*

1. INTRODUCTION

LiDAR has been gaining its popularity as a remote sensing technique in recent decades in many areas. It has become a main data source of many applications in many engineering fields, such as machine learning, pattern recognition, data mining and knowledge extraction. The advantage of LiDAR is that it requires less effort to have 3D data with respect to traditional data sources. Airborne LiDAR system is generally mounted on an aircraft and assisted with Global Positioning System (GPS) and Inertial Navigation System (INS) systems. 3D dense point cloud data accurately collected by basically sending a laser pulse from a transmitter and receiving the scattered back photons. Using the travel time between signal emission and reception 3D point cloud data is created. Airborne LiDAR data has been being used by many researchers especially for feature extraction and ground modeling & DTM generation applications (Liu 2008; Chen *et al*. 2017). To extract features such as building, trees etc. and/or create ground models firstly separation between ground and non-ground has to be implemented. So that, extracted ground points can be employed for terrain modeling and Digital Elevation Model (DEM) generation. DEM studies are also widely used which are created using LiDAR data (Büyüksalih and Gazioğlu, 2019). Particularly, ground extraction and modeling are important in terms of usage for model water flow, planning applications, classification of objects, volume calculation and other applications (Canaz Sevgen, 2019; Yılmaz and Uysal, 2017).

Ground can shortly be described as a solid surface of the earth while non-ground represent the objects that do not belong to the ground or pertaining to the ground surface. Extraction of the ground surface and generating a model from LiDAR data with filtering algorithms were studied by many researchers (Kraus and Pfeifer 2001; Liu and Zhang 2008; Yuan *et al*. 2009; Wang and Tseng 2010; Mongus and Zalik 2012, Mongus *et al*. 2014, Uysal and Polat, 2014; Zeybek *et al*., 2015). In literature, filtering algorithms for ground modeling can be classified into groups such as interpolation-based (surface-based) filtering algorithms (Kraus and Pfeifer 1998; Chen *et al*. 2007; Lee and Younan 2003), Sloped-Based filtering algorithms (Vosselman 2000; Zhang *et al*., 2003), Morphological Filtering algorithms (Kilian *et al*. 1996; Lohmann *et al*. 2000; Zakšek and Pfeifer 2006), and Segmentation-Based Filters (Filin and Pfeifer 2006; Tovari and Pfeifer 2005).

Point-cloud data also can be generated from photographs (Akçay *et al*., 2017). In recent years, some researchers also studies ground extraction to create digital terrain models from point clouds generated from photogrammetric aerial photographs instead of using LiDAR data. For instance, Yilmaz *et al*. (2018) investigates the performances of seven widely used ground filtering algorithms from commercial and non-commercial software's on UAV-based point clouds. Wallace *et al*. (2016) another example of UAV-based point cloud filtering algorithm investigation study. Zeybek and Şanlıoğlu (2019) filtered UAV-based 3D raw point cloud data and compared four different filtering algorithms; curvature based (Multiscale Curvature Classification-MCC), surface-based filtering (FUSION), progressive TIN based (LasTool-LasGround module-commercial) and physical simulation processing (Cloth Simulation Filtering-CSF). Wang *et al*. (2014) also filtered Point Cloud Extracted from UAV Images. Point clouds generated from aerial photographs are dense comparing with LiDAR data; however, in some cases it is not possible to create point clouds from photograph since creating point clouds needs overlapping images. More specifically, in contrast to laser scanning, 3D data can be only derived from overlapping imagery whenever conjugate features have been identified and the intersection of the respective spatial rays is mathematically described (Canaz and Habib 2013). Therefore, in this study source of the data was chosen as LiDAR.

On the other hand, some researchers created ground filtering algorithms by focusing on ground extraction from LiDAR data on urban areas. Urban areas are abundant on non-ground objects, which means that sudden height differences occur in these areas such as ground to building facades, or roof of buildings and cars. In view of the fact that urban areas have more non-ground object compared with the bare territory, many researchers developed algorithms to extract ground on urban areas. For instance, Shan and Sampath (2005) extracted ground for urban areas performing a forward and backward labeling algorithm, which uses slope and elevation difference, and they created DEM for urban areas from airborne LiDAR data. Wang and Zhang (2016) extracted ground points by utilizing the scan line information in LiDAR data and using similarity measurement. Furthermore, a combination of slope based method and region growing was studied for ground extraction from LiDAR data in urban areas by Feng *et al*. 2009. Three windows with different sizes; small, average and large are created and a height difference threshold, was used for separating ground and non-ground points in each local window by Rashidi and Rastiveis (2017). Meanwhile, the best threshold values for the size of windows are considered based on physical characteristics of the ground surface and size of objects. In this study, the algorithm is proposed to not have any threshold entered by users. Hence, the proposed algorithm does not require any user input threshold to label and extract ground points.

Recently, a Cloth Simulation Filter (CSF) algorithm was developed by Zhang *et al.* (2016) for generating DTM from point cloud data. The authors firstly turning point cloud upside to down, and then rigid cloth is used to cover the inverted surface. Their algorithm analyzes the cloth nodes and the corresponding LiDAR points` intersection. Finally, the generated surface are compared with the original surface for extracting the ground points from the LiDAR point cloud. In this study, the proposed algorithm's ground extraction result was compared with the CSF algorithm results.

An elevation based algorithm for separation of ground and non-ground points for urban areas from airborne LiDAR data was proposed in this study. The algorithm cuts the large area of LiDAR data to into small windows size and then height difference for each point to randomly selected points were calculated. The number of below and upper points label the point as ground or non-ground. The algorithm based on that ground points generally do not have lower points from them. Most advantageous part of the proposed algorithm is that it does not require any threshold entered by the

users, and separate ground and non-ground points without any user interference. The proposed algorithm was tested with three different datasets, which differ from each other in point density, vegetation density, and building data type, The result of the proposed algorithm was compared with data provider's ground classification, which was performed by LAStools and TerraScan LiDAR processing software package, and the CSF algorithm (Zhang *et al*. 2016) ground extraction results. The proposed algorithm gives reliable results for extracting ground points from LiDAR data for urban areas according to the comparison result.

2. METHODOLOGY

Urban areas generally have dense non-ground objects such as trees, buildings, cars etc. For these areas, airborne LiDAR data consist of points which are scattered back from both ground points and any points which belong to non-ground points. Starting from this point, the proposed algorithm was developed to extract ground points from LiDAR data automatically for urban areas by simply using ground points and non-ground points height differences. The details of the methodology are explained in next sections.

To extract ground points from raw LiDAR data of an urban area, an algorithm was proposed, and a stepwise approach was followed. The proposed algorithm firstly start with creating *n* number of *m* by *m* meters sized windows of LiDAR data. In this study, 30 meters windows were chosen since mainly in urban areas 900 m^2 are enough to present non-ground points of objects and ground points. If there are no non-ground points (i.e. cars, trees, buildings) in the window area, the algorithm assigns all the points as ground points by simply checking height differences in the current window. The proposed algorithm firstly performs windows creation, and using points in the windows, classification of non-ground and ground points from LiDAR data was performed. The algorithm firstly, creates *n* number of 30×30 meters windows in XY planimetric space.

The proposed algorithm mainly have one condition. The condition is that non-ground points in the current window area higher than ground points. To calculate heights differences, firstly for each point to randomly selected points, distances are calculated in the Z axis. The points are randomly selected to prevent compare height distance from only same classes (ground/non ground) then, a number of height distances less than zero and more than 1 meters is counted. In other words, a number of positive and negative distances are counted for each point. Since LiDAR data standard deviation in Z axis generally changes 10 cm to 1 meter (Liu, 2011), 1 meter is intentionally chosen to prevent counting points which are in the same class and very close to each other. For instance, in LiDAR data points which are on the ground have generally 10 cm to 1 meters height differences even if they are in the same plane, and this is occurring because of LiDAR data nature. So that, to not count these point for positive distance 1 meter was intentionally chosen. After that, minimum height in the current window is found and used to check labeled ground points if they are too high than the local height, the point checked again if it is non-ground points by using the other labeled ground points.

The proposed algorithm lay on a logic, if a positive number of distance points more than the negative number of distance points, then the point is assigned as non-ground points. Since non-ground points are higher than ground points in the window size area (Fig. 1).

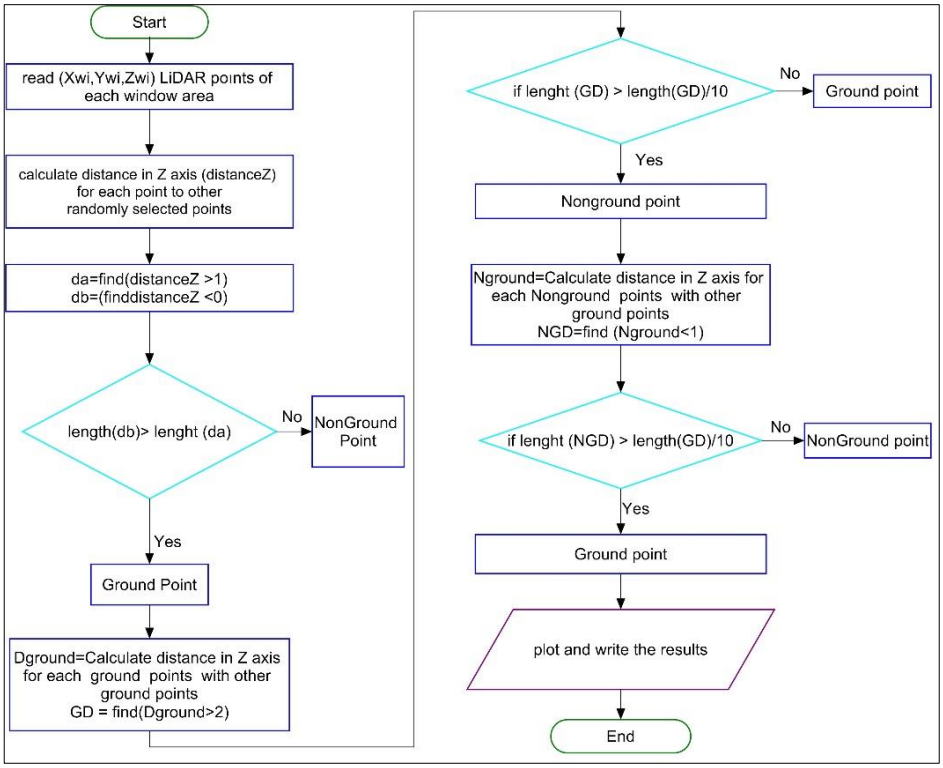

Fig. 1. Flowchart of the proposed methodology

The logic behind the proposed algorithm is illustrated in Fig. 2. In the figure red point is the selected as a sample point. Blue points represent non-ground points, while ground points are displayed as green. For the red point, if distance higher than 0 and less than 1 meter is calculated with randomly selected points, there will be more number of points that are higher than red points. Therefore, the red point will be assigned as ground point.

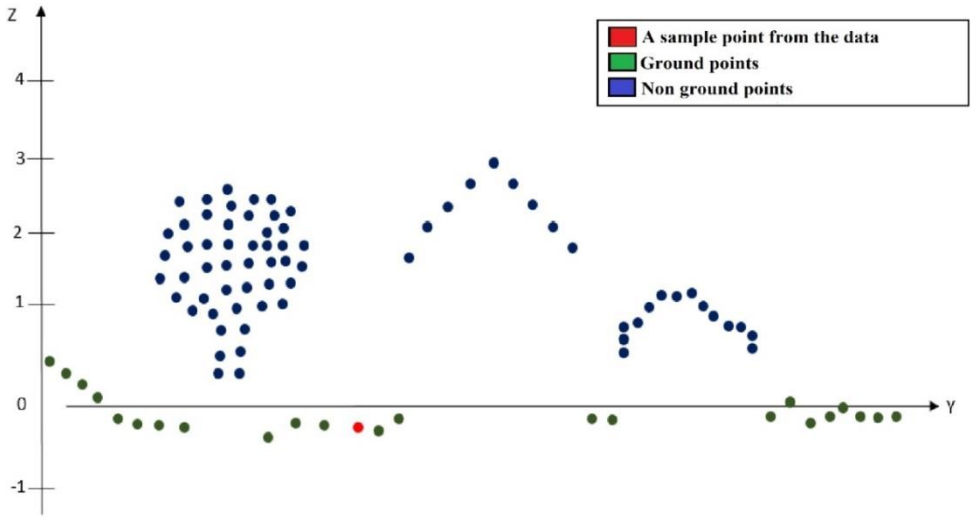

Fig. 2. Illustration of the condition for the proposed algorithm

After the proposed algorithm assigns ground and non-ground points, a quick quality control was employed to check the points labeled correctly. The control starts with a calculating distance of each assigned ground point to other ground points. If the distance from a ground point to other ground points have much distance in Z, the ground point is assigned as non-ground points and it will be removed from ground point class. The logic behind this calculation is that in the window size data, ground points should not have such a huge height difference even in the sloped areas.

For the final analysis of the results, quality controls were applied. Firstly visual inspection was carried out. The visual quality control is simply performed by plotting and comparing the classified ground and non-ground points with the plotted reference. Reference ground extraction was employed by data provider which conducted by using LAStools and TerraScan LiDAR processing software package and the CSF algorithm. LAStools classify ground basically using Adaptive Triangulated Irregular Network (ATIN) algorithm (Axelsson, 2000). A search windows are created and angle criteria was used to classify ground points in LAStools. According to visual inspection, the proposed algorithm gives reliable results, which can be seen in the results section in the figure of results.

On the other hand, quantitative quality control was performed by comparing each point's classes with reference classes. The proposed algorithm labels points 0 and 1 as non-ground and ground points, respectively. After sorting reference and the proposed algorithm result and reference classes according to X, Y and Z axes, the classified points and reference point's classes (i.e. the CSF algorithm's results) were compared one by one. For the quantitative quality control, error matrices were created and overall and producers' accuracy were calculated. The details of the quality control are discussed in the results section in details.

3. RESULTS AND DISCUSSION

The proposed ground extraction algorithm was tested with three different dataset which contain only urban areas. The first data set is downloaded from a package of a LiDAR processing tool *LAStools* (2017) and the data is called as *Fusa* in this study *(https://rapidlasso.com/lastools/).* Reference Ground Classification of *Fusa* data set was already conducted by *Lastools* software package. The data contains approximately 277K points. The total area of the data is 0.06 km^2. The second data used in this study is from Istanbul (Bimtaş Co., Istanbul) and named as *Istanbul* hereafter. The area of *Istanbul* data is 0.37 km^2 and total number of points is 1.8M. The third data is from California U.S. (obtained from Digital Mapping, Inc. (DMI), U.S.) It has 1M points and its area is 5.23 km^2 (Table 1). Reference Ground Classification of *Istanbul* and *California* was employed by data provider using TerraScan software. The details of the data can be seen in Table 1. *California* data set's area is bigger than *Fusa* and *Istanbul* data area, while these two data sets are denser compared with *California* data set. Furthermore, *Istanbul* data sets have taller buildings comparing with *California* and *Fusa* data sets, while *Istanbul* has less tree in contrast to the two other data sets. Aforementioned proposed algorithm partitions the data into 30×30 meters window in XY plane, and a total number of windows for each dataset is given in Table 1.

Table 1. LiDAR data sets' details

Data Name	Number of Points	Ave. Point Density	Dimensions (m)	Area (km^2)	# of Windows (30×30 m)
Fusa	277,354	4.44	249X249	0.06	**81**
Istanbul	1,845,761	4.93	534X700	0.37	**432**
California	1,023,432	0.19	2729X1918	5.23	**5,824**

Ground/non-ground classification points in the Fusa data set's result is shown in Fig. 3. Fig. 3a is the classified reference data set by LAStools software package, Fig. 3b is the proposed algorithm's classification results, Fig. 3c is the CSF algorithm result. The green area of the figure represent the ground points, while red points are non-ground points (buildings, cars, trees etc.)

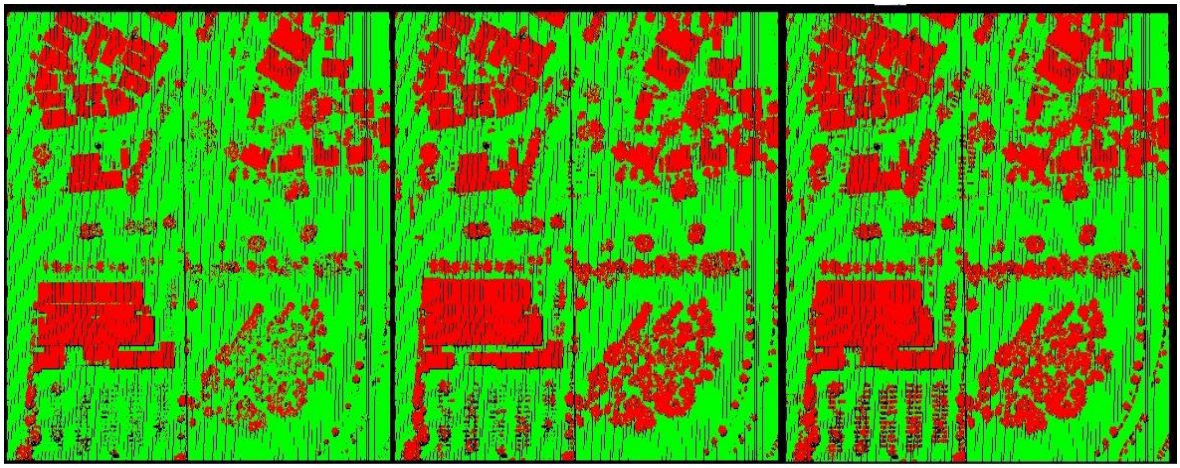

Fig. 3. Ground extraction result for Fusa data sets. (a) data provider classification result (Lastools), (b) the proposed algorithm result, (c) the CSF algorithm result.

To evaluate result visually, the study area for the Fusa data set given in the below (Fig. 4). According to the below images, and the results above, it can be said that all the classification results are correctly labeled by comparing the images and the results.

Fig. 4. Ortophoto images for Fusa data sets (Source: Google web services)

To examine result visually, randomly selected part of the areas from the result was zoomed and showed in Fig. 5 for Fusa data set. Fig. 5 has also 3D view of the closer examined results. Left columns are 2D views of the selected parts (XY plane), and right columns are their 3D representation. Upper selected part of the result has both trees and houses as non-ground objects, while bottom part includes only trees as non-ground objects. According to visual inspection of the result, it can be easily observed that the algorithm worked very well, and ground points are successfully extracted.

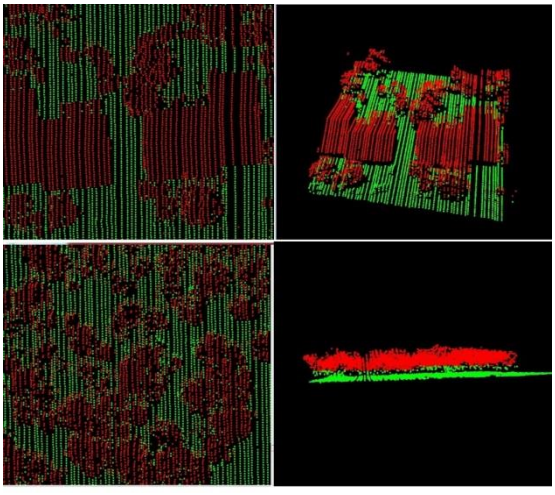

Fig. 5. Closer examination of ground/non-ground classification result of Fusa data set by proposed algorithm

Istanbul data set classified ground and the non-ground result is illustrated in Fig. 6. Fig. 6a shows classified ground and non-ground points in reference

data, whereas Fig. 6b is the result of the proposed algorithm, and Fig. 6c is the CSF algorithm result. It can be easily observed that the proposed algorithm gives very reliable results, by comparing Fig. 6a, 6b, and 6c. Ground points are successfully extracted from the whole Istanbul LiDAR data set.

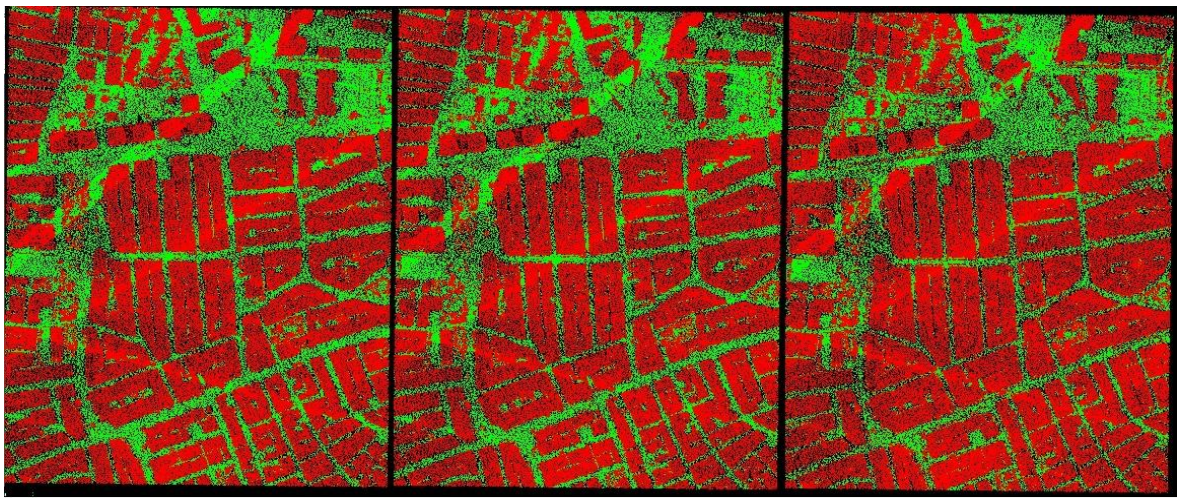

Fig. 6. Istanbul data set results; (a) data provider classification result (by TerraScan), (b) the proposed algorithm result, (c) the CSF algorithm result.

Orthophoto imagery of the Istanbul data set area is shown in Fig. 7, the buildings can be easily seen in the image, and these buildings and non-ground area were successfully classified by the proposed algorithm (Fig. 6b)

Fig. 7. Orthophoto images for İstanbul data sets

For qualitative quality control, randomly chosen areas are zoomed and shown in Fig. 8 from Istanbul data set result. Here again, left columns are selected areas from the result in 2D coordinates system (XY axes), right columns are their 3D view. Istanbul data has very tall building and it is observed that the proposed algorithm work very well with data sets that have tall non-ground objects.

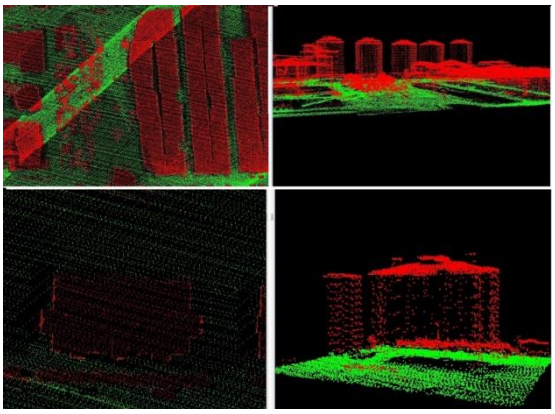

Fig. 8. Closer examination of ground- non-ground classification result of Istanbul data set

Finally, the result for the California data set can be seen in the below (Fig. 9). As mentioned before, red areas represent non-ground points of the data. The area is large and has very big size houses in contrast to two previous data sets. The result for the proposed algorithm represented in Fig. 9b.

Fig. 9. California data set results; (a) data provider classification result (by TerraScan), (b) the proposed algorithm result, (c) the CSF algorithm result.

The study are for the California data set shown in the below orthophoto image, as it can be seen in the image, the area has so many houses, and the area is slightly complex. However, overall it can be observed that the proposed algorithm was extracted ground reliable by comparing the Fig. 10 and Fig 9b.

Fig. 10. Ortophoto images for California data sets (Source: Google web services)

Fig. 11 is an example of closer examination from results in California data set and it shows how the proposed algorithm gives reliable results. Upper left figure includes results of non-ground points (houses) and big size ground part, and its 3D view can be seen on the right upper part in the figure. On the other side, bottom figure is an example of non-ground that includes tree and houses. According to visual closer quality control. Only a few points were wrongly labeled in these randomly selected part of the result.

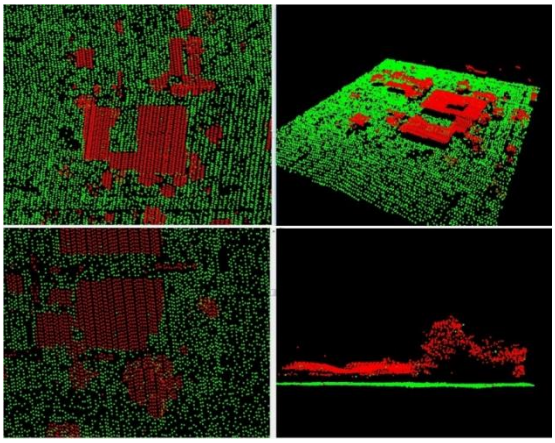

Fig. 11. Closer examination of ground- non-ground classification of California data set result

The results from the proposed algorithm were compared with reference result qualitatively and quantitatively. Qualitative evaluation is carried out by visual interpretations of the results. Nevertheless, a quantitative evaluation is conducted by calculating overall accuracy and producer's accuracy. To conduct quantitative quality control, error matrix is created. Table 2 shows the error matrices and total accuracy as well producer's accuracy (1) and (2).

$$\boldsymbol{Overall_{Accuracy}} = \frac{\boldsymbol{Exracted\ (Ground + Non-ground)}}{\boldsymbol{Total\ points}} \boldsymbol{x100} \qquad (1)$$

$$\boldsymbol{Producer's_{Accuracy}} = \frac{\boldsymbol{Extracted\ Ground\ or\ Non-G\ Points}}{\boldsymbol{Total\ Ground\ or\ Non-ground\ Points}} \boldsymbol{x100} \qquad (2)$$

Table 2 Error matrices for the proposed ground extraction algorithm versus reference result

Fusa	Ground Points	Non-ground Points	Total reference
Ground Points	191475	6785	198260
Non-ground Points	1000	78094	79094
Total Proposed Algorithm	192475	84879	277354
Producer's Accuracy (%)	96.58	98.74	Overall Accuracy= 97%
Istanbul Area	**Ground Points**	**Non-ground Points**	**Total** reference
Ground Points	681405	25894	707299
Non-ground Points	194	1138268	1138462
Total Proposed Algorithm	681599	1164162	1845761
Producer's Accuracy (%)	96.33	99.98	Overall Accuracy= 98%
California	**Ground Points**	**Non-ground Points**	**Total** reference
Ground Points	471448	6374	477822
Non-ground Points	44769	500841	545610
Total Proposed Algorithm	516217	507215	1023432
Producer's Accuracy (%)	98.66	91.79	Overall Accuracy= 95%

According to the quantitative quality control for the proposed ground extraction algorithm, overall accuracy is calculated 95%, 97%, 98% for California, Fusa and Istanbul, respectively. According to quantitative quality control, it can be said that the algorithm gives reliable results for extraction of the ground points automatically in urban areas.

Finally, the proposed algorithm ground/non-ground extraction was compared with the CSF algorithm result. The overall accuracy was observed between 95-97%. Producer's accuracy was found between 90-99%.

Table 3 Error matrices for the proposed ground extraction algorithm versus CSF Results

Fusa	Ground Points	Non-ground Points	Total CSF
Ground Points	183495	183	183678
Non-ground Points	8980	84696	93676
Total Proposed Algorithm	192475	84879	277354
Producer's Accuracy (%)	99.99	90.41	Overall Accuracy= 97%
Istanbul Area	**Ground Points**	**Non-ground Points**	**Total CSF**
Ground Points	587186	7076	594262
Non-ground Points	94413	1157086	1251499
Total Proposed Algorithm	681599	1164162	1845761
Producer's Accuracy (%)	98.80	92.45	Overall Accuracy= 95%
California	**Ground Points**	**Non-ground Points**	**Total CSF**
Ground Points	465816	5502	471318
Non-ground Points	50401	501713	552114
Total Proposed Algorithm	516217	507215	1023432
Producer's Accuracy (%)	98.83	90.87	Overall Accuracy= 95%

4. CONCLUSIONS

In conclusion, terrain modeling and creating DEM have vital importance in the usage of hydrological modeling, telecommunication industry etc. 3D data is necessary to create terrain modeling. LiDAR technology have the ability to collect 3D data fast and directly using laser pulses. Since LiDAR advantage of the dense 3D data set, it was chosen as the main dataset for this study. An algorithm was proposed to extract ground and non-ground points from LiDAR data in the urban areas. In the literature there are many algorithms that extracts ground points, while automatically study of extraction of the ground points are limited for the urban areas. The most advantageous of the proposed algorithm is that it does not require any threshold input and extract the ground/non-ground points automatically using the height difference of the point with the randomly selected other points in urban areas. The algorithm was tested with three different LiDAR data sets, and the results were compared with the data provider reference ground points and the CSF algorithm result. Error matrices were

created overall accuracy is calculated between 95-98%, while producer's accuracy calculated as 86-99%. Furthermore, qualitative quality control carried out simply plotting inspecting the reference data and the proposed algorithm results visually. According to both qualitative and quantitative quality control, it is observed that the proposed algorithm gives reliable result in urban areas. Consequently, the algorithms extract ground points in the urban area from LiDAR data set automatically. The most advantage part of the proposed algorithm is that it is fully automated. For the future work, the algorithm will be developed for the areas that does not only include urban areas.

ACKNOWLEDGEMENTS

The authors would like to acknowledge Digital Mapping, Inc. (DMI) U.S. and Bimtaş, Istanbul, for sharing LiDAR data to use in our academic study.

REFERENCES

Akçay, Ö , Erenoğlu, R , Avşar, E (2017). The Effect Of Jpeg Compression In Close Range Photogrammetry. *International Journal of Engineering and Geosciences* , 2 (1) , 35-40 . foi: 10.26833/Ijeg.287308

Axelsson P (2000) DEM generation from laser scanner data using adaptive TIN models. *International Archives of Photogrammetry and Remote Sensing* 33 (B4/1): 110–117.

Büyüksalih İ., Gazioglu C (2019). New Approach in Integrated Basin Modelling: Melen Airborne LIDAR. *International Journal of Environment and Geoinformatics (IJEGEO*) 6: 22-32. 10.30897/ ijegeo.530272.

Canaz S, Habib A (2013) Photogrammetric features for the registration of terrestrial laser scans with minimum overlap. *J. Geod. Geoinf.* 2013, 2, 1–8.

Canaz Sevgen, S . (2019). Airborne Lidar Data Classification In Complex Urban Area Using Random Forest: A Case Study of Bergama, Turkey. *International Journal of Engineering and Geosciences* , 4 (1) , 45-51 .doi: 10.26833/ijeg.440828

Chen Z, Gao B, Devereux B (2017) State-of-the-art: DTM generation using airborne LIDAR data. *Sensor*s 2017, 17, 150.

Chen Q, Gong P, Baldocchi D, Xin G (2007). Filtering airborne laser scanning data with morphological methods. *Photogrammetric Engineering and Remote Sensing* 73(2), 175-185.

Filin S, Pfeifer N (2006) Segmentation of airborne laser scanning data using a slope adaptive neighborhood. *ISPRS Journal of Photogrammetry and Remote Sensing* 60, 71–80.

Kilian J, Haala N, Englich M (1996) Capture and evaluation of airborne laser scanner data, International Archives of Photogrammetry. *Remote Sensing and Spatial Information Sciences* 31(B3), 383-388.

Kraus K, Pfeifer N (2001) Advanced DTM generation from LIDAR data. International Archives of the Photogrammetry. *Remote Sensing and Spatial Information Sciences*, XXXIV (Pt. 3/W4) (2001), pp. 23-30.

Kraus K, Pfeifer N (1998) Determination of terrain models in wooded areas with airborne laser scanner data. *ISPRS Journal of Photogrammetry and Remote Sensing* 53(4), 193-203.

LAStools (2017) Award-winning software for efficient LiDAR processing with LASzip, obtained from https://rapidlasso.com/LAStools/

Lee HS, Younan NH (2003) DTM extraction of LiDAR returns via adaptive processing. *IEEE Transactions on Geoscience and Remote* Sensing 41(9), 2063-2069.

Liu X, Zhang Z (2008) Lidar data reduction for efficient and high quality DEM generation. *Int. Arch. Photogram. Remote Sens. Spat. Inform. Sci*. vol. 37 (pg. 173 -178).

Liu X (2008) Airborne LiDAR for DEM generation: some critical issues. *Prog. Phys. Geog*. 32, 31-49.

Liu XY (2011) Accuracy assessment of LiDAR elevation data using survey marks. *Surv Rev* 43:80–93. doi: 10.1179/003962611X12894696204704

Lohmann P, Koch A, Schaeffer M (200) Approaches to the filtering of laser scanner data. *International Archives of Photogrammetry, Remote Sensing and Spatial Information Sciences* 33(B3), 540-547.

Mongus D, Žalik B (2012) Parameter-free ground filtering of LiDAR data for automatic DTM generation. *ISPRS J. Photogrammetry* 67, 1–12

Mongus D, Lukač N, Žalik B (2014) Ground and building extraction from LiDAR data based on differential morphological profiles and locally fitted surfaces. *ISPRS J. Photogramm. Remote Sens.* Vol; 93, 145–156.

Rashidi P, Rastiveis H, (2017) Ground Filtering Lidar Data Based On Multi-Scale Analysis Of Height Difference Threshold. *The International Archives of the Photogrammetry, Remote Sensing and Spatial Information Sciences*, Volume XLII-4/W4, 2017 Tehran's Joint ISPRS Conferences of GI Research, SMPR and EOEC 2017, 7–10 October 2017, Tehran, Iran

Shan J, Sampath A (2005) Urban DEM generation from raw LiDAR data: a labeling algorithm and its performance. *Photogrammetric Engineering and Remote Sensing* 71, 217–26

Tovari D, Pfeifer N (2005) Segmentation based robust interpolation – a new approach to laser data filtering. *IAPRS* Vol XXXVI, 3/W3, Enschede, the Netherlands.

Uysal, M. Polat, N (2014) Investigating Performance Of Airborne Lidar Data Filtering With Triangular Irregular Network (TIN) Algorithm, Int. Arch. Photogramm.

Remote Sens. Spatial Inf. Sci., XL-7, 199-202, https://doi.org/10.5194/isprsarchives-XL-7-199-2014, 2014.

Vosselman G (2000) Slope based filtering of laser altimetry data, *International Archives of Photogrammetry, Remote Sensing and Spatial Information Sciences.* 33(part B3/2), 935-934.

Wang CK, Tseng YH (2010) DEM generation from airborne LiDAR data by adaptive dual-directional slope filter. *Int. Arch. Photogram. Remote Sens. Spat. Inform. Sci* 38(Part 7B), 628–632.

Yuan F, Zhang J X, Zhang L, Gao J (2009) DEM generation from airborne LIDAR data. *Inter-national Archives of the Photogrammetry, Remote Sensing and Spatial Information Sciences* Vol XXXVIII-7/C4 : 308-312

Yuan F, Zhang J, Zhang L (2009) Urban DEM generation from airborne Lidar data[C]. *Urban Remote Sensing Event*, 2009 Joint. IEEE, pp 1–5.

Zakšek K, Pfeifer N (2006) An improved morphological filter for selecting relief points from a LiDAR point cloud in steep areas with dense vegetation, *Luubljana, Slovenia and Innsbruck, Austria: Institute of Anthropological and Spatial Studies*, Scientific Research Centre of the Slovenian Academy of Sciences and Arts, and Institute of Geography, Innsbruck University.

Zhang Y, Wang L (2016) Computer Vision and Pattern Recognition LiDAR Ground Filtering Algorithm for Urban Areas Using Scan Line Based Segmentation. Cornell University*Computer Vision and Pattern Recognition*

Zhang KQ, Chen SC, Whitman D, Shyu ML, Yan JH, Zhang CC (2003) A progressive morphological filter for removing nonground measurements from airborne LiDAR data, *IEEE Transactions on Geoscience and Remote Sensing* 41(4), 872-882.

Zhang WM, Qi JB, Wan P, Wang HT, Xie DH, Wang XY, Yan GJ (2016) An Easy-to-Use Airborne LiDAR Data Filtering Method Based on Cloth Simulation. *Remote Sens*. 2016, 8, 501

Zeybek M., Şanlıoglu İ., Genc A (2015) Yüksek Çözünürlüklü Yersel lazer tarama verilerinin filtrelenmesi ve filtrelemelerin heyelan izlemeye etkisi. Dogal Afetler ve Cevre Dergisi, 1:11 – 20, 2015.

Zeybek M., Şanlıoğlu İ (2019) Point cloud filtering on UAV based point cloud. *Measurement* 133, 99-111.

Yilmaz Serifoglu C, Yilmaz V, Gungor O (2018) Investigating the performances of commercial and non-commercial software for ground filtering of UAV-based point clouds. *International Journal of Remote Sensing.*

Yilmaz, M , Uysal, M (2017). Comparing Uniform And Random Data Reduction Methods For Dtm Accuracy. International Journal of Engineering and Geosciences , 2 (1) , 9-16 . doi: 10.26833/ijeg.286003

Wallace L, Lucieer A, Malenovský Z, Turner D, Vopěnka P (2016) Assessment of Forest Structure Using Two UAV Techniques: A Comparison of Airborne Laser Scanning and Structure from Motion (Sfm) Point Clouds *Forests*. 7 (3): 62. doi:10.3390/f7030062.

Wang Q, Wu L, Wu Z, Tang H, Wang R, Li F (2014) A progressive morphological filter for point cloud extracted from UAV images." *In IEEE International Geoscience and Remote Sensing Symposium (IGARSS)* doi: 10.1109/ IGARSS. 2014. 6946860.

Turkish Journal of Engineering

Turkish Journal of Engineering (TUJE)
Vol. 4, Issue 3, pp. 123-128, July 2020
ISSN 2587-1366, Turkey
DOI: 10.31127/tuje.646926
Research Article

THE CLASSICAL AES-LIKE CRYPTOLOGY VIA THE FIBONACCI POLYNOMIAL MATRIX

Orhan Dişkaya [*1], Erdinç Avaroğlu [2] and Hamza Menken [3]

[1] Mersin University, Graduate School of Natural and Applied Sciences, Ciftlikkoy, Mersin, TURKEY
ORCID ID 0000-0001-5698-7834
orhandiskaya@mersin.edu.tr

[2] Mersin University, Computer Engineering Department, Ciftlikkoy, Mersin, TURKEY
ORCID ID 0000-0003-1976-2526
eavaroglu@mersin.edu.tr

[3] Mersin University, Department of Mathematics Ciftlikkoy, Mersin, TURKEY
ORCID ID 0000-0003-1194-3162
hmenken@mersin.edu.tr

* Corresponding Author
Received: 14/11/2019 Accepted: 23/12/2019

ABSTRACT
Galois field, has an important position in cryptology. Advanced Encryption Standard (AES) also used in polynomial operations. In this paper, we consider the polynomial operations on the Galois fields, the Fibonacci polynomial sequences. Using a certain irreducible polynomial, we redefine the elements of Fibonacci polynomial sequences to use in our cryptology algorithm. So, we find the classical AES-like cryptology via the Fibonacci polynomial matrix. Successful results were achieved with the method used.

Keywords: *Fibonacci Numbers, Fibonacci Polynomial Numbers, Cassini Identity, Fibonacci Matrix, Galois Field*

1. INTRODUCTION

The Advanced Encryption Standard (AES), also known by its original name Rijndael (Daemen and Rijmen, 2003), is a specification for the encryption of electronic data established by the U.S. National Institute of Standards and Technology (NIST) in 2001. The AES block encryption algorithm is used for the algorithmic part of the developed system. AES is the applicable block encryption standard developed by J. Daemen and V. Rijmen in 1997 and adopted as a standard in 2000. AES is an iterative block cipher based on a design principle known as a substitution-permutation network (SPN). AES operates on a 4×4 column-major order matrix of bytes, called the state. Matrix calculations are done in a special finite field. AES supports 128-, 192-, 256- bit keys. The number of cycles of repetition for 128-bit, 192-bit, and 256-bit keys are 10, 12, and 14, respectively. These stages include key addition, byte substitution, ShiftRow, and MixColumn (Avaroğlu, Koyuncu, Özer and Türk, 2015). We too created a new encryption algorithm (known as AES-like) by using the AES algorithm. In AES-like, Galois field arithmetic is used in most layers, especially in matrix operations. We give an introduction to Galois fields as needed for this purpose before we introduced with the algorithm. A background on Galois fields is not needed for a basic understanding of AES-like. So, we will obtain a basic entrance to Galois fields (Paar and Pelzl, 2009; Stewart, 1990). Information on the following classical cryptology benefit in (Klima and Sigmon, 2012).

1.1. Definition : In (Paar and Pelzl, 2009). A field F is a set of elements with the following features:

1. All elements of F form an additive group with the group operation + and the neutral element 0.
2. All elements of F except 0 form a multiplicative group with the group operation × and the neutral element 1.
3. When the two group operations are mixed, the distributive law holds, i.e., for all $a,b,c \in F$:

$$a(b+c) = ab + ac .$$

In extension fields $GF(2^m)$ elements are not represented as integers but as polynomials with coefficients in $GF(2)$. However, we take $m = 5$ for the next process. In AES-like the finite field contains 32 elements and is denoted as $GF(2^5)$. In the field, $GF(2^5)$, which is used in AES-like, each element $A \in GF(2^5)$ is thus represented as:

$$A(x) = a_4x^4 + a_3x^3 + a_2x^2 + a_1x + a_0,$$
$$\{a_i\} \in GF(2) = \{0,1\}$$

Note that there are exactly $32 = 2^5$ such polynomials. The set of these 32 polynomials is the finite field $GF(2^5)$. Each elements of this polynomial correspond to one letter of the alphabet.

1.2. Definition : (Addition and subtraction in $GF(2^5)$). In (Paar and Pelzl, 2009). Let $A(x), B(x) \in GF(2^5)$. The sum and the subtraction of the two elements are then computed according to:

$$A(x) \pm B(x) = (a_4 \pm b_4)x^4 + (a_3 \pm b_3)x^3 + (a_2 \pm b_2)x^2 + (a_1 \pm b_1)x + (a_0 \pm b_0),$$
$$(a_i \pm b_i) \bmod 2 \quad \text{for } i \in \{0,1,2,3,4\}$$

1.3. Example: For $A(x) = x^4 + x^2 + x$ and $A(x) = x^4 + x^3 + x^2 + 1$, the sum $A(x) + B(x)$ of two elements from $GF(2^5)$ is computed:

$$A(x) + B(x) = x^3 + x + 1.$$

1.4. Definition: (Multiplication in $GF(2^5)$). In (Paar and Pelzl, 2009). Let $A(x), B(x) \in GF(2^5)$ and let

$$P(x) = p_0 + p_1x + p_2x^2 + p_3x^3 + p_4x^4 + p_5x^5,$$
$$p_i \in GF(2^5)$$

be an irreducible polynomial. Multiplication of the two elements $A(x), B(x)$ is performed as

$$A(x).B(x) \bmod P(x).$$

The irreducible polynomials of $GF(2^5)$ are as follows,
$x^5 + x^2 + 1$,
$x^5 + x^3 + 1$,
$x^5 + x^3 + x^2 + x + 1$,
$x^5 + x^4 + x^3 + x + 1$,
$x^5 + x^4 + x^3 + x^2 + 1$,
$x^5 + x^4 + x^2 + x + 1$.
For AES, the irreducible polynomial
$P(x) = x^8 + x^4 + x^3 + x + 1$
is used. It is part of the AES specification. For AES-like, we consider the irreducible polynomials as following,
$P(x) = x^5 + x^2 + 1$.

1.5. Example: For $A(x) = x^4 + x^2 + 1$ and $B(x) = x^3 + x$ in the field $GF(2^5)$, the multiplication $A(x).B(x)$ according to the irreducible polynomial $P(x) = x^5 + x^2 + 1$ is
$A(x).B(x) = x^7 + x = x^2(x^2 + 1) + x = x^4 + x^2 + x$.
Especially, we are concerned with software implementations of the Galois fields. Hence, we know
$A(x) = x^4 + x^2 + 1 = (10101)_2 = 21_{10}$
$B(x) = x^3 + x = (01010)_2 = 10_{10}$.
The field elements, are normally stored as bit vectors in the computers. If we look at the multiplication from the previous example, the following very atypical operation is being performed on the bit level:
$A(x).B(x) = (x^4 + x^2 + 1)(x^3 + x) = x^4 + x^2 + x$
$(10101)(01010) = (10110)$

This computation is not identical to integer arithmetic. The result would have been $(01101)_2 = 13_{10}$, which is clearly not the same as the Galois field

multiplication product. Inversion in $GF(2^5)$ is the core operation to decrypt of the matrix polynomial.

1.6. Definition: In (Paar and Pelzl, 2009). For a given field $GF(2^5)$ and the corresponding irreducible reduction polynomial $P(x)$, the inverse A^{-1} of a nonzero element $A \in GF(2^5)$ is defined as:

$$A^{-1}(x)A(x) = 1 \bmod P(x).$$

1.7. Definition: In (Koshy, 2018; 2019). The Fibonacci sequence $\{F_n\}_{n\geq 0}$ is

$$F_0 = 0,\ F_1 = 1 \text{ and } F_{n+2} = F_{n+1} + F_n.$$

Here, F_n is the nth Fibonacci number. The first few members of this sequence is given as follow;

n	0	1	2	3	4	5	6	7	8	...
F_n	0	1	1	2	3	5	8	13	21	...

Table 1. A few the Fibonacci numbers

1.8. Definition: In (Koshy, 2018; 2019). The Fibonacci Polynomial sequence $\{f_n(x)\}_{n\geq 0}$ is

$$f_0(x) = 0,\ f_1(x) = 1 \text{ and } f_{n+2}(x) = xf_{n+1}(x) + f_n(x).$$

The first few members of this sequence is given as follow;

Table 2. A few the Fibonacci polynomial numbers

n	0	1	2	3	4	5	...
$f_n(x)$	0	1	x	x^2+1	x^3+2x	x^4+3x^2+1	...

According to irreducible polynomial $P(x)$ the Fibonacci polynomials $f_n(x)$ are as follows;

Table 3. A few the irreducible polynomial numbers

n	$f_n(x)$	Z_2
0	0	mod 2
1	1	mod 2
2	x	mod 2
3	$x^2 + 1$	mod 2
4	x^3	mod 2
5	$x^4 + x^2 + 1$	mod 2
6	$x^2 + x + 1$	mod 2
7	$x^4 + x^3 + x + 1$	mod 2
8	$x^4 + x^2$	mod 2
9	$x^4 + x^2 + x$	mod 2
...	...	...

The following identity is non-zero, which tells us that Fibonacci polynomial matrix can be reversed,

1.9. Theorem (Cassini Identity): In (Koshy, 2018; 2019). Let $f_n(x)$ denote the nth Fibonacci polynomial sequence. Then,

$$f_{n+1}(x)\, f_{n-1}(x) - f_n^2(x) = (-1)^n, \quad n \geq 1.$$

1.10. Theorem (Fibonacci Polynomial Matrix): In [3, 4]. Let,

$$Q(x) = \begin{pmatrix} x & 1 \\ 1 & 0 \end{pmatrix}$$

It then follows by inductive method that,

$$Q^n(x) = \begin{pmatrix} f_{n+1}(x) & f_n(x) \\ f_n(x) & f_{n-1}(x) \end{pmatrix}$$

where $n \geq 1$. $Q^n(x)$ is called the Fibonacci polynomial matrix.

1.11. Theorem (Inverse of a 2x2 Matrix): Let $Q^n(x)$ be a Fibonacci Polynomial Matrix. Let $Q^n(x)$ be the Fibonacci polynomial matrix. Then, the determinant of $Q^n(x)$ is

$$\left|Q^n(x)\right| = f_{n+1}(x)\, f_{n-1}(x) - f_n^2(x) = 1.$$

and inverse of $Q^n(x)$ is given by

$$Q^n(x)^{-1} = \begin{pmatrix} f_{n-1}(x) & f_n(x) \\ f_n(x) & f_{n+1}(x) \end{pmatrix}.$$

Polynomials of the Galois field are equivalent of each alphabet is as following,

Table 4.The polynomials are equivalent of each alphabet

No	Bit	Polynom	Alphabet
0	00000	0	A
1	00001	1	B
2	00010	x	C
3	00011	$x + 1$	Ç
4	00100	x^2	D
5	00101	$x^2 + 1$	E
6	00110	$x^2 + x$	F
7	00111	$x^2 + x + 1$	G
8	01000	x^3	Ğ
9	01001	$x^3 + 1$	H
10	01010	$x^3 + x$	I
11	01011	$x^3 + x + 1$	İ
12	01100	$x^3 + x^2$	J
13	01101	$x^3 + x^2 + 1$	K
14	01110	$x^3 + x^2 + x$	L
15	01111	$x^3 + x^2 + x + 1$	M
16	10000	x^4	N
17	10001	$x^4 + 1$	O
18	10010	$x^4 + x$	Ö
19	10011	$x^4 + x + 1$	P
20	10100	$x^4 + x^2$	R
21	10101	$x^4 + x^2 + 1$	S
22	10110	$x^4 + x^2 + x$	Ş

23	10111	$x^4 + x^2 + x + 1$	T
24	11000	$x^4 + x^3$	U
25	11001	$x^4 + x^3 + 1$	Ü
26	11010	$x^4 + x^3 + x$	V
27	11011	$x^4 + x^3 + x + 1$	W
28	11100	$x^4 + x^3 + x^2$	X
29	11101	$x^4 + x^3 + x^2 + 1$	Y
30	11110	$x^4 + x^3 + x^2 + x$	Z
31	11111	$x^4 + x^3 + x^2 + x + 1$	Q

2. MAIN RESULTS

In the present work, we consider a message text in ns lengths (called the n-letter). Then, this messaging creates a cryptology algorithm using certain mathematical rules (Fibonacci polynomial matrix). We obtain a decryption algorithm by applying inversely of the stated mathematical rules. Similar investigations on the following algorithm were given in (Uçar, Taş, and Özgür, 2017).

2.1. The Fibonacci Blocking Algorithm: The Coding Algorithm

Step 1. Consider a text of length n and assume that each letter represents one length.

Step 2. Divide the text into 2s blocks and transform it into 2×1 matrices. 2×1 matrices are multiplied by the *n-th* Fibonacci polynomial matrix in 2×2 . If there is an ascending letter in the text that is converted into 2s block, its letters are multiplied $f_n(x)$.

Step 3. Divide the latest created text into 3s blocks and transform it into 3×1 matrices. 3×1 matrices are multiplied by the key matrix in 3×3 :

$$\text{Key matrix} = \begin{pmatrix} B & B & C \\ Ç & E & \breve{G} \\ K & E & Y \end{pmatrix} = \begin{pmatrix} 1 & 1 & 2 \\ 3 & 5 & 8 \\ 13 & 5 & 30 \end{pmatrix}$$

If there is an ascending 2 letter in the text that is converted into 3s block, it letters is multiplied by 2.key matrix in 2×2 :

$$\text{2.Key Matrix} = \begin{pmatrix} E & A \\ O & D \end{pmatrix} = \begin{pmatrix} 5 & 0 \\ 17 & 4 \end{pmatrix}$$

If there is an ascending letter in the text that is converted into 3-block, its letters are multiplied by polynomial *"F"*.

Step 4. New text created in step 3 is addition by Fibonacci polynomial numbers $\sum_{i=1}^{n} f_i(x)$ respectively by starting from the left.

$$\sum_{i=1}^{n} f_i(x) = f_1(x) + f_2(x) + f_3(x) + \ldots + f_n(x).$$

The Decoding Algorithm

Step 1. Consider encrypted a text of length n and assume that each letter represents one length.

Step 2. Encrypted text is addition by Fibonacci polynomial numbers $\sum_{i=1}^{n} f_i(x)$ respectively by starting from the left:

$$\sum_{i=1}^{n} f_i(x) = f_1(x) + f_2(x) + f_3(x) + \ldots + f_n(x).$$

Step 3. Divide the encrypted text into 3s blocks and transform it into 3×1 matrices. 3×1 matrices are multiplied by the inverse of the key matrix in 3×3 :

$$\text{Inverse Key matrix} = \begin{pmatrix} F & Ç & Z \\ S & \breve{G} & N \\ V & T & G \end{pmatrix} = \begin{pmatrix} 6 & 3 & 30 \\ 22 & 8 & 16 \\ 26 & 23 & 7 \end{pmatrix}$$

If there is an ascending 2 letter in the encrypted text that is converted into 3s block, its letters are multiplied by the inverse of the 2.Key Matrix.

$$\text{Inverse 2.Key Matrix} = \begin{pmatrix} T & A \\ \breve{G} & H \end{pmatrix} = \begin{pmatrix} 23 & 0 \\ 8 & 9 \end{pmatrix}.$$

If there is an ascending letter in the encrypted text that is converted into 3s block, its letters are multiplied by *"L"* polynomial.

Step 4. Divide the encrypted text into 2s blocks and transform it into 2×1 matrices. 2×1 matrices are multiplied by the *n*th inverse of the Fibonacci polynomial matrix. If there is an ascending letter in the encrypted text that is converted into 2s block, it letters is multiplied the inverse of $f_n(x)$.

2.2. Example of the Fibonacci Blocking Algorithm:

Consider the following message text in 5s lengths (called the 5-letter):
"HELLO"

The Application of The Coding Algorithm

Step 1. HELLO is 5-letter that means $n=5$.

Step 2.

$$Q^5(x) = \begin{pmatrix} f_6(x) & f_5(x) \\ f_5(x) & f_4(x) \end{pmatrix} = \begin{pmatrix} x^2 + x + 1 & x^4 + x^2 + 1 \\ x^4 + x^2 + 1 & x^3 \end{pmatrix}$$

It is known that

$$9 = (01001) = x^3 + 1 = H$$

$$5 = (00101) = x^2 + 1 = E$$

$$14 = (01110) = x^3 + x^2 + x = L$$

$$17 = (10001) = x^4 + 1 = O$$

So, It is

$$\begin{pmatrix} f_6(x) & f_5(x) \\ f_5(x) & f_4(x) \end{pmatrix}\begin{pmatrix} H \\ E \end{pmatrix} = \begin{pmatrix} x^2+x+1 & x^4+x^2+1 \\ x^4+x^2+1 & x^3 \end{pmatrix}\begin{pmatrix} x^3+1 \\ x^2+1 \end{pmatrix}$$
$$= \begin{pmatrix} x^4+1 \\ 1 \end{pmatrix} = \begin{pmatrix} O \\ B \end{pmatrix},$$
$$\begin{pmatrix} f_6(x) & f_5(x) \\ f_5(x) & f_4(x) \end{pmatrix}\begin{pmatrix} L \\ L \end{pmatrix} = \begin{pmatrix} x^2+x+1 & x^4+x^2+1 \\ x^4+x^2+1 & x^3 \end{pmatrix}\begin{pmatrix} x^3+x^2+x \\ x^3+x^2+x \end{pmatrix}$$
$$= \begin{pmatrix} x^2+x+1 \\ x^4+x^2+x+1 \end{pmatrix} = \begin{pmatrix} G \\ T \end{pmatrix}$$

And

$$(f_5(x))(x^4+1) = (x^4+x^2+1)(x^4+1) = x = C.$$

It results HELLO→OBGTC.

Step 3. Turn into blocks of 3s and multiply with the key matrix,

$$\begin{pmatrix} B & B & C \\ Ç & E & Ğ \\ K & E & Y \end{pmatrix}\begin{pmatrix} O \\ B \\ G \end{pmatrix} = \begin{pmatrix} 1 & 1 & x \\ x+1 & x^2+1 & x^3 \\ x^3+x^2+1 & x^2+1 & x^4+x^3+x^2+1 \end{pmatrix}\begin{pmatrix} x^4+1 \\ 1 \\ x^2+x+1 \end{pmatrix}$$
$$= \begin{pmatrix} x^4+x^3+x^2+x \\ x^3+x^2+x \\ x^4+x^3+x^2+x+1 \end{pmatrix} = \begin{pmatrix} Z \\ L \\ Q \end{pmatrix}$$

If there is an ascending 2 letter in the text that is converted into 3s block, it letters is multiplied by 2.key matrix in 2×2 .

$$\begin{pmatrix} E & A \\ O & D \end{pmatrix}\begin{pmatrix} T \\ C \end{pmatrix} = \begin{pmatrix} x^2+1 & 0 \\ x^4+1 & x^2 \end{pmatrix}\begin{pmatrix} x^4+x^3+x^2+x+1 \\ x \end{pmatrix}$$
$$= \begin{pmatrix} 1 \\ x^3+x^2+1 \end{pmatrix} = \begin{pmatrix} B \\ K \end{pmatrix}.$$

It results OBGTC→ZLQBK

Step 4.

$Z + f_1(x) = x^4 + x^3 + x^2 + x + 1 = Q$
$L + f_2(x) = x^3 + x^2 + x + x = x^3 + x^2 = J$
$Q + f_3(x) = x^4 + x^3 + x^2 + x + 1 + x^2 + 1$
$= x^4 + x^3 + x = V$
$Z + f_4(x) = 1 + x^3 = x^3 + 1 = H$
$K + f_5(x) = x^3 + x^2 + x + 1 + x^4 + x^2 + 1$
$= x^4 + x^3 = U$

It results ZLQBK → QJVHU.

The Application of The Decoding Algorithm:

Step 1.

$Q + f_1(x) = x^4 + x^3 + x^2 + x + 1 + 1$
$= x^4 + x^3 + x^2 + x = Z$
$J + f_2(x) = x^3 + x^2 + x = L$
$V + f_3(x) = x^4 + x^3 + x + x^2 + 1$
$= x^4 + x^3 + x^2 + x + 1 = Q$
$H + f_4(x) = x^3 + 1 + x^3 = 1 = B$
$U + f_5(x) = x^4 + x^3 + x^4 + x^2 + 1 = x^3 + x^2 + 1 = K$

It results QJVHU → ZLQBK .

Step 2. Divide encrypted text into 3s blocks and transform it into 3×1 matrices. 3×1 matrices are multiplied by inverse of the key matrix in 3×3 :

$$\begin{pmatrix} F & Ç & Z \\ S & Ğ & N \\ V & T & G \end{pmatrix}\begin{pmatrix} Z \\ L \\ Q \end{pmatrix} = \begin{pmatrix} O \\ B \\ G \end{pmatrix}$$

If there is an ascending 2 letter in the encrypted text that is converted into 3s block, its letters are multiplied by the inverse of the 2.key matrix:

$$\begin{pmatrix} T & A \\ Ğ & H \end{pmatrix}\begin{pmatrix} B \\ K \end{pmatrix} = \begin{pmatrix} T \\ C \end{pmatrix}$$

It results ZLQBK → OBGTC.

Step 3. Divide the encrypted text into 2s blocks and transform it into 2×1 matrices. 2×1 matrices are multiplied by the *n*th inverse of the Fibonacci polynomial matrix in 2 . If there is an ascending letter in the encrypted text that is converted into 2s block, its letters are multiplied the inverse of $f_n(x)$.

$$Q^5(x)^{-1} = \begin{pmatrix} x^3 & x^4+x^2+1 \\ x^4+x^2+1 & x^2+x+1 \end{pmatrix}$$

and

$$\begin{pmatrix} x^4+1 \\ 1 \end{pmatrix} = \begin{pmatrix} O \\ B \end{pmatrix}, \quad \begin{pmatrix} x^2+x+1 \\ x^4+x^2+x+1 \end{pmatrix} = \begin{pmatrix} G \\ T \end{pmatrix}$$

It is know that,

$$\begin{pmatrix} x^3 & x^4+x^2+1 \\ x^4+x^2+1 & x^2+x+1 \end{pmatrix}\begin{pmatrix} x^4+1 \\ 1 \end{pmatrix} = \begin{pmatrix} x^3+1 \\ x^2+1 \end{pmatrix} = \begin{pmatrix} H \\ E \end{pmatrix},$$
$$\begin{pmatrix} x^3 & x^4+x^2+1 \\ x^4+x^2+1 & x^2+x+1 \end{pmatrix}\begin{pmatrix} x^2+x+1 \\ x^4+x^2+x+1 \end{pmatrix} = \begin{pmatrix} x^3+x^2+x \\ x^3+x^2+x \end{pmatrix} = \begin{pmatrix} L \\ L \end{pmatrix}$$

and let's $f^{-1}(x) = x^4 + x^3 + x$.
So, It is
$f^{-1}(x).C = (x^4 + x^3 + x)(x) = x^4 + 1 = O.$
It results OBGTC→HELLO.

3. CONCLUSION

Rijndael found the AES (Advanced Encryption Standard) with the help of polynomials in Galois fields. We too created a new encryption algorithm with the help of Fibonacci polynomials and polynomials in Galois _elds and this algorithm is called Classical AES-like Cryptology via Fibonacci Polynomial Matrix. First, we present the mathematical basis necessary for understanding the specifications followed by the design rationale and the description itself. Subsequently, the implementation aspects of the cipher and its inverse are treated.

ACKNOWLEDGEMENTS

This work was presented at the Second *Cilicia International Symposium on Engineering and Technology (CISET 2019).*

REFERENCES

Uçar, S , Taş, N., and Özgür, N. (2019). "A New Application to Coding Theory via Fibonacci and Lucas Numbers". *MSAEN 7: 62-70.*

Paar, C., and Pelzl, J. (2009). "Understanding cryptography: a textbook for students and practitioners." *Springer Science, Business Media*.

Koshy, T. (2018). "Fibonacci and Lucas Numbers with Applications." Volume 1, *John Wiley & Sons, New Jersey*.

Koshy, T. (2019). "Fibonacci and Lucas Numbers with Applications." Volume 2, *John Wiley & Sons, New Jersey*.

Stewart, I. (1990). "Galois theory." *Chapman and Hall/CRC.*

Klima, R. E., and Sigmon, N. P. (2012). "Cryptology: classical and modern with maplets." *Chapman and Hall/CRC.*

Daemen,, J., and Rijmen, V. (2003). "AES Proposal: Rijndael". *National Institute of Standards and Technology. p. 1. Archived from the original on 5 March 2013*. Retrieved 21 February 2013.

Avaroğlu, E., Koyuncu, I., Özer, A. B., and Türk, M. (2015). "Hybrid pseudo-random number generator for cryptographic systems." *Nonlinear Dynamics*, *82*(1-2), 239-248.

Turkish Journal of Engineering

Turkish Journal of Engineering (TUJE)
Vol. 4, Issue 3, pp. 129-141, July 2020
ISSN 2587-1366, Turkey
DOI: 10.31127/tuje.652358
Research Article

CLASSIFICATION PERFORMANCE COMPARISONS OF DEEP LEARNING MODELS IN PNEUMONIA DIAGNOSIS USING CHEST X-RAY IMAGES

Osman Doğuş Gülgün *[1] and Hamza Erol [2]

[1] Mersin University, Graduate School of Natural and Applied Sciences, Department of Computer Engineering, Mersin, Turkey
ORCID ID 0000 – 0003 – 1824 – 4401
dogusgulgun@gmail.com

[2] Mersin University, Engineering Faculty, Department of Computer Engineering, Mersin, Turkey
ORCID ID 0000 – 0001 – 8983 – 4797
herol@mersin.edu.tr

* Corresponding Author
Received: 28/11/2019 Accepted: 23/12/2019

ABSTRACT
In recent years, the analysis of medical images using deep learning techniques has become an area of increasing popularity. Advances in this area have been particularly evident after the discovery of deep artificial neural network models and achieving more successful performance results than other traditional models. In this study, the performance comparison of different deep learning models used to efficiently diagnose pneumonia on chest x-ray images was performed. The data set used in the study consists of a total of 5840 chest x-ray images of individuals. In order to classify these data, three different deep learning models are used: Convolutional Neural Network, Convolutional Neural Network with Data Augmentation and Transfer Learning. The images in the data set were classified into two categories as pneumonia and healthy people using these three deep learning models. The performances of these three deep learning models used in classification were compared in terms of loss and accuracy. In the comparison of three different deep learning models with two different performance values, 5216 chest x-ray images in the data set were used to train the deep learning model and the remaining 624 were used to test the model. At the end of the study, the most successful performance result was obtained by convolutional neural network model applied with data augmentation technique. According to the best results of this study, this model was able to accurately predict the class of 93.4% of the test data.

Keywords: *Deep Learning, Medical Diagnosis, Data Augmentation, Convolutional Neural Network, Transfer Learning*

1. INTRODUCTION

In this section, previous studies about medical image classification and deep learning in the literature are discussed and the techniques used in these studies are explained.

In recent years, there have been significant developments in medical image analysis and machine learning. The most important developments in this field have been experienced especially after the emergence of deep artificial neural network models and performing better than other models. Following the intense use of artificial neural networks, the number of studies on medical imaging, medical data analysis and disease diagnosis has increased and many of them have been realized with significant potential in this field. In their study, Lundervold and colleague examined the deep learning and machine learning studies in the field of medical imaging performed on MRI images and gave information about current studies in this field (Lundervold and Lundervold, 2019). In their studies, they examined a wide range of studies such as data generation using generative adversarial network model, image classification with convolutional neural networks. They discussed current reference works in this field. Especially convoluted neural networks have shown very good results in the classification of images in the field of medical image analysis, the detection of abnormalities in medical images, and the identification of the most important features on medical images. In addition to data analysis, features obtained from convolutional neural networks can also be used for different purposes, such as the generation of new data, very similar to the original. Therefore, because of the successful performance of deep learning models observed in previous studies in this field, it was considered appropriate to use deep learning techniques to diagnose pneumonia on x-ray images in this study.

Convolutional neural networks are one of the most powerful computerized vision techniques in terms of usability for different tasks. Recent studies in the field of computer vision have shown that the features obtained using convolutional neural can be used in a classifier other than the original network structure after the completion of neural network training. Van Ginneken *et al*, the study of the detection of nodules in the lung on computed tomography images, can be given as an example of studies on this subject (Van Ginneken *et al*., 2015). In this study, 865 computed tomography scanning images of publicly available LIDC data set were used. The images were evaluated by 4 qualified radiologists and the classes of the images were determined. Using 2 dimensional sagittal, coronal and axial parts in all images, 4096 features were extracted for each image. These features were classified using a linear support vector machine.

Recent studies have shown that deep learning techniques have significant advantages over traditional methods based on handmade attributes. However, deep learning techniques also have some limitations due to the similarities and differences of the data in different classes caused by class diversity in various medical scenarios. In order to reduce these limitations, Zhang *et al*. proposed a synergic deep learning model in their study (Zhang *et al*., 2019). In their synergic deep learning model, more than one convolutional neural network model was used and they enabled each other to learn from each other. Both convolutional neural networks were designed according to the ResNet50 architecture. If one of the convolutional neural network performs the correct classification while the other performs the wrong classification, this false creates an extra synergic force for updating the weights of the faulty model. Therefore, in this synergic model, networks are mutually learned through classification errors. The model used in the study was evaluated using 4 different data sets. According to the results, the synergic deep learning model obtained the best results for each data set.

Recent research in the field of deep learning reveals that deep neural networks are highly sensitive to small irregularities and differences in images. Although this provides an advantage in some special studies, it is a significant disadvantage that may adversely affect the classification performance. Li *et al*. conducted studies with 3D brain MRI images to examine the effect of such adverse conditions on the medical image processing field (Li *et al*., 2019). In their study, they were interested in designing deep learning models that could predict the age of subjects on 3D brain MR images. Their data set consists of 3D brain MRI images of 3921 subjects obtained from 7 different data sets. The subjects were between 4 and 94 years old and the mean age was 25.5 years. They used two different models for estimating images: a conventional deep neural network and a hybrid deep learning model using attributes reported by the anatomical context. In addition, they succeeded in creating incorrect results in age estimation by adding noise to the images. They found that their hybrid model obtained more successful estimation results on noisy images. As a result of the noise they added to the images, they realized that the age of a 19-year-old person could be estimated as 80 due to the noise in the image. This reveals that differences and noise in images significantly affect results in deep learning models.

Due to the limitations of data sources and the unbalanced number of samples of different classes in the data set, it is difficult to perform computer-assisted segmentation of 3D medical images at high levels of success using deep learning methods. Indraswari *et al*. proposed an advanced deep learning model for segmentation of 3D images (Indraswari *et al*., 2019). They used three different data sets in their studies. The first and second data sets were used for brain tumor segmentation and the third data set was used for dental segmentation of the jaw images of individuals. The first two sets of data were MRI images of low and high-grade glioma patients, while the third data set consisted of human jaw scanning images taken with cone beam computed tomography. They propose a convolutional autoencoder architecture consisting of encoder and decoder structures to perform segmentation of the image data they use. Since the input images used in the proposed architecture are 3D, these images are first decomposed into axial, coronal and sagittal components to obtain a 2D image component for each plane. The images are passed in three sets of convolution and deconvolution layers to obtain the most important information separately for each plane. The information obtained from axial, coronal and sagittal slices are combined after the final pooling process to obtain the actual input vector of the model. Then, the combined input information is convolution to obtain the most important features. They also proposed a special cost function for their models. The proposed cost function

adds a weight to the network model to take into account the probability of each class in the data classes. Despite the imbalance of the class data in 3 different data sets, they achieved good results with the proposed cost function and model approach.

In another important study in this field, Şengür *et al*. proposed a hybrid classification model approach to perform optical disc detection on eye retinal images (Şengür *et al*., 2018). They used convolutional neural network architecture together with the k nearest neighbors classifier. The features in the fully connected layer of the convolutional neural network model, which were previously trained on retinal images, were extracted and these features were used to classify optic disc and non-optic disc regions with k nearest neighbor classifier. Using the AlexNet architecture as a convolutional neural network, they extracted 4096 dimensional feature vectors of each image. They used 3 different retinal image data sets to create the training and test data of the model they created. Patches of 280 x 280, 500 optical discs and 1565 non-optical discs were collected from the datasets, and then the patches were scaled to 227 x 227 to extract feature from these patches. The k nearest neighbor classifier was trained and tested on the generated features, and 165 retinal images were used in the test phase. The accuracy, sensitivity and specificity criteria of the hybrid model were examined in order to test the hybrid model. According to their results, the models reached 95.74% accuracy, 84.46% sensitivity and 99.08% specificity.

Determining the laterality of speech before the operations performed is very important in terms of predicting the possible risks accurately. Toroman *et al*. have studied the use of non-invasive machine learning techniques to determine speech laterality over EEG signals (Toroman *et al*., 2019). In their study, they used data obtained from 67 subjects diagnosed as healthy according to EEG examination in the 18-65 age range. In the data used, 35 of the subjects were individuals of right dominant type and the speech center was located in the left hemisphere of the brain. The remaining 32 subjects are left dominant individuals and the speech center is located in the right hemisphere of the brain. In this study, a spectrogram image was created for each of the 18 EEG channels using various convolutional neural network architecture including VGG16, VGG19, ResNet, MobileNet, NasNet and DenseNet. Then, attributes were extracted from the images using these network architectures. Extracted attributes were classified using support vector machines. According to the results obtained from the study, it was observed that VGG16 network architecture is more successful than other architectures.

The most dangerous type of sleep disorder is obstructive sleep apnea syndrome (OSAS) that occurs during sleep and can cause sudden death of patients. This disease depends on many parameters and the diagnosis of the disease is laborious and time consuming for the experts. Tuncer *et al*. have studied the design of a deep learning-based decision support system to diagnose OSAS with PPT signals (Tuncer *et al*., 2019). In their study, they used only Pulse Transition Time (PTT) signal parameter in classification of patients and healthy individuals instead of classical diagnostic parameters used in the literature. In the study, feature extraction from PPT signals was performed using AlexNet and VGG16 convolutional neural network models. Then, healthy and patient individuals were classified by using this extracted features with k nearest neighbors and support vector machines classifiers. At the end of the study, the best results were obtained by classifying the features extracted using VGG16 network architecture with support vector machines classifier. This hybrid structure was able to accurately predict the classes of 92.78% of the test data.

In another study on the detection of abnormalities from medical images, Setio *et al*. proposed a computer-assisted detection system using a multi-view convolutional artificial neural network (ConvNets) for pulmonary nodule detection (Setio *et al*., 2016). The artificial neural network used in their studies was formed by using the features of three different convolutional neural networks previously used in the detection of solid, subsolid and large nodules. They used data augmentation and dropout techniques to prevent overfitting problems during the training of their models. Tested their model on 888 lung tomography scans containing 1186 lung nodules. The model succeeded in detecting 1016 of 1186 nodules and reached 85.7% detection accuracy rate.

In another similar study, Roth *et al*. conducted a study to improve the performance of the three computer-aided detection systems previously established (Roth *et al*., 2015). They were interested in detecting colon polyps from computed tomographic colonography images. In addition, they studied for the detection of enlarged lymph nodes and the detection of spinal metastases on body computed tomography images. In this study, they benefited from the CNN architecture and they applied data augmentation technique to their existing model images by randomly rotating them up to 100 degrees on three orthagonal axes. The models developed as a result of the methods used were evaluated over 3 different data sets consisting of 1186 for detecting colon polyps, 176 for detecting enlarged lymph nodes and 59 for detecting spinal metastases. According to the results, the sensitivity of lesion detection was increased in the range of 13-34% for 3 models developed independently for each data set. Sensitivity values increased from 57% to 70%, 43% to 77% and 58% to 75% for spine metastasis detection, enlarged lymph node detection and colon polyp detection models, respectively.

Gastroscopy is a diagnostic method in which the gastrointestinal system structure can be examined directly. This method is widely used in gastrointestinal examinations. Diagnosis of gastrointestinal diseases through endoscopy images requires considerable experience and can only be diagnosed by experienced physicians. It is difficult for clinicians other than specialist physicians to correctly diagnose such diseases. In order to overcome this problem, Zhu *et al*. proposed a computer-assisted lesion detection system that works on endoscopy images (Zhu *et al*., 2015). They also used a convolutional neural network model to extract the most important features from images. They used image features from the fully connected layer of convolutional neural network to train and test a support vector machine classifier. At the end of the study, they observed that their models performed better than other endoscopic image classification models in the literature.

Histopathology images are obtained from tissues suspected of disease. These images are examined under a light microscope and used in the definitive diagnosis of many diseases, especially cancer. In order to benefit from the definitive diagnosis of histopathology images, Wang

et al. proposed a classification model that provides diagnosis by performing classification directly on these images (Wang *et al*., 2017). In their models, they used a different network architecture called Bilinear CNN (BCNN) by making use of convolutional neural network architecture. In the first step, histopathology images are divided into two different components. Afterwards, these image components are evaluated with different convolutional neural networks and feature extraction is performed separately from the components. The feature vectors obtained from two separate convolutional neural networks for two different components are combined to obtain a high dimensional feature vector. A support vector machine (SVM) classifier is trained using this high dimensional feature vector, and then the performance of the trained model is tested. At the end of the study, the proposed BCNN based classification model accurately predicted the class of most of the test data and reached a classification accuracy rate of 92.6%. In addition, the proposed model achieved 92.8% sensitivity and 98.9% specificity. This study has achieved the most successful results in terms of correct classification of images when compared with other studies in this field in the literature.

The studies described in this section show that deep learning techniques can be used for different purposes such as classification, object detection and data generation in the medical field. The results obtained from previous studies with deep learning techniques show that deep learning techniques can be used efficiently in this field. In our study, we propose different model architectures that can be used to diagnose pneumonia with chest x-ray images using deep learning techniques. After creating the proposed models, we compare the performance of these models.

The dataset, used in this study, containing chest x-ray images consists of image data belonging to two classes (Kermany and Goldbaum, 2018). The two classes in the data set refer to pneumonia and healthy people. The data set was obtained from x-ray images of children aged one and five years from Guangzhou Women's and Children's Medical Center. All chest x-ray images of the patients were taken as part of their routine clinical care. In order to perform accurate analysis of chest x-ray images, low quality or incomprehensible images were identified from all lung graphs and extracted from the data set and quality control of the images was ensured.

The diagnosis of the dataset images for the training of the artificial neural network system used in the deep learning model was first made by two specialist doctors. The data set was also checked by a third specialist to take into account any possible misconceptions of specialist physicians evaluating the data. Chest x-ray images of 5840 individuals are included in the data set. Of these images, 5216 were used to train the deep learning model and 624 were used to test the model (Kermany and Goldbaum, 2018). The deep learning models used will be trained with 89% of the image data set and thus will be able to diagnose pneumonia on the x-ray image. The trained models will then be tested on the remaining 11% of the same data set. In this way, the data will be evaluated by observing the success performance of the models in the classification and the success comparison of the models will be made. An exemplary chest x-ray image from the data set is given in Fig. 1.

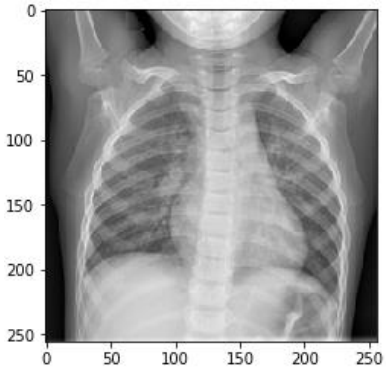

Fig. 1. A sample chest x-ray image in the data set ("Chest X-Ray Images", 2019).

2. DEEP LEARNING METHODS APPLIED

In this section, the dataset consisting of chest x-ray images of 5840 individuals into two categories as pneumonia and healthy individuals. Convolutional neural network, convolutional neural network with data augmentation and transfer learning deep learning models will be explained for classification of dataset of chest x-ray images.

2.1. Classification Using Convolutional Neural Network Model

In order to diagnose pneumonia from the image data, the convolutional neural network deep learning model was used first. In the design of the convolutional neural network model, keras library was used in the software. By applying deep learning methods to image data, it is necessary to introduce the images to computer systems first in the diagnosis of diseases with computer systems. Therefore, the images need to be converted to digital format that computer systems can detect.

All images are made up of digital units called pixels. Pixel is the name given to the smallest unit of the image in a digital environment. Many pixels come together to form images. Each pixel value is between 0 and 255 according to the image color tone. Images must be converted to digital matrix format in order to be perceived by computer systems. Each element of this matrix corresponds to one pixel. Digitization and pixel values of the images are shown in Fig. 2.

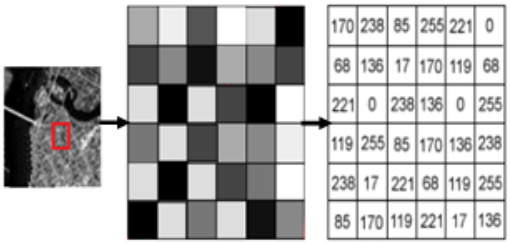

Fig. 2. Digitization and pixel values of an image ("Image Pixels", 2019).

In order to process image data in the applied model, image matrices (64x64) of the data set are obtained first. When classifying images in convoluted neural networks,

it is necessary to extract the feature map which affects the class of an image via image matrices. These features may represent a simple shape such as a line or corner in the image, as well as more complex convex shapes. In the applied model, it determines the class of the test images in the test phase and determines the class of the related image depending on whether these features are detected in the image or not. Therefore, the resulting image matrices are first convolution in the convolution layer with filters of a certain size to extract the feature map from the images. In this way, it is provided to detect the distinctive parts in the images and to find the features that affect the classification.

While convolution is performed, image matrices are screened with filters. In the convolution process, the numerical values of the filter matrix to be applied in certain dimensions are multiplied by the numerical values of the portion of the image matrix up to the filter size starting from the beginning of the image matrix and these multiplication results are added. The new total value obtained; it becomes the new singular value on the image matrix, representing the corresponding area in the filter matrix size. This process is repeated by shifting the filter matrix over the image matrix with a certain step size. Thus, convolution is performed to filter the image matrix by filter. As a result of this process, the classifier properties of the image matrices are determined. The convolution layer and the convolution process are shown in Fig. 3.

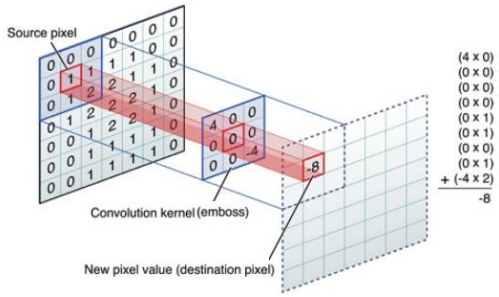

Fig. 3. Convolution layer and convolution process ("Convolution Operation", 2019).

In the convolutional neural network model used in the study, the obtained image matrices are transformed with 3x3 size filters in order to obtain classifying properties. In this way, it is provided to determine the desired parts in the images and find the desired features (Aghdam and Heravi, 2017). As a result of convolution, the size of the original image matrix decreases. Decreasing the image matrix size increases the processing speed of the models used and is advantageous in time. However, this reduction in size also leads to a certain level of information loss. As a result of the convolution process, the size of the image matrix after the process and the possible loss of information can be calculated with the following formulas: Eq. 1 and Eq. 2 (Krizhevsky *et al.*, 2012). Width of output matrix is defined by G.

$$G = \frac{W-F+2P}{S} + 1 \quad (1)$$

Where W: means the width of the image matrix, F: the width of the filter matrix used, P: the padding element depending on the padding technique used, and S indicates how many units the filter advances on the image matrix at each step in the convolution process. Height of the output matrix is defined by Y.

$$Y = \frac{H-F+2P}{S} + 1 \quad (2)$$

Where H: means the height of the image matrix, F: the height of the filter matrix used, P: the padding element depending on the padding technique used, and S: how many units the filter advances on the image matrix in each step in the convolution process.

Using these formulas, the amount of reduction in the size of the image matrix in each convolution layer can be calculated. In order to prevent such loss of information due to the decrease in the size of the image matrix, padding technique can be utilized in such models. When this technique is applied, the size of the image matrices presented as input to the convolution process does not change and a matrix of the same size is obtained as the result of the process. This prevents the loss of information from the image data as a result of convolution. In the study, the same padding technique, which is one of the mentioned padding methods, was used. In the same padding technique, before the convolution is applied to the image matrix, a frame consisting of 0 elements is added around this matrix and after this addition, convolution is performed. As a result of the convolution process applied, both the size of the image matrix is preserved and the loss of information especially in the pixels close to the corners of this matrix is prevented. The same padding technique is shown in Fig. 4.

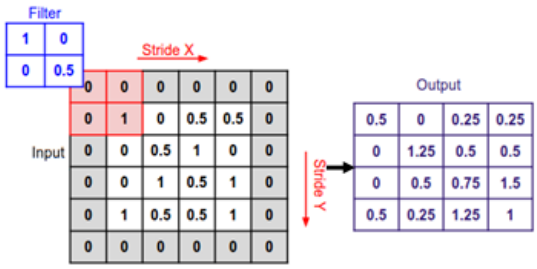

Fig. 4. The same padding technique ("Same Padding", 2019).

The number of filters used in the convolution layer can vary depending on the designer and the images. After convolution, the image matrices in the convolution layer are included in an activation function. In this study, relu activation function was used at this stage. The main reason for using the relu activation function in the model is its complexity-increasing structure. With the use of this activation function, convoluted neural networks perform better in detecting complex nonlinear shapes during the determination of classifying properties in images. When negative values are given as input to Relu activation function, the function gives 0 as the output and if positive values are given, the function gives the same value as the output. Therefore, these positive outputs produced with the same magnitude versus positive inputs enable the function to show better results in complex and non-linear situations. The relu activation function is shown in Fig. 5.

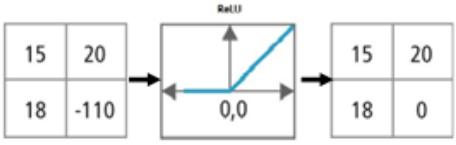

Fig. 5. The relu activation function ("Relu Activation Function", 2019).

The convolution layer is then transferred to the image matrices by the model to the pooling layer. In this layer, the number of pixels is reduced by reducing the image size (Krizhevsky *et al*., 2012). In this way, the number of parameters and operations used in the network is reduced, the performance of the network increases, and consequently the performance and speed of the model are increased and the processing time is reduced. Different pooling techniques such as max, min and avarage can be applied in the pooling layer. In the max pooling technique, the image matrix is divided into areas of a certain size. Then, the pixels with the highest numerical value are selected from the pixels in these fields, and this field is now expressed with this single pixel, thus reducing the number of pixels as the other pixels are disabled. The same process applies to all areas separated in the image matrix. In another pooling technique, min pooling, the image matrix is similarly divided into areas of the same size, but the pixel with the lowest numerical value is selected to represent the areas. In the Avarage pooling technique, after the image matrix is divided into areas of the same size, the pixel values in each area are averaged and the area is represented by this single average numerical pixel value. Max pooling technique is shown in Fig. 6.

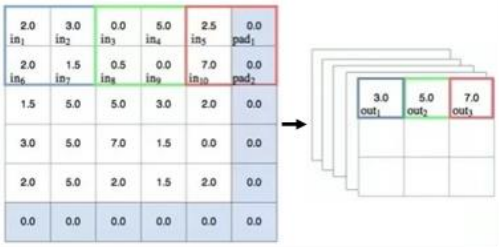

Fig. 6. Max pooling technique ("Max Pooling", 2019).

In this study, max pooling technique was used in the model among these techniques. In this way, it is provided to increase the performance and speed of the model, while avoiding the problem of producing incorrect results based on memorization due to the over-learning of the model called overfitting (Goodfellow *et al*., 2016). After this step in the applied model, the image matrices are passed through a different convolution layer for the second time. In this way, the possibility of detecting the features of classifiers in the images that are effective for the determination of classes increases. This enables the image classes of the model to be detected more accurately. Therefore, the second convolution layer applied in the model is included in the model architecture in order to improve the classification performance of the model.

After this step, the image matrices are transferred back to the pooling layer for the second time. In this way, the performance of the model is increased and especially the "overfitting" problem is prevented. In this pooling layer, max pooling technique was used similar to the first pooling layer, and the highest pixel values of the areas allocated in the pool size were selected to represent the relevant areas in the image. In the model, the image matrix data is transferred to a different convolution layer after the 2nd pooling layer for the third and last time. With the first two convolution layers applied, low and medium level classifying properties were determined which were effective in determining the classes in the image data. However, in order to increase the classification performance and obtain a higher percentage of accurate classification, it is necessary to determine the more complex high-level classifier properties. Consequently, the third convolution layer applied at this stage is included in the model to determine the more complex high-level classifier properties.

In this layer, as in the first two convolution layers, the same padding technique was used to preserve the size of the image matrix and prevent loss of information. Also, similar to the first two convolution layers, relu activation function is used in this layer and thus the probability of detecting nonlinear features in the images is increased. After this stage, the image data is transferred to a different pooling layer for the third and last time. In this layer, max pooling technique was applied similar to the first two pooling layers, thus reducing the processing time and further reducing the possibility of "overfitting" problem. Therefore, since the image matrix data is transferred to the model as input, a total of 3 convolutions and 3 times are included in the pooling layer.

32 filters were used in the first convolution layer and 64 filters were used in the second and third convolution layers. After all these steps, the processed image matrix data with classifier properties are transferred to the fully connected layer by the model used. Fully coupled layer is the section where image classification is performed depending on the presence or absence of classifier properties in image matrices. Therefore, the diagnosis of the test images in the data set will be performed in this section. The model performs the classification process and therefore the diagnosis by means of an artificial neural network in this layer. The general structure of the artificial neural network in the fully connected layer is shown in Fig. 7.

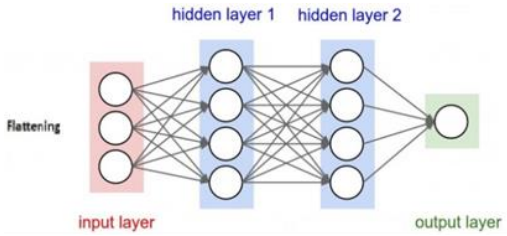

Fig. 7. The general structure of the artificial neural network in the fully ("Fully Connected Layer", 2019).

However, the artificial neural network in the layer cannot process the image data in matrix format. Therefore, said image matrix data must be supplied to the artificial neural network in vector format. Therefore, in this layer, the image matrices are first converted to a vector by flattening operation so that the data of the images can be input to the artificial neural network in this layer. The

flattening process is shown in Fig. 8.

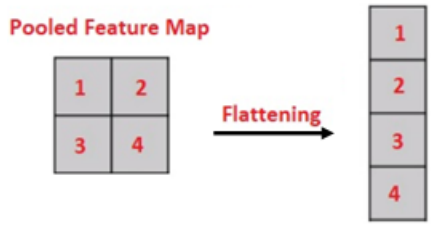

Fig. 8. The flattening process ("Flattening", 2019).

The vectors carrying the generated image data are transferred to an artificial neural network with 512 neurons. Depending on the input training image data, the weights of the artificial neural network are rearranged in an iterative manner and as a result, it gains the ability to classify the artificial neural network image data in this layer and thus diagnose the disease. The trained model is then tested over the image data reserved for the test stage in the data set and the classification accuracy percentage and performance of the model is tested. In this stage, artificial "sigmoid" function was used as the activation function in the artificial neural network. Sigmoid function is an activation function that can be used in neural networks in two class classification problems.

In this study, sigmoid function, which is more suitable for 2-class classification problems, was preferred at this stage, since there were a total of 2 classes, sick and healthy, in the classification and diagnosis of image data. The sigmoid function is shown in Fig. 9.

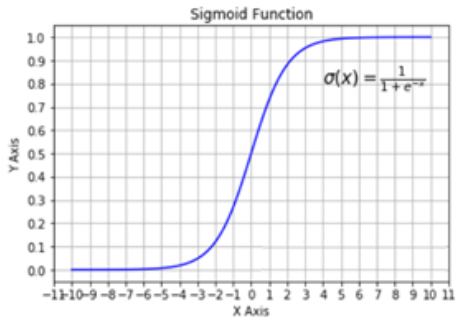

Fig. 9. The sigmoid function ("Sigmoid Function", 2019).

In addition, overfitting problem can be seen in this type of neural network as described previously. In this problem, depending on the excessive learning of the model by the model, the model outputs the results of incorrect classification based on the memorization. Therefore, as an additional step to prevent this problem, dropout technique is also utilized in this layer. Dropout technique is a regulation method used to train artificial neural network in this layer (Srivastava *et al*., 2014). With this technique, half of the neurons are disabled in different iterations with different possibilities during data processing in the artificial neural network. Thus, in each iteration, a certain number of weights are changed instead of all the weights of the artificial neural network in this layer. Thus, the effect of any image input to the model on the weights of the neural network is limited, which prevents the network from performing misclassifications due to over-learning by heart. Dropout technique is shown in Fig. 10.

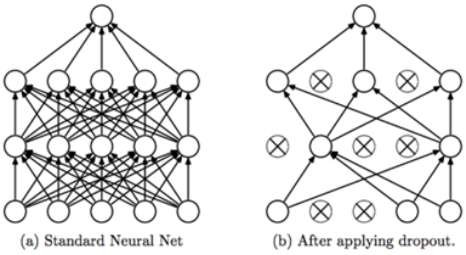

Fig. 10. Dropout technique ("Dropout", 2019).

The first model used is shown in Fig. 11.

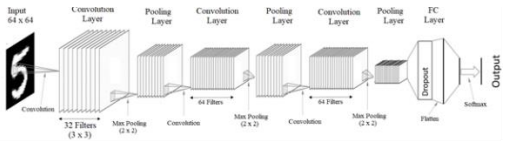

Fig. 11. The first model used ("First Model", 2019).

Therefore, the model described in this stage is the first of the three different deep learning models used in the study, and the results of the diagnostic performance obtained from the model and the correct classification percentage of the test data of the model are included in the results section.

2.2. Classification Using Convolutional Neural Network with Data Augmentation Model

The second deep learning model used to diagnose pneumonia from image data is a convective neural network model similar to the first deep learning model used. However, in this second model, data augmentation technique was applied unlike the first model. In the data augmentation technique applied to the model, the images in the image data set are given to the model both in their original format and through some changes. The changes are made by displaying images at different angles and at different distances (zooms) to the model (Wong *et al*., 2016). As the model re-evaluates the same images from different angles and different distances, the possibility of identifying the classifying features in the image in question is increased. Therefore, with the higher probability of detecting these features, the model can learn and analyze the problem better via image data, and consequently, the classification performance of the model increases.

This technique is applied for training data to be transferred as input to the model. The testing phase of the model is performed only on the test data as in the first model used. Therefore, with this technique, it is aimed to train the model more successfully by transferring the training data to the model in different formats. Data augmentation is shown in Fig. 12.

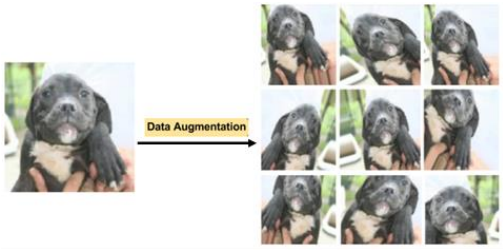

Fig. 12. Data augmentation technique ("Data Augmentation", 2019).

In the data set used in the study, 5216 images are used to train the model. This image data is transferred to the model in 32 size packages while training the model according to the software created. Therefore, with the transfer of images to 163 models performed in 1 cycle, all 5216 training images can be transferred to the model. However, in the software prepared for analysis, the model receives 200 of these 32 packets as input in 1 cycle. Therefore, the model takes a total of 6400 images as input in 1 cycle. Of the 6400 images taken as input of the model, 5216 are the original data set images, while the remaining 1184 images are the images created by the software using the data augmentation technique. The said 1184 images are created by replacing the original images with the software used.

Changes to images can be described as: First, images are rotated randomly to the right at a value between 0-30 degrees. Second, images are rotated randomly to the left at a value between 0-30 degrees. Third, the images are enlarged by 30% (Zoom in). Fourth, images are reduced by 30% (Zoom out). Fifth, images are rotated 90 degrees to the right. Sixth, images are rotated 90 degrees to the left.

The images that have been modified above are also used during the training of the model. The changes that may be made in the data are not limited to this and may vary according to the preferences of the software developer. Therefore, the rotation angle, direction and magnification ratios of the images can also be arranged in different ways. However, these parameters were adjusted as specified, considering the operating performance and processing time of the model. In addition, normalization pretreatment is applied to all of the image data in question. With this pre-treatment, the value range of all pixels of the images with pixels in the 0-255 value range is changed and this range is set to the 0-1 value range. Thus, the classification performance of the model is improved by filtering the defective pixels in the images. Apart from this technique, the model used in this stage is the same as the convolutional neural network model described in the first stage. Therefore, this model consists of a total of 7 layers, 3 convolution, 3 pooling and 1 fully connected layer. Also, as in the first stage model, 32 filters were used in the first convolution layer and 64 filters were used in the second and third convolution layers. The pooling, padding and dropout techniques used in the first model are also applied in this model. The percentage of classification accuracy and performance evaluation obtained from the model is given in the results section. The second model used is shown in Fig. 13.

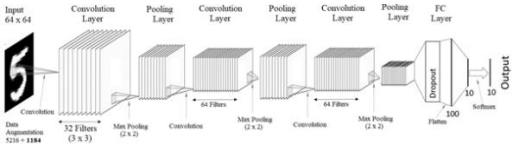

Fig. 13. The second model used ("Second Model", 2019).

2.3. Classification Using Transfer Learning Model

Transfer learning technique was used in the formation of the third model to be used for the diagnosis of pneumonia from the image data. The basis of this technique is based on the idea of storing the information previously obtained while solving a problem and then applying that information to a different but similar problem. Therefore, in this technique, the weights of an artificial neural network model which has been previously trained over a large data set for solving a problem and which is known to be successful in solving this problem are transferred to a different model in order to solve a similar problem. The output layer of the new model created using this technique is rearranged in accordance with the new problem to be solved, and after these arrangements, the model can now be used to solve the new problem. The transfer learning method is shown in Fig. 14.

In the present study, weights of the VGG16 neural network, previously trained on a 1000-class data set, will be used to classify lung x-ray image data (Shin *et al*., 2016). The output layer of the VGG16 model has been rearranged and this new model has been adapted to this 2 class problem. The VGG16 model is basically a simple network model and the difference is that the convolution layers are used in 2s and 3s. There are 4096 neurons (artificial neural network cells) in the full coupling layer of this model. This network has been developed for the solution of a classification problem of 1000 classes as previously mentioned, and the model calculates approximately 138 million parameters.

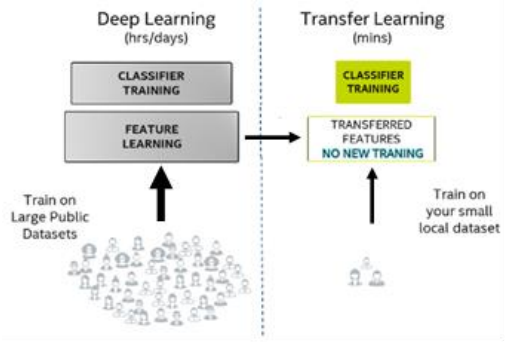

Fig. 14. The transfer learning method ("Transfer Learning", 2019).

As the depth of the model increases, the size of the image matrices decreases from the input layer to the output layer, while the depth value, ie the number of channels, increases. The filters with different weights are calculated at each convolution layer output of the model, and as the number of layers increases, the classifying properties in the filters represent the depths of the image.

The VGG16 model architecture is shown in Fig. 15.

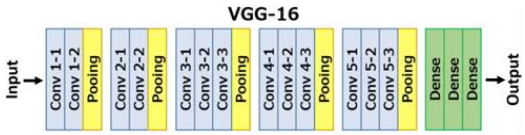

Fig. 15. The VGG16 model architecture ("VGG16 Model", 2019).

The most important advantage of this technique and therefore of the model used is that this model has already been optimally trained by a multidimensional data set. Therefore, the feature map of the model is highly developed. In this way, the model can detect the differences on the images and according to the findings can be divided into classes. The classifier features of the VGG16 model are shown in Fig. 16. The classification results obtained from the model and evaluations of the model's performance in diagnosis are given in the results section.

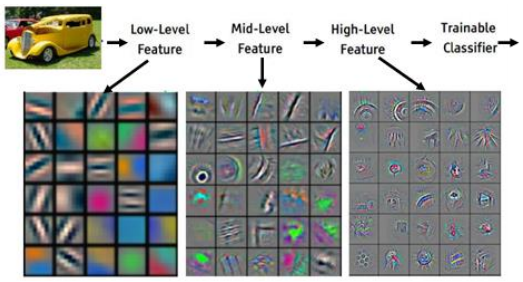

Fig. 16. The classifier features of the VGG16 model ("Features", 2019).

3. PERFORMANCE CALCULATIONS OF DEEP LEARNING METHODS APPLIED

In comparison of three different deep learning models with two different performance values, 5216 of chest x-ray images in the data set were used to train the deep learning model and the remaining 624 were used to test the model. Three deep learning models used in the classification; loss and classification accuracy values were calculated with the software prepared in python environment. As a result of the calculation, graphs of performance values were created for deep learning models.

3.1. Calculation of Classification Performance Values of Convolutional Neural Network Model

The classification performance values of the convolutional neural network model: loss and classification accuracy values were calculated with the software prepared in python environment. Graphs of the values obtained as a result of the calculation are given.

3.1.1. Loss Performance Values

The graph of loss performance values obtained as a result of the application of convolutional neural network model is shown in Fig. 17.

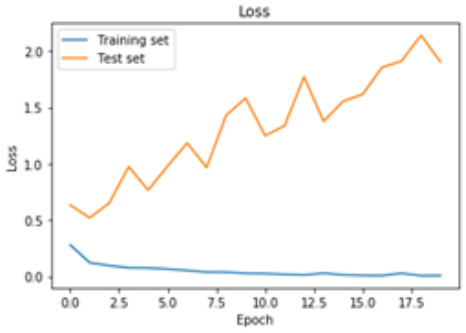

Fig. 17. The graph of loss performance values obtained as a result of the application of convolutional neural network model.

3.1.2. Classification Accuracy Values

The graph of the classification accuracy values obtained from the application of convolutional neural network model is shown in Fig. 18.

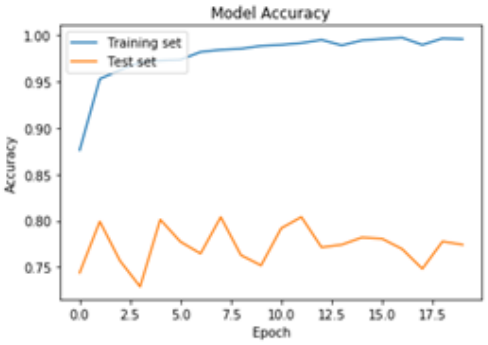

Fig. 18. The graph of the classification accuracy values obtained from the application of convolutional neural network model.

3.1.3. Performance Evaluation of Model

It is seen that the percentage of correct classification of test data in the test stage of the model trained with this data set is 75-80%. The best classification performance of the model is 80.4% accuracy at 12th iteration. It can be said that the CNN model used in this stage shows a successful classification performance and is suitable for diagnosis purposes, but it is seen that the same model gives better results when a "data augmentation" technique is used in the next stage. The confusion matrix results obtained from the classification task performed are given in Fig. 19.

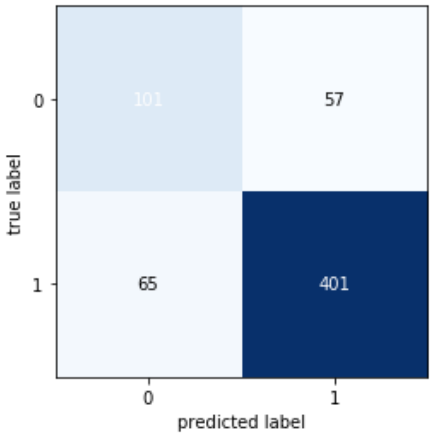

Fig. 19. Confusion matrix results of the first model.

When the results are examined, it is seen that the model misclassifies 122 of 624 test samples and the remaining samples correctly classify.

3.2. Calculation of Classification Performance Values of Convolutional Neural Network with Data Augmentation Technique

The classification performance values of the convolutional neural network model applied by data augmentation technique: loss and classification accuracy values were calculated with the software prepared in python environment. Graphs of the values obtained as a result of the calculation are given.

3.2.1. Loss Performance Values

The graph of the loss performance values obtained as a result of the application of the convolutional neural network model applied by data augmentation technique is shown in Fig. 20.

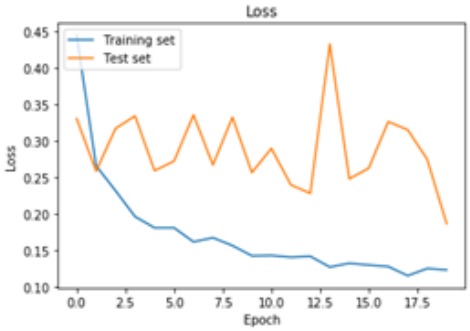

Fig. 20. The graph of the loss performance values obtained as a result of the application of the convolutional neural network model.

3.2.2. Classification Accuracy Values

The graph of classification accuracy performance values obtained as a result of the application of convolutional neural network model applied by data augmentation technique is shown in Fig. 21.

Fig. 21. The graph of classification accuracy performance values obtained as a result of the application of convolutional neural network model.

3.2.3. Performance Evaluation of Model

When the results obtained from the model are examined, it is seen that the model has reached the lowest loss (total error) value in the 20th iteration and this value is 0.1864. It is seen that the percentage of correct classification of test data in the test stage of the model trained with this data set is 89-93%. The best classification performance of the model is 93.4% accuracy at the 20thiteration. Therefore, the model was able to accurately predict the class of 93.4% of the test data. At this stage, it can be seen that the data augmentation technique used in convolutional neural network model increases the model success and classification performance and when these results are compared with the results obtained in the previous stage.

The data augmentation technique is better, the model was able to extract the classifying features of the disease more successfully from the changing images (in terms of size, angle and proximity). Thus, the model showed a higher classification performance compared to the previous stage. It can be seen in the results that the model created here is suitable for use at the point of diagnosis on images. The confusion matrix results obtained from the classification task performed are given in Fig. 22.

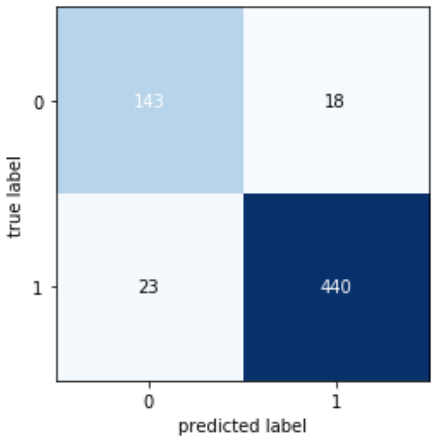

Fig. 22. Confusion matrix results of the second model.

When the results are examined, it is seen that the model misclassifies 41 of 624 test samples and the remaining samples are classified correctly.

3.3. Calculation of Classification Performance Values of Transfer Learning Model

The classification performance values of loss and classification accuracy values of the classification model created by transfer learning technique were calculated with the software prepared in python environment. Graphs of the values obtained as a result of the calculation are given.

3.3.1. Loss Performance Values

The graph of the loss performance values obtained as a result of the application of the transfer learning model is shown in Fig. 23.

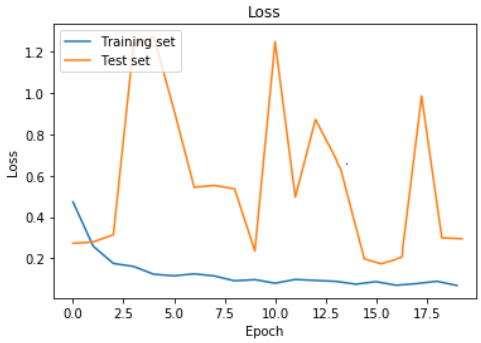

Fig. 23. The graph of the loss performance values obtained as a result of the application of the transfer learning model.

3.3.2. Classification Accuracy Values of Model

The graph of the classification accuracy values obtained from the application of transfer learning model is shown in Fig. 24.

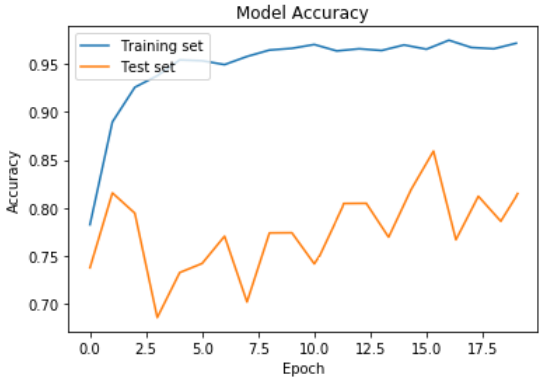

Fig. 24. The graph of classification accuracy performance values obtained as a result of the application of transfer learning model.

3.3.3. Performance Evaluation of Model

When the results obtained from the model are examined, it is seen that the lowest loss value reached by the model is 0.17. It is seen that the correct classification percentage of the test data is in the range of 70-82% at the test stage of the model trained with this data set. The best classification performance of the model was calculated as 85.6% accuracy. The confusion matrix results obtained from the classification task performed are given in Fig. 25.

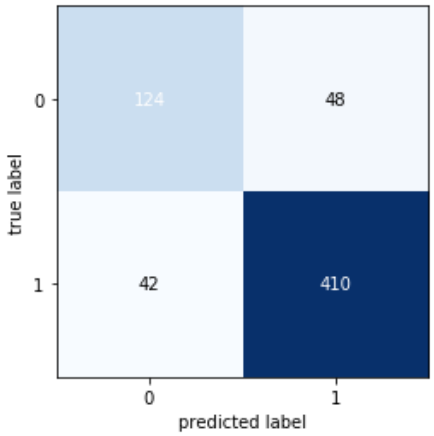

Fig. 25. Confusion matrix results of the third model.

3.4. Samples Pneumonia Detection in Chest X-ray Images

In order to examine the classification estimation performances of the models used in this study, experiments were performed with sample images. The described models take a chest x-ray image as input and give the class possibilities of this image as output. From the outputs of the models, information of the likelihood of a sample being pneumonia or healthy can be obtained. Sample experiments were carried out with the created models. Two sample experiments using convolutional neural network with data augmentation model are given. The output result obtained from the model for the chest x-ray image of a person known to have pneumonia is shown in Fig. 26.

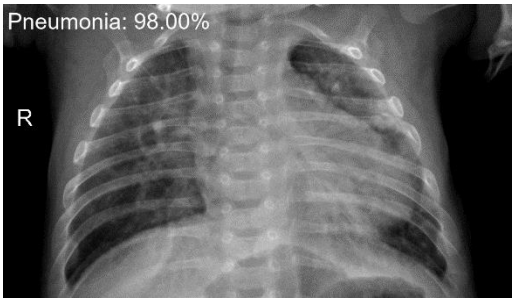

Fig. 26. The output result obtained from the model for the chest x-ray image of a person known to have pneumonia.

According to the output result, pneumonia was detected in this person's image with a probability of 98% and the estimate was correct. In another example, the output of the model for a chest x-ray image of a person known to be healthy is shown in Fig. 27.

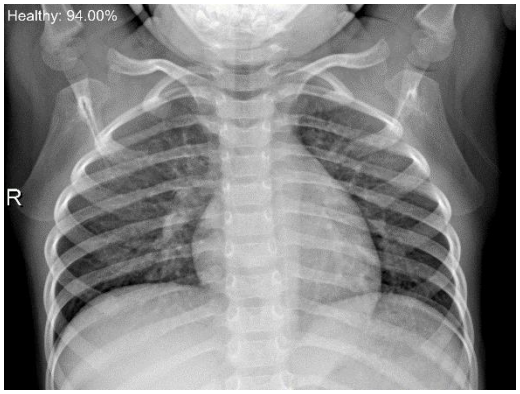

Fig. 27. The output of the model for a chest x-ray image of a person known to be healthy.

According to the output, this person was estimated to be 94% likely to be healthy, and this estimate is also true. In the examples, the model was able to accurately predict the classes of two different image samples. The model adds the forecast class label and probability information to the images as output.

4. CONCLUSIONS AND SUGGESTIONS

When the results of the models applied in the study were examined, it was observed that the correct classification rate of the convolutional neural network model, which is the first model, reached 80.4%. On the other hand, the second neural network model, which was created by using data augmentation technique on this model, showed that the correct classification rate of the test data reached up to 93.4%. Therefore, it is understood that applied data enhancement technique increases the classification performance of the model. The last model applied in the study was obtained by using the structure of VGG16 model, which has been obtained by training with a data set of 1000 classes, by using feature learning transfer technique. The output layer of this model is arranged in accordance with the two-class classification problem in the study. According to the results, the model succeeded in classifying the test data with an accuracy rate of 85.6%. All performance value results obtained from the models are shown in Table 1.

Table 1. All performance value results obtained from the models

Models	Accuracy	Loss
CNN	80.4	0.7645
CNN with Data Augmentation	93.4	0.1864
Transfer Learning	85.6	0.3984

Considering the performance of three different deep learning models at the point of classification of the image data in the data set, the most successful classification results were obtained with convolutional neural network model with data increase. Therefore, it is understood from the results that data augmentation and dropout techniques used in convective neural networks have a positive effect on the classification diagnostic performance of the model. In addition, these techniques prevent the problem of overfitting in the deep learning models, which causes the model to produce incorrect results by heart.

ACKNOWLEDGEMENTS

We would like to thank anonymous refrees for their revision ideas that add depth to the article.

REFERENCES

Aghdam, H. H. and Heravi, E. J. (2017). Guide to Convolutional Neural Networks, NY: Springer, New York, USA

Chest X-Ray Images, https://www.kaggle.com/paultimothymooney/chest-xray-pneumonia [Accessed 20 July 2019].

Convolution Operation, https://medium.com/@bdhuma/6-basic-things-to-know-about-convolution-daef5e1bc411 [Accessed 21 July 2019].

Data Augmentation, https://developers.google.com/machine-learning/practica/image-classification/preventing-overfitting [Accessed 26 July 2019].

Dropout, https://medium.com/@amarbudhiraja/https-medium-com-amarbudhiraja-learning-less-to-learn-better-dropout-in-deep-machine-learning-74334da4bfc5 [Accessed 26 July 2019].

Features, https://medium.com/abraia/getting-started-with-image-recognition-and-convolutional-neural-networks-in-5-minutes-28c1dfdd401 [Accessed 29 July 2019].

First Model, http://fourier.eng.hmc.edu/e176/lectures/ch10/node8.html [Accessed 27 July 2019].

Flattening, https://www.kaggle.com/kanncaa1/convolutional-neural-network-cnn-tutorial/notebook [Accessed 25 July 2019].

Fully Connected Layer, http://cs231n.github.io/convolutional-networks/ [Accessed 22 July 2019].

Goodfellow, I., Bengio, Y., and Courville, A. (2016). *Deep learning*, MIT press, Massachusetts, USA.

Image Pixels, https://ai.stanford.edu/~syyeung/cvweb/tutorial1.html [Accessed 20 July 2019].

Indraswari, R., Kurita, T., Arifin, A. Z., Suciati, N. and Astuti, E. R. (2019). "Multi-projection deep learning network for segmentation of 3D medical images." *Pattern Recognition Letters*, Vol. 125, pp. 791-797.

Kermany, D. K., & Goldbaum, M. (2018). Labeled optical coherence tomography (OCT) and Chest X-Ray images for classification. Mendeley Data, 2.

Krizhevsky, A., Sutskever, I. and Hinton, G. E. (2012). "Imagenet classification with deep convolutional neural networks." *Neural Information Processing Systems 2012*, NIPS, Lake Tahoe, Nevada, USA, pp. 1097-1105.

Li, Y., Zhang, H., Bermudez, C., Chen, Y., Landman, B. A. and Vorobeychik, Y. (2019). "Anatomical context protects deep learning from adversarial perturbations in medical imaging." *Neurocomputing*.

Lundervold, A. S. and Lundervold, A. (2019). "An overview of deep learning in medical imaging focusing on MRI." *Zeitschrift für Medizinische Physik*, Vol. 29, No. 2, pp. 102-127.

Max Pooling, http://adventuresinmachinelearning.com/convolutional-neural-networks-tutorial-tensorflow/[Accessed 22 July 2019].

Relu Activation Function, https://www.kaggle.com/kanncaa1/convolutional-neural-network-cnn-tutorial/notebook [Accessed 25 July 2019].

Roth, H. R., Lu, L., Liu, J., Yao, J., Seff, A., Cherry, K., Kim, L. And Summers, R. M. (2015). "Improving computer-aided detection using convolutional neural networks and random view aggregation." *IEEE Transactions on Medical Imaging*, Vol. 35, No. 5, pp. 1170-1181.

Same Padding, https://medium.com/@ayeshmanthaperera/what-is-padding-in-cnns-71b21fb0dd7 [Accessed 21 July 2019].

Second Model, http://fourier.eng.hmc.edu/e176/lectures/ch10/node8.html [Accessed 27 July 2019].

Setio, A. A. A., Ciompi, F., Litjens, G., Gerke, P., Jacobs, C., Van Riel, S. J., Wille, M. M. W., Naqibullah, M., Sanchez, C. I. and van Ginneken, B. (2016). "Pulmonary nodule detection in CT images: false positive reduction using multi-view convolutional networks." *IEEE Transactions on Medical Imaging*, Vol. 35, No. 5, pp. 1160-1169.

Shin, H. C., Roth, H. R., Gao, M., Lu, L., Xu, Z., Nogues, I. and Summers, R. M. (2016). "Deep convolutional neural networks for computer-aided detection: CNN architectures, dataset characteristics and transfer learning." *IEEE transactions on medical imaging*, Vol. 35, No. 5, pp. 1285-1298.

Sigmoid Function, http://buyukveri.firat.edu.tr/2018/04/16/derin-ogrenme-yapay-sinir-aglari-3/ [Accessed 26 July 2019].

Srivastava, N., Hinton, G., Krizhevsky, A., Sutskever, I. and Salakhutdinov, R. (2014). "Dropout: a simple way to prevent neural networks from overfitting." *The journal of machine learning research*, Vol. 15, No 1, pp. 1929-1958.

Şengür, A., Akılotu, B. N., Tuncer, S. A., Kadiroğlu, Z., Yavuzkılıç, S., Budak, Ü. and Deniz, E. (2018). "Optic disc determination in retinal images with deep features." *Proc., 2018 26th Signal Processing and Communications Applications Conference (SIU)*, Izmir, Turkey, pp. 1-4.

Toraman, S., Tuncer, S. A. and Balgetir, F. (2019). "Is it possible to detect cerebral dominance via EEG signals by using deep learning?" *Medical hypotheses*, Vol. 131, 109315.

Transfer Learning, https://mlconf.com/blog/use-transfer-learning-for-efficient-deep-learning-training/ [Accessed 28 July 2019].

Tuncer, S. A., Akılotu, B. and Toraman, S. (2019). "A deep learning-based decision support system for diagnosis of OSAS using PTT signals." *Medical hypotheses*, Vol. 127, pp. 15-22.

Van Ginneken, B., Setio, A. A., Jacobs, C. and Ciompi, F. (2015). "Off-the-shelf convolutional neural network features for pulmonary nodule detection in computed tomography scans." *Proc., 2015 IEEE 12th International Symposium on Biomedical Imaging (ISBI)*, New York, USA, pp. 286-289.

VGG16 Model, https://neurohive.io/en/popular-networks/vgg16/ [Accessed 28 July 2019].

Wang, C., Shi, J., Zhang, Q. and Ying, S. (2017). "Histopathological image classification with bilinear convolutional neural networks." *Proc., 2017 39th Annual International Conference of the IEEE Engineering in Medicine and Biology Society (EMBC)*, Seogwipo, South Korea, pp. 4050-4053.

Wong, S. C., Gatt, A., Stamatescu, V., and McDonnell, M. D. (2016). "Understanding data augmentation for classification: when to warp?." *Proc., 2016 international conference on digital image computing: techniques and applications (DICTA)*, IEEE, Canberra, Australia, pp.1-6.
Zhang, J., Xie, Y., Wu, Q. and Xia, Y. (2019). "Medical image classification using synergic deep learning." *Medical Image Analysis*, Vol. 54, pp. 10-19.

Zhu, R., Zhang, R. and Xue, D. (2015). "Lesion detection of endoscopy images based on convolutional neural network features." *Proc., 2015 8th International Congress on Image and Signal Processing (CISP)*, Shenyang, China, pp. 372-376.

Turkish Journal of Engineering

Turkish Journal of Engineering (TUJE)
Vol. 4, Issue 3, pp. 142-153, July 2020
ISSN 2587-1366, Turkey
DOI: 10.31127/tuje.644597
Research Article

DESULPHURIZATION OF SYNGAS PRODUCED FROM BIOMASS USING DOLOMITE AS ADSORBENT

Ademola Stanford Olufemi *[1], Olusegun Samson Osundare [2], Isaiah Oluwadamilare Odeyemi [3] and Mirwais Kakar [4]

[1] Osmangazi University, Department of Chemical Engineering, Eskişehir, Turkey
ORCID ID: 0000-0003-4523-1454
e-mail: 503520181006@ogrenci.ogu.edu.tr

[2] University of Glasgow, School of Engineering, Glasgow, UK
ORCID ID: 0000-0001-9668-9030
e-mail: sammie1308@gmail.com

[3] Istanbul University, Department of Chemistry, Istanbul, Turkey
ORCID ID: 0000-0002-8369-9130
e-mail: i.odeyemi@ogr.iu.edu.tr

[4] Osmangazi University, Department of Chemistry, Eskişehir, Turkey
ORCID ID: 0000-0002-4215-9795
e-mail: 501520181002@ogrenci.ogu.edu.tr

* Corresponding Author
Received: 08/11/2019 Accepted: 24/12/2019

ABSTRACT
This article deals with the cleaning of generated gas for energy use in high-temperature fuel cells by the method of high-temperature adsorption in the potential utilization according to Industry 4.0. The study presents the methods of preparation of a wide range of sorbents, test equipment, used analytical methods and overview of achieved results. This project focused on high-temperature removal of acidic components such as hydrogen sulfide, Carbonyl sulfide, hydrogen chloride and hydrogen floride (H_2S, COS, HCl and HF), using laboratory-made or commercial sorbents, from the gas resulting from the gasification of biomass. In the theoretical part of the biomass and its gasification, cleaning possibilities of the raw gas and, above all, of selecting a suitable adsorbent for high-temperature removal of unwanted components was the major focus. The possibilities of using purified gas in fuel were also mentioned in the article and the properties and structure of the fuel cell. The experimental part of the project addressed the testing of specific adsorbents at different temperatures. The task was to find a sorbent that would clean the raw gas at the specified temperature to the desired concentrations of undesirable components in order to enter as fuel into a high-temperature fuel cell. Commercial and naturally obtained dolomite were modified and tested. The effective time range of sorbents at atmospheric pressure (101.325 kPa) and at different temperatures ranging from 300 to 600 °C were also measured. From the results obtained, modified dolomite was established to be more effective adsorbent for the removal of hydrogen sulphide gas from syngas produced from biomass.

Keywords: *Industry 4.0, High-Temperature Adsorption, Hydrogen Sulfide, Dolomite, Syngas*

1. INTRODUCTION

The expectation from Industry 4.0 is high, and one of the major demands is energy as its utilization plays an indispensable role. One of the possibilities for energy generation or recovery is the gasification of solid waste or biomass. Fossil fuels, as the main sources of the world energy, do not only pose a threat in term of their reserve limits but also their environmental emissions. The emissions of greenhouse gases and other combustion-related pollutants have caused non-negligible consequences such as global warming and air pollution, which are seriously threatening the biosphere (Yin & Yip, 2017). Therefore, it is imperative to explore alternative sources of energy, which are sustainable by nature and pose less or no environmental concerns.

Biomass is one of the potential resources, which is renewable/sustainable, abundant, and carbon neutral. Utilization of energy from biomass will reduce dependence on fossil resources and the environmental hazards associated with the use of fossil resources. Gasification of biomass with steam is more beneficial than with air or oxygen as higher hydrogen concentration and yield is obtained (Chutichai *et al.,* 2015; Kalinci *et al.,* 2009; Li *et al.,* 2018; Parthasarathy & Narayanan, 2014). Therefore, product gas with a higher heating value can be obtained (Kalinci *et al.,* 2009; Li *et al.,* 2018; Mahishi & Goswami, 2007).

During biomass gasification, a gas blend containing mainly hydrogen, carbon monoxide, carbon dioxide, water-vapour and methane (H_2, CO, CO_2, H_2O and CH_4) is generated together with certain unwanted byproducts, in which their concentrations depend on the feedstock, gasifier design, and process conditions (Cheah *et al.,* 2009). The undesired byproducts include organic tars, sulfur and nitrogen heteroatom species such as (thiophene, pyridine), and inorganic substances such as sulfur (H_2S, COS) chlorine (HCl) Nitrogen (NH_3, HCN), and alkali metals (Cheah *et al.,* 2009; Leppdahti & Koljonen, 1995).

The usage of dolomite sorbent is a promising way for the removal of acidic gases from biomass gasification products. Dolomite ($CaMg(CO_3)_2$) has abundant reserves and it is comparatively inexpensive. Upon calcination of dolomites, decomposes to form a highly porous CaO/MgO compound (Su *et al.,* 2019; Valverde *et al.,* 2015). Exposure of dolomite to the high temperature of gasification conditions makes the minerals undergo calcination reaction as stated below:

$$CaCO_3 + MgCO_3 \leftrightarrow CaCO_3 + MgO + CO_2 \leftrightarrow CaO + MgO + 2CO_2$$

The CaO is the active component, while MgO is inert (Abbasian *et al.,* 1990; Husmann *et al.,* 2016).The desulfurization step is as follows:

$$CaO + H_2S \leftrightarrow CaS + H_2O$$

The equilibrium of the desulfurization reaction depends majorly on the temperature of the reaction environment and the steam content (Bakker *et al.,* 2003; Husmann *et al.,* 2016). The high content of steam in the syngas (as water is formed during desulfurization step) is disadvantageous for the residual H_2S content in the gas downstream of a desulfurization unit.

In addition, the use of zinc and copper oxides on alumina-shaped cylinders as commercial sorbents for removal of acidic gas in biomass gasification product. The zinc-based sorbents are currently the leading sorbent contenders (Gupta & Brien, 2000). Zinc oxide has a high sulfur adsorption capacity (Wu *et al.,* 2018). On fractional desulfurization basis, zinc can be accepted up to 1,149.85 °C with ZnS as the sulfide form while the stable form is ZnO with excess. However, zinc-based sorbents do suffer from metal volatility (ZnO reduces to Zn above 499.85 °C and volatilizes at 699.85 °C) (Lee & Feng, 2012). Whereas copper-based sorbents do not suffer from metal volatility problems, they were determined serviceable at the temperature of 799.85 °C and above (Lee & Feng, 2012). By reducing atmospheres, copper oxides are reduced to Cu or CuO at a temperature above 199.85 °C. The equilibrium of Cu-based sorbents with H_2S concentrations are very low, about 1-5 ppm at 726.85 °C. However, Cu in a mixed oxide state can reduce the sulfur level to below 1 ppm (Lee & Feng, 2012).

The objective of this study is to perform a suitability test on a naturally sourced limestone (dolomite) for removal of acid gas components from syngas produced during the gasification of biomass.

2. EXPERIMENTAL

2.1. Material and Sample Preparation

Two types of sorbents were used. The first was a metamorphic limestone, classified as dolomite natural material harvested from Ikpeshi, Akoko-Edo Area of Edo State, Nigeria (Latitude 070 11' mN and Longitude 060 15' mE). These dolomite- sorbent materials were calcinated by annealing in an oven (PRECISION, Model 6525) at 700 °C for about 1 hour and at 850 °C and 950 °C for approximately 30 minutes to a constant weight. The sample was thoroughly washed in distilled water to remove the sludge off the surfaces so that the dolomite is cleaned.

It was subsequently cooked for about 7 minutes, filtered, dried for 1 hour at 110 °C, and finally, after drying, the sample was annealed for one hour in an oven at 700 °C.

The exact elemental composition of the dolomite limestone was determined using a Rigaku MiniFlex300 X-Ray Diffractometer with Cu-K α radiation ($\lambda \approx 0.154$ nm) which shows that the dolomite contains $CaCO_3$ 61.59 %, $MgCO_3$ 33 %, SiO_2 2.99 %, Al_2O_3 1.57 % and Fe_2O_3 0.297 %.

The second sorbent was a commercial dolomite of a given composition in the shape of small cylinders of 5.2 x 3.2 mm. These dolomites have been tested for natural and readily available sources with the composition of ZnO 46 %, CuO 33 % and Al_2O_3 21 %.

Other reagents and chemicals were obtained from two different manufacturers they include hydrofluoric acid (38 – 40 %), hydrochloric acid (36 %) and sodium hydroxide, potassium nitrate, lead acetate from Spolana and potassium nitrate from Erba Lachema.

The microstructure of the natural, calcined and sulphated dolomite was visualized in a scanning electron microscope (Hitachi TM3000) with a magnification capacity of up to 30,000 times, with 5 kV and 15 kV beams. The samples were placed on an aluminium stand when viewed. A JEOL JSM 6060 scanning electron microscope with an accelerating voltage of 0.3 to 30 kV

and a magnification capacity of up to 300,000 times was also used. In this microscope the visualization was made after metallization of the dolomite limestone particles with gold.

Specific area and pore volume were determined by BET method in specific area analyser (Quantachrome Nova 1000), with nitrogen as adsorption gas. Samples were pre-treated in vacuum for 3 hours at 300 °C. In the particle size analysis, a laser granulometer (Cilas 1180) was used. Sample density was determined on a Quantachrome MVP-1 multi-helium gas pycnometer.

2.2 GC-MS Analysis of the Produced Bio-Gas

The chemical composition of the gaseous mixture (representing the gas produced by biomass gasification) produced gas was determined using PerkinElmer Clarus 500 GC Gas chromatograph which is equipped with a flame ionization detector (FID) and a capillary column (Elite– 5), 60 m x 0.32 mm x 0.25 mm with a packing of 5 % phenyl/95 % dimethylpolysiloxane. The analysis was done using the method reported by Wauton and Ogbeide (Wauton & Ogbeide, 2019).

2.3 Experimental Set-up

Tests for the absorptive efficiency of the syngas produced from biomass has been carried out through the bench-scale experimental rig illustrated schematically in Fig. 1. The materials used to test the properties of selected sorbents include: For the measurements, two types of reactor, double-walled, were used (small) with the dolomite test frit and single-shell (large) reactor for commercial measurement sorbent and also a dolomite based material from Ikpeshi, Akoko-Edo, Nigeria.

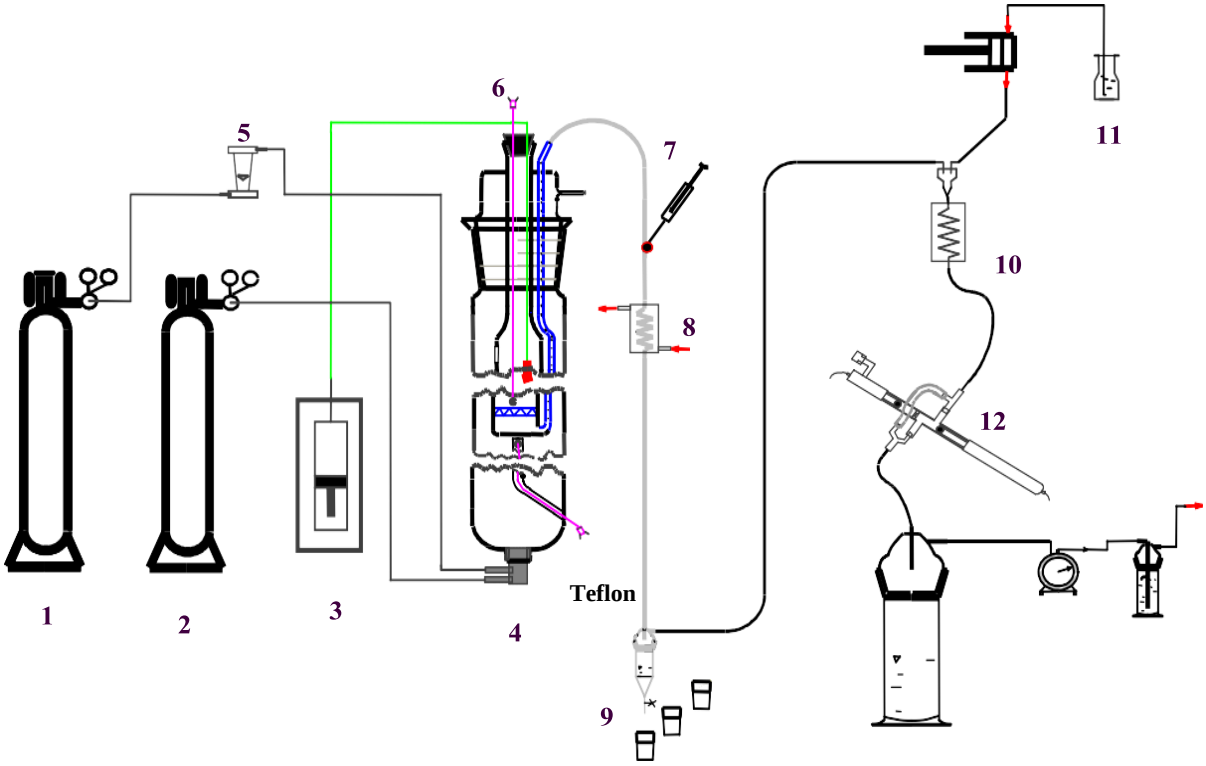

Fig. 1. The Schematic Diagram of the Experimental Set-up

Legend to Fig. 1:

1 gas mixture
2 nitrogen
3 linear pump
4 furnace with the reactor (inside)
5 rotameter
6 thermocouple
7 syringe for dispensing distilled water
8 cooler
9 sampling for liquid chromatography
10 absorber
11 NaOH solution tank
12 a sulfide electrode filled with KNO_3 solution

2.4. Experimental Procedure

The gas mixture produced after the biomass gasification (100 ppm sulphate content), passes from the cylinder (1) through the flowmeter (5) to the lower part of the reactor (4). The volumetric flow of the gas mixture is set to 85 L/h. Nitrogen (2) is also injected into the bottom of the reactor, which is used to flush the apparatus before and after the measurement. Flushing is important for two reasons. First, leakage of the whole unit is checked and secondly, the air (oxygen) that could form an explosive mixture with the hydrogen contained in the gaseous mixture (limits of explosive hydrogen are in the range of 4–75 %). The reactor head comes with an aqueous solution of acids (HCl and HF), which evaporates in the gas mixture. Acids are delivered to the device by a linear metering pump (3). The dosage is set at a flow rate of 9.026 mL/hr, resulting in a water concentration (13 %), HCl (150 ppm) and HF (20 ppm) after evaporation of the mixture.

In this study, two reactors (small and large), were made of quartz glass. The gas mixture enriched with the evaporated aqueous acid solution passes through the bed of the reactor containing the sorbent to be tested. The reactor was placed in an oval heating chamber (oven) which was heated to attain the coveted measuring temperature.

The gaseous mixture passed through the adsorbent bed emerges from the reactor head and continues into the condenser (8) where it is cooled to the condensation temperature of the acids and the sulphate remains in the gas phase. To improve the condensate drain, a syringe filled with distilled water (7) is injected into the liquid chromatography sampling device (9) and is injected at the site between the reactor and the condenser. A temperature measuring device is located at the outlet of the heat sink, where it is used to check that the temperature does not fall below the value at which the sulphate may be accidentally condensed.

The hydrogen gas mixture containing hydrogen sulfide continues into the absorber (10), where it is also supplied from the reservoir (11) by the sodium hydroxide solution. There is a dissociation of NaOH and H_2S and the increase of the S^{2-} ion potential is recorded by the sulfide electrode (12) on the potentiometer display (in mV). The electrode is filled with KNO_3 solution, which has the salt bridge function. The gas further passes through a container in which papers soaked in lead acetate are placed. If the sulfate concentration in the gas exceeds 1 ppm, the paper begins to blackout. After leaving this vessel the gas goes into the fume cupboard.

The weighed test material was poured into the reactor bed located in the furnace. In the case of a double-jacketed reactor, weighing was approximately 2 g of sample with a particle size range between 50 - 500 µm, and in a single-shell reactor, different heights of a 2 to 10 cm measured sorbent layer were tested with a particle size of 4 mm, corresponding to about 18 - 90 g of the sample. A potassium nitrate solution was added to the sulfide electrode and sodium hydroxide solution was added to the reservoir. The rectangular shaped paper was soaked in lead acetate and placed in a vessel that is connected to the electrode and serves to visualize the hydrogen sulfide penetration.

The temperature at which the oven was to be heated was set on the furnace display. Our temperature ranges from 300 to 600 °C. Prior to the measurement, it was necessary to flush the entire apparatus with nitrogen. Thereafter, the nitrogen inlet was closed, a gas cylinder containing a gaseous mixture (simulating the composition of the gas from the biomass gasification) was opened, and it was also possible to start an aqueous solution of HCl and HF by means of a linear pump. Both streams were mixed and penetrated through a test sorbent located on the reactor bed, where sulfate, HCl and HF were captured. Exhaust gas emerges from the reactor head. Subsequently, it is cooled in the cooler to a temperature at which acid condensation occurs and the sulphate is still in the gaseous state. Every 10 minutes the pH of the condensate is checked using litmus paper. If the paper begins to turn red, it means that the pH of the condensate is in the acidic area and the measured sorbent is no longer picking up the acid. The acid-containing condensate is withdrawn every 30 minutes for liquid chromatography.
Hydrogen sulphide remains in the gaseous state and passes through a sorbent filled with sodium hydroxide where dissociation occurs. The increase in the potential of S^{2-} ions is recorded on the potentiometer using a sulfide electrode filled with KNO_3 solution. The gas further passes through a container in which papers soaked in lead acetate are placed. If the sulfate concentration in the gas exceeds 1 ppm, the paper begins to black out. After the measurement was completed, the apparatus was also purged with nitrogen again.

2.5. Analytical Methods

Determination of outlet concentrations of undesirable acidic components of the gas after purification (H_2S, HCl and HF) was performed by two analytical methods.

The first was the hydrogen sulphide content determination, which was done potentiometrically using a sulfide electrode filled with KNO_3 solution. An indication of the penetration point of H_2S (above 1 ppm) by lead acetate.

The second is the concentration of HCl and HF in the condensate resulting from the cooling of the gas exiting the reactor was determined by ion chromatography.

2.6. Chemistry of Adsorbent Reaction

The performance of the solid sorbent depends on its affinity for hydrogen sulfide, porosity, mechanical resistance, and resistance to high operating temperatures ranging from 500-800 °C. Emphasis is also placed on the possibilities of regeneration, the durability of consumed sorbent and the cost of the sorbent.

The high-temperature removal of sulfur components by means of a solid sorbent is based on the following reactions:

$$Me_xO_y + xH_2S + (y-x)H_2 \leftrightarrow xMeS + zH_2O$$

$$Me_xO_y + + xCOS + (y-x)CO \leftrightarrow xMeS + zCO_2$$

Regeneration of the sorbent used takes place according to these reactions and depends on whether unwanted side reactions occur:

$$xMeS + \left(x + \frac{y}{2}\right) O_2 \rightarrow Me_xO_y + xSO_2$$

$MeS + H_2O \leftrightarrow MeO + H_2S$

$xMeS + \left(\frac{y}{2}\right) SO_2 \rightarrow Me_xO_y + (\frac{y}{2}) S$

$$xMeS + (x + y/2)O_2 \rightarrow Me_xO_y + xSO_2$$
$$MeS + H_2O \leftrightarrow MeO + H_2S$$
$$xMeS + (y/2)SO_2 \rightarrow Me_xO_y + (y/2)S$$

Westmoreland *et. al*., (1977) analyzed the gas desulphurization of 28 metal oxides at high temperature by minimizing free energy in the C-H-N-O-S system, which was in contact with the excess of the tested oxide at a constant pressure of 2 MPa and temperature in the range of 360 to 1560 °C. From their experiment, only the following 11 metal oxides - Fe, Zn, Mo, Mn, V, Ca, Sr, Ba, Co, Cu and W - appeared to be suitable.

3. RESULTS AND DISCUSSION

From the experimental setup shown in Fig. 1, for the determination of the adsorption capacity, the adsorbed gas quantity was determined in four (4) steps at different values of temperature between 300 to 600 °C. A digital technical balance with an accuracy of 10-12 g was employed to determine the quantity of adsorbate adsorbed in the fixed bed, by subtracting the mass of packed bed after the adsorption from its initial mass.

3.1. Dolomity

Dolomite-based sorbents from Ikpeshi, Akoko, Edo State, Nigeria were measured into both small and large reactors. The dolomite material was tested, which was used directly without further processing and was calcined at various temperatures (700 °C, 850 °C and 950 °C) subsequently flushed with distilled water. The modifications made were believed to improve the efficiency of the sorbent.

Measurement on a double-jacketed reactor was carried out at a temperature of 600 °C with an average particle size of 50-500 μm, measured by laser particle size and the results are summarized in Tables A1 and A2, which shows that neither different dolomite treatments had a great effect on the capture of hydrogen sulphide. The penetration occurred at the beginning of the measurement, but even after the sorption broke, a certain amount of sulfate was retained. In the case of acid seizure, the dolomite exhibited good results, especially in crude dolomite No. 2 and in the calcined sorbent. Even after the penetration of the dolomite, there was still another seizure of acids.

When measuring a single-shell reactor, the same height of the sorbent layer was 2 cm, the sample having a grain size of 4 mm (gravel). The difference between the dolomite samples was at different calcination temperatures and also at the various temperatures at which the measurements were made. Even in large reactor testing, sulphide sorption was not sufficient. The acid uptake improved with the decreasing measurement temperature and the best results were achieved at 300 °C. The better adsorption mechanism of dolomites can be attributed to the fact that after calcination and emission of CO_2, what is left of dolomite is the mixture of CaO and MgO. Since MgO does not react with H_2S, this leaves a higher porosity for H_2S to fill in the core of the grains according to Puigjaner (2011).

3.2. Commercial Sorbent

In addition, commercial sorbents - zinc and copper oxides on alumina-shaped cylinders measuring 5.2 x 3.2 mm were tested. Their effectiveness was measured at different temperatures (500 °C, 400 °C and 300 °C) and different layer heights (10 cm, 4 cm and 2 cm). When measured at a temperature of 500 °C, the elemental zinc was reduced to block the apparatus, therefore the temperature and the height of the layer decreased due to shorter testing time. At a temperature of 400 °C and a layer height of 4 cm, the acid did not penetrate and the hydrogen sulfide seizure was at a good level, therefore, in this case, the height of the layer was reduced. In spite of this reduction of the layer, good results were obtained during testing as well as at 300 °C.

By testing, it was found that the commercial sorbent is particularly suitable for capturing sulfate, whereby the desired concentration can be below 1 ppm. Mineral acid sorption is also advantageous.

Based on this, the adsorbed mass of the sample (Mads) and adsorption capacity denoted as q (mg/g), can be unveiled. The adsorbed gas quantity, the initial and final conditions which were considered as vital parts were calculated with the relationship:

$$\frac{dq}{dt} = k_f\left(C - C^*\right) \quad (1)$$

$$M_{ads} = QC_0\int_0^t\left(1 - \frac{C}{C_0}\right)dt \quad (2)$$

$$q = \frac{C_0 - C}{M}V \quad (3)$$

Where C_0 represents the initial concentration (mg/L), C stands for the outlet concentration (mg/L); the adsorbent dosage is denoted by M and measured in (g); Q connotes the flow rate and V as the volume of the reactor. This reaction is used during adsorption and desorption (purge) stage.

Next, the pressurized–depressurized stages need to obey the ideal gas law (PV= nRT).

The percentage deviation is given by:

$$Percentage\ Deviation = \sum\left(\frac{C_{pred} - C_{obs}}{C_{obs}}\right)\frac{100}{n} \quad (4)$$

3.3. Characterization of Natural Dolomite

Dolomitic limestone is characterized by its compact structure when observed under a scanning electron microscope, as it is a metamorphic limestone (Fig. 2). However some pores and uneven surface formed by steps were also observed. It has been shown that a dolomitic limestone has a less compact structure than a calcitic limestone (Mazlumoğlu and Gülaboğlu, 2017).

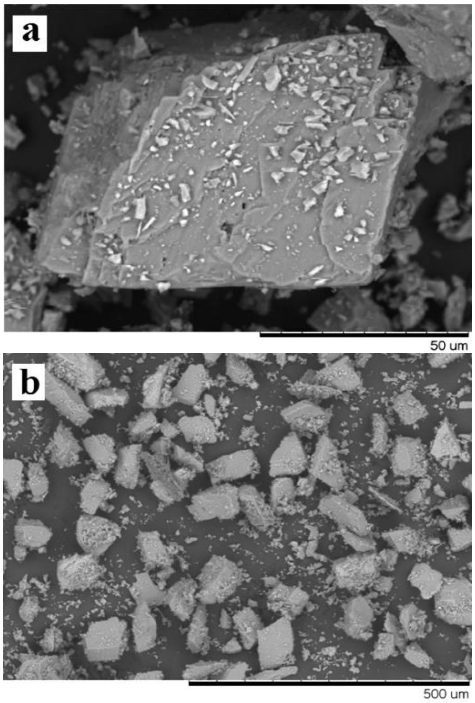

Fig. 2. SEM micrographs of in natural dolomite limestone. a) compact surface, b) particle size distribution

Due to the structure and origin, the specific area measured and the pore volume were low, and are presented in Table A3, along with the particle size distribution as measured by laser particle size. As a rule, dolomite limestone rocks have low initial porosity (Rubiera *et. al.*, 1991). The particle size range used had an average diameter of ~ 50 μm, but with some particles >100 μm. $D_{10\%}$ was represented by very fine particles smaller than 3.81 μm.

3.4. Characterization of Calcined Dolomite

The calcination of dolomitic limestone in the furnace was performed to analyze the texture and microstructure developed at 850 °C in air at atmospheric pressure. Calcination caused a reduction in the average and relative diameter of the particles according to surface fractures, and this reduction was similar for calcination by gradual heating and thermal shock. In Fig. 3d we can observe the greater amount of fines due to fracture, when compared to limestone in natura (Fig. 2b). According to the particle size distribution data presented in Table A4, it can be seen that in the granulometry used for dolomitic limestone, the reduction of mean and relative diameter during calcination at 850 °C in the furnace is not so expressive, being the main one is gas-solid contact, decreasing the resistance to intraparticle diffusion (Fuertes *et. al*., 1995).

During the calcination, high temperatures and CO_2 diffusion change the texture and microstructure of the dolomite, being marked by the opening of porosity and micro and macrofractures that eventually favor the complete rupture of larger particles and therefore the increase in fine particles; this is important in order to increase the reactive surface area of the particle. Fig. 3 shows the microstructure of the calcareous particle after calcination. The microstructure did not vary with regard to gradual heating or thermal shock calcination, and was marked by some fractures and small pores on the surface (Fig. 3).

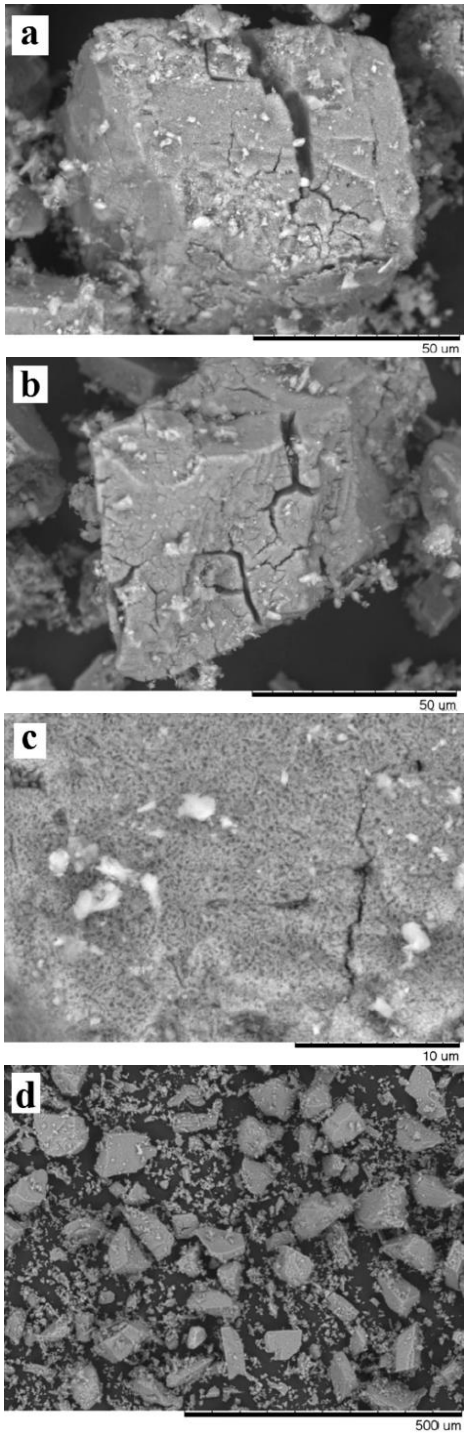

Fig. 3. SEM micrographs of calcined dolomite; a, c) gradual heating and b) thermal shock d) particle size after calcination on furnace.

3.5. Effect of the Inlet Concentration

As the affinity of adsorbate for a given adsorbent is dependent on its size, shape, polarity of the fluid and the system temperature, the importance of the partial pressure as in gases, or concentration in fluid cannot be over

emphasized. The optimization data were investigated using the commercial sorbent and the locally sourced dolomite material. Breakthrough curves were drawn to determine the adsorption capacity or efficiency for different concentrations of fluorine and chlorine and the quantity of H_2S adsorbed at different temperatures and masses. Here, the results obtained for the gas flow rate at 0.2 L/min and the adsorbed H_2S were analyzed and at different inlet concentrations are as shown in Figs. 4-6 below.

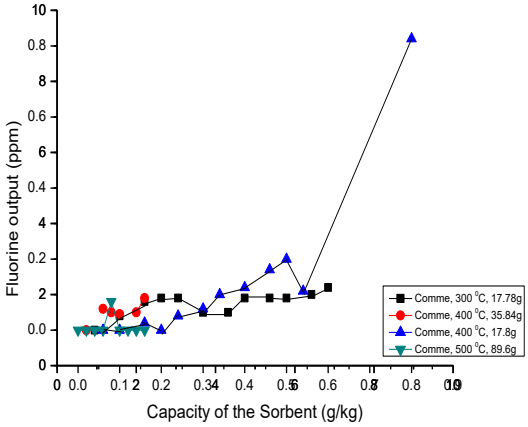

Fig. 4. Breakthrough curves of commercial sorbent for different fluoride temperatures

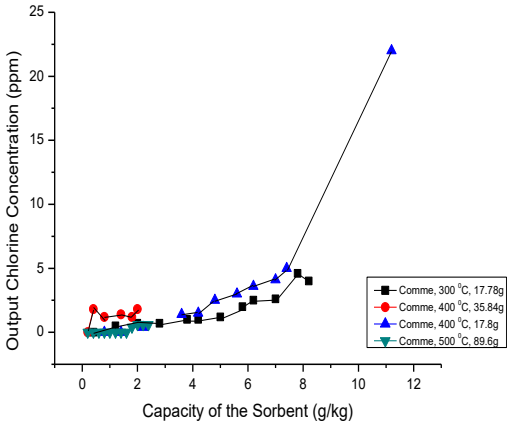

Fig. 5. Breakthrough curves for commercial sorbent for different chloride temperatures

As shown in Figs. 4 and 5, the commercial sorbent was optimized at 400 °C and 17.8 g appear to possess a higher absorption capacity.

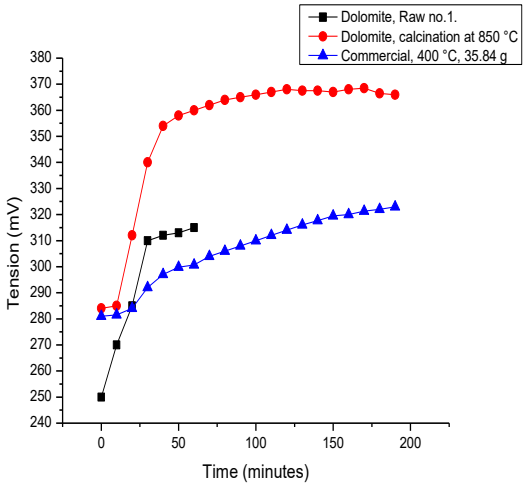

Fig. 6. Breakthrough representatives of the penetration curves for all H_2S graphs.

As it can be seen in Fig. 6, the potential difference, which corresponds to the amount of sulphide deposited from the effluent gas, is proportional to the equilibration time; it can be observed that the raw natural dolomite has a short equilibration time which shows its weakness sorption capacity but when modified at a temperature of 850 °C, its efficiency increased.

It can also be seen that as the sorption capacity increases, the breakthrough curve is shifted to the right, which is of longer breakthrough times because more molecules of the adsorbate are held by the adsorbent. Fig. 6 shows that at increased temperature of calcination of the locally sourced adsorbent, the percentage removal of adsorbed H_2S increases as well as the rate of adsorption.

3.6. Effect of Temperature on Modified Adsorbent

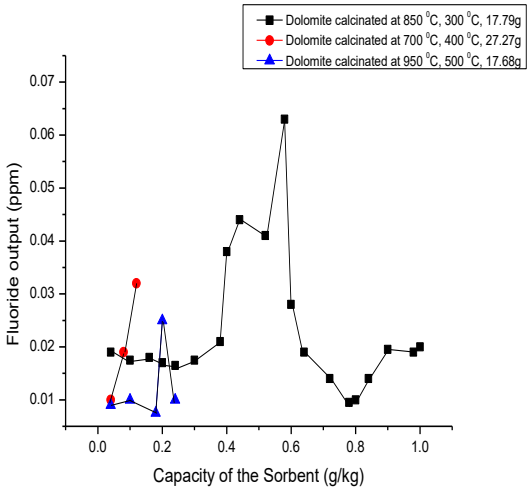

Fig. 7. Fluoride adsorbed in the dolomite for different degrees of temperature modification.

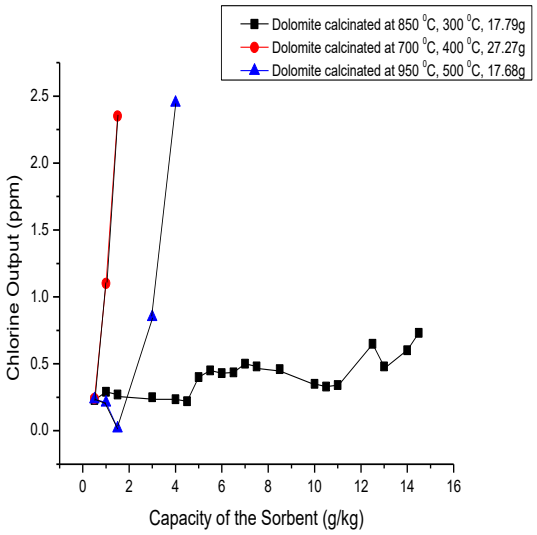

Fig. 8. Chloride adsorbed in the dolomite for different degrees of temperature modification.

In Fig. 7 and 8, it is presented that the dolomite modified at 850 ºC and 17.68 g has a more sorption capacity for fluoride than the other ones modified at 700 ºC and 950 ºC. Its weakness was obvious in Fig. 6 against chlorine even when the sorption capacity was increased. But the modified dolomite at 950 ºC, 17.68 g has a faster output which shows that at high temperature of modification, dolomites can give a large quantity of chorine.

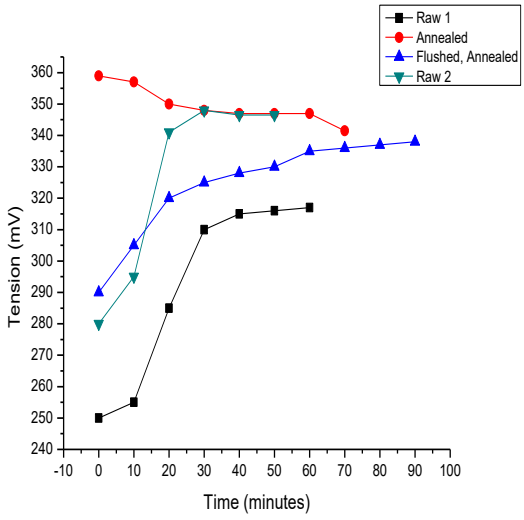

Fig. 9. Small reactor dolomite penetration curves at 600 °C for H_2S

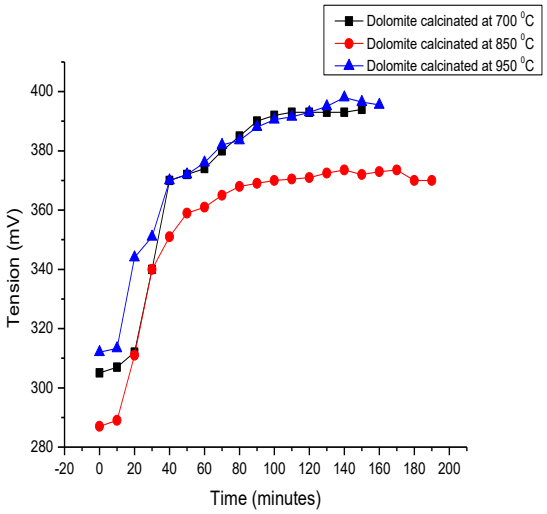

Fig. 10. Small reactor slot curves of dolomite sorbent for H_2S sorption at different temperatures of treatment

According to the results presented in Fig. 9, it can be seen that the amount of sulphide left in effluent increases with temperature. An equal weight of calcinated dolomite was used to adsorb the components of a fixed concentration of biogas mixtures. Fig. 10 shows that Dolomite calcinated at 850 °C shows the most effective optimization. Calcinated dolomite at 850 °C possess the lowest amount of Sulphide deposit after adsorption which shows that more sulphate had been adsorbed by the adsorbent. The 850 °C calcinated dolomite also shows an extended equilibration time, which affirms its higher adsorption capacity, according to the work of Delgado & Aznar (1997).

The percentage removal of adsorbed H_2S increases as well as the rate of adsorption.

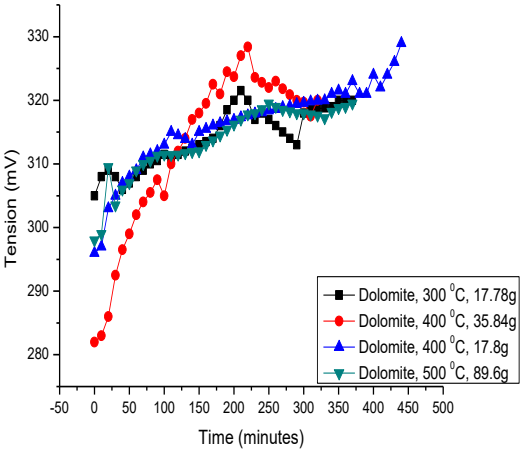

Fig. 11. Large reactor slot curves of dolomite sorbent for H_2S sorption at different temperatures of treatment

The amount of sulphide removed according to Fig. 11 shows that the dolomite material modified at 400 °C and at a capacity of 17.8 g was more effective than others. This is in line with the work of Delgado & Aznar (1997). The constant parameters (a, b, c, d, k_1 and k_2) presented in the kinetic equations were calculated by linear

regression analysis. Table A5 presents the R-squared, percentage deviation, estimated value of all statistical parameters; a, b, c, d, k_1 and k_2 included. The R^2 values and % deviations can be seen in table A5 shows there is correlation between the three kinetic equations. The power function shows the least correlation with an R^2 value ranging between 64 and 80 %, while the proffered equation demonstrates an optimum correlation with an R^2 value ranges between 97 and 99 %.

According to the R^2 value and the percentage deviation obtained, the 950 °C modified dolomite's kinetic was observed to have the least correlation as possesses an R^2 value of 90 % and a lower percentage deviation when compared to other dolomites calcined at different temperatures.

The dolomite calcined at 400 °C have the highest value of R^2 and lowest percentage deviation values. This colludes with the results obtained by other researchers which claims the ability of the simple Elovich equation to satisfactorily explain the kinetics of adsorption on lignite and cashew nut shell (Gu & Ding, 1996; Senthilkumar *et al.,* 2011). The order of adequate correlations for all modified dolomites and the predicted percentage deviation with Power Function (PF), Simple Elovich (SE) and the Proposed Equation (PE) also affirms the order;

$$PE > SE > PF$$

It can therefore be concluded that the proffered equation can adequately describe the kinetics of the modified dolomites.

3.7. GC-MS Analysis of The Purified Syngas

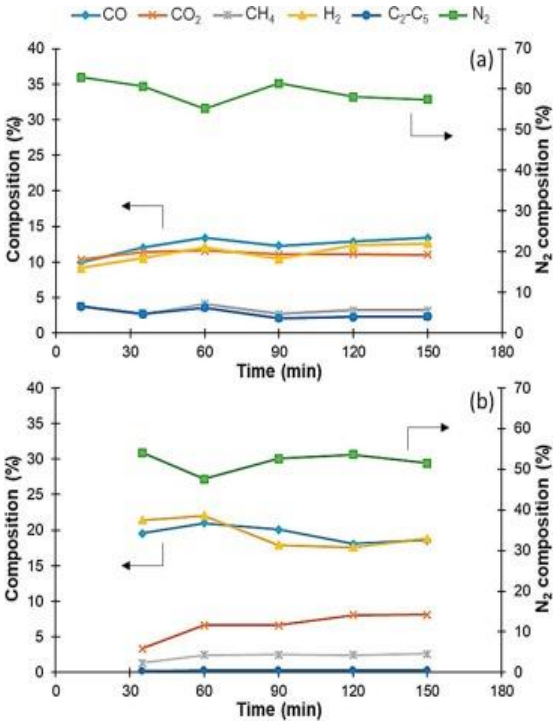

Fig. 12. GC-MS Analysis of the purified gas mixture

The chromatogram in Fig. 12 above is the actual response of the gas mix on the parallel configuration. The neat thing about the first cluster is the gas peak from the GC followed by the separation of the other components (less the H_2S) on the mol-sieve. It was found to contain CO 20 %, H_2 17.5 %, CO_2 8.6 %, H_2S 100 ppm and N_2 residue.

4. CONCLUSION

Considering the environmental and efficiency standpoint, gasification technologies have proven to be among the prime auspicious means of generating electrical power as they allow thorough and nondetrimental use of coal and other carbonaceous materials assorted with coal with high Sulphur byproducts included.

The goal of this study was to improve the removal of these by-products from the produced syngases. Considering its low cost in reducing H_2S in biomass gasification and its properties, natural dolomite which has affinity of reaction with H_2S so as to form calcium sulphate was selected among several earth-alkaline compounds for this study. Tests were carried out using dolomite obtained from Ikpeshi, Edo State, Nigeria. This dolomite sorbent was modified by calcination at different temperatures without chemical blending before being used. The dolomite was sulphurized in a pressurized fixed bed using a mixture of gases that acts as the gasification gas. The factors that affect sulphurization conditions such as gas velocity, bed length, the effect of temperature on the modified dolomite, effect of gas concentration, and gas composition were investigated.

This study established that dolomites can be used as effective adsorbents for the removal of hydrogen sulphide gas from syngas produced from biomass.

REFERENCES

Abbasian, J., Rehmat, A., Leppin, D., & Banerjee, D. D. (1990). Desulfurization of Fuels with Calcium-based Sorbents. *Fuel Processing Technology*, *25*, 1–15.

Bakker, W. J. W., Kapteijn, F., & Moulijn, J. A. (2003). A high capacity manganese-based sorbent for regenerative high temperature desulfurization with direct sulfur production Conceptual process application to coal gas cleaning. *Chemical Engineering Journal*, *96*, 223–235. https://doi.org/10.1016/j.cej.2003.08.022

Cheah, S., Carpenter, D. L., & Magrini-bair, K. A. (2009). Review of Mid- to High-Temperature Sulfur Sorbents for Desulfurization of. *Energy & Fuels*, *23*, 5291–5307. https://doi.org/10.1021/ef900714q

Chutichai, B., Patcharavorachot, Y., & Assabumrungrat, S. (2015). Parametric analysis of a circulating fluidized bed biomass gasifier for hydrogen production. *Energy*, *82*, 406–413. https://doi.org/10.1016/j.energy.2015.01.051

Delgado, J., & Aznar, P. M. (1997). Biomass Gasification with Steam in Fluidized Bed : Effectiveness of CaO , MgO , and CaO - MgO for Hot Raw Gas Cleaning. *Ind. Eng. Chem. Res.*, *35*, 1535–1543. https://doi.org/10.1021/ie960273w

Fuertes, A.B., Velasco, G., Alvarez, T., Fernandez, M.J. (1995). Sulfation of dolomite particles at high CO_2 partial pressures, *Termochim. Acta*, 254, 63.

Gu, J. M., & Ding, D. R. (1996). A study on the characteristics of adsorption for Zn2+, Cu2+, Pb2+ ions onto peat and lignite. *Environmental Chemistry*, *15*, 343–346.

Gupta, R. P., & Brien, W. S. O. (2000). Desulfurization of Hot Syngas Containing Hydrogen Chloride Vapors Using Zinc Titanate Sorbents. *Industrial & Engineering Chemistry Research*, *39*, 610–619. https://doi.org/10.1021/ie990533k

Husmann, M., Zuber, C., Maitz, V., Kienberger, T., & Hochenauer, C. (2016). Comparison of dolomite and lime as sorbents for in-situ H_2S removal with respect to gasification parameters in biomass gasification. *Fuel*, *181*, 131–138. https://doi.org/10.1016/j.fuel.2016.04.124

Kalinci, Y., Hepbasli, A., & Dincer, I. (2009). Biomass-based hydrogen production : A review and analysis. *International Journal of Hydrogen Energy*, *34*(21), 8799–8817. https://doi.org/10.1016/j.ijhydene.2009.08.078

Lee, J., & Feng, B. (2012). A thermodynamic study of the removal of HCl and H_2S from syngas. *Chemical Engineering Science*, *6*(1), 67–83. https://doi.org/10.1007/s11705-011-1162-4

Leppdahti, J., & Koljonen, T. (1995). Review Nitrogen evolution from coal , peat and wood during gasification : Literature review. *Fuel Processing Technology*, *43*, 1–45.

Li, Q., Song, G., Xiao, J., Sun, T., & Yang, K. (2018). Exergy analysis of biomass staged-gasification for hydrogen-rich syngas. *International Journal of Hydrogen Energy*, *44*(5), 2569–2579. https://doi.org/10.1016/j.ijhydene.2018.11.227.

Puigjaner, L. (2011). Syngas from Waste: Emerging Technologies *Green Energy and Technology*. Springer Science & Business Media, 127.

Mahishi, M. R., & Goswami, D. Y. (2007). Thermodynamic optimization of biomass gasifier for hydrogen production. *International Journal of Hydrogen Energy*, *32*, 3831–3840. https://doi.org/10.1016/j.ijhydene.2007.05.018

Mazlumoğlu, H., & Gülaboğlu, M. (2017). Effect of Temperature on SO_2 Absorption. *Journal of the Turkish Chemical Society B*, 1(1), 135–48.

Parthasarathy, P., & Narayanan, K. S. (2014). Hydrogen production from steam gasification of biomass: Influence of process parameters on hydrogen yield - A review. *Renewable Energy*, *66*, 570–579. https://doi.org/10.1016/j.renene.2013.12.025.

Rubiera, F., Fuertes, A.B., Pis, J.J., Artos, V., & Marbàn, G. (1991). Changes in textural properties of limestone and dolomite during calcinations, *Termochim. Acta*, 179, 125.

Senthilkumar, P., Ramalingam, S., Sathyaselvabala, V., Kirupha, S. D., & Sivanesan, S. (2011). Removal of copper (II) ions from aqueous solution by adsorption using cashew nut shell. *Desalination*, *266*(1–3), 63–71. https://doi.org/10.1016/j.desal.2010.08.003

Su, Y., Han, R., Gao, J., Wei, S., Sun, F., & Zhao, G. (2019). Novel method for regeneration/reactivation of spent dolomite-based sorbents from calcium looping cycles. *Chemical Engineering Journal*, *360*(August 2018), 148–156. https://doi.org/10.1016/j.cej.2018.11.095

Valverde, J. M., Perejon, A., Medina, S., & Perez-maqueda, L. A. (2015). Thermal decomposition of dolomite under CO2: insights from TGA and in situ XRD analysis. *Physical Chemistry Chemical Physics*, *17*, 30162–30176. https://doi.org/10.1039/c5cp05596b

Wauton, I., & Ogbeide, S. E. (2019). Characterization of pyrolytic bio-oil from water hyacinth (Eichhornia crassipes) pyrolysis in a fixed bed reactor. *Biofuels*, *0*(0), 1–6. https://doi.org/10.1080/17597269.2018.1558838.

Westmoreland, P.R., Gibson, J.B. & Harrison, D.P. (1977). Comparative kinetics of high-temperature reaction between hydrogen sulfide and selected metal oxides. *Environmental Science & Technology*. 11(5), 488-491.

Wu, J., Liu, D., Zhou, W., Liu, Q., & Huang, Y. (2018). Status of Coal Gas H_2S Removal. In *High-Temperature H_2S Removal from IGCC Coarse Gas* (pp. 21–55). Springer Singapore.

Yin, H., & Yip, A. C. K. (2017). A Review on the Production and Purification of Biomass-Derived Hydrogen Using Emerging Membrane Technologies. *Journal of Catalysts and Catalyzed Reactions*, *7*(297), 1–31. https://doi.org/10.3390/catal7100297

Appendix

Table A 1: Dolomite measurement results on a small reactor

	Sample	Weighing	$T_{calcination}$ °C	T_{try} °C	Capacity of H_2S-dolomite penetration (g/kg)	Capacity of H_2S-dolomite adsorbed at max. (g/kg)	Capacity of dolomite penetration (g/kg)	Capacity of dolomite end (g/kg)
Small reactor	Dolomite No.1.	2g	Not executed	600	0.00	5.98	0.00	5.44
	Dolomite No.2.	2 g	Not executed	600	1.00	2,99	4.46	7.12
	Dolomite	2 g	700	600	0.00	0.00	3.96	11.50
	Dolomite	2 g	700+hydr.	600	0.00	8.95	0.51	4.72

Table A 2: Dolomite measurement results on a big reactor

	Sample	Weighing	$T_{calcination}$ °C	T_{try} °C	Capacity of H_2S-dolomite penetration (g/kg)	Capacity of H_2S-dolomite adsorbed at max. (g/kg)	Capacity of dolomite penetration (g/kg)	Capacity of dolomite end (g/kg)
Big reactor	Dolomite	27.3 g, 2 cm	700	400	0.15	1.10	1.60	1.60
	Dolomite	17.7 g, 2 cm	950	500	0.11	1.71	3.74	3.74
	Dolomite	17.8 g, 2 cm	850	300	0.11	1.92	Not reached	15.15

Table A 3: Particle size distribution and texture data for natural dolomite

	Sample size (µm)
$D_{10\%}$ <	3.81
$D_{50\%}$ <	54.07
$D_{90\%}$ <	83.42
D_{medium}	48.48
Surface density (m^2/g)	4.9
Pore volume (cm^3/g)	0.0064
Density (g/cm^3)	2.86

Table A 4: Particle size distribution, texture and weight loss for calcined dolomite

Sample size (µm)	**Gradual heating**	**Thermal shock**
$D_{10\%}$ <	5.54	5.92
$D_{50\%}$ <	31.14	31.6
$D_{90\%}$ <	60.80	59.53
D_{medium}	32.80	32.84
Surface density (m^2/g)	14.5	12.1
Pore volume (cm^3/g)	0.022	-
Density (g/cm^3)	2.69	-
Weight loss (%)	32.3	28.4

Table A 5: Parameters from six different kinetic equations

Absorbate (Calinated at ^{0}C)	**Power Function** $C_{ads} = at^b$				**Simple Elovich** $C_{ads} = C + d\ln t$				**Proposed Equation** $C_{ads} = \frac{k_1 t}{1 + k_2 t^2}$			
	$a\times10^{-4}$	b	R^2	% *Dev.*	$C\times10^4$	$d\times10^4$	R^2	% *Dev.*	$k_1\times10^6$	$k_2\times10^2$	R^2	% *Dev.*
Dolomite at 300 ^{0}C	1.90	0.459	0.748	0.801	4.12	1.15	0.847	0.528	1.87	2.24	0.996	3.43
Dolomite at 400 ^{0}C	6.94	1.251	0.540	8.88	9.35	7.16	0.966	0.210	8.32	2.60	0.998	1.28
Dolomite at 500 ^{0}C	2.00	0.273	0.733	0.747	1.78	1.28	0.891	2.332	1.14	0.430	0.992	3.28
Dolomite at 700 ^{0}C	1.52	0.202	0.643	0.634	5.79	1.63	0.899	0.520	0.430	1.41	0.991	2.10
Dolomite at 850 ^{0}C	2.86	1.224	0.740	0.759	7.09	7.00	0.909	6.591	5.29	1.23	0.997	3.81
Dolomite at 950 ^{0}C	1.80	0.305	0.759	0.740	2.85	2.82	0.892	1.238	2.61	1.439	0.990	1.73

Turkish Journal of Engineering

Turkish Journal of Engineering (TUJE)
Vol. 4, Issue 3, pp. 154-163, July 2020
ISSN 2587-1366, Turkey
DOI: 10.31127/tuje.650238
Research Article

ESSENTIALS OF A SUSTAINABLE LAND USE PLANNING APPROACH FOR RURAL AREAS AND A MODEL PROPOSAL TO BE APPLIED UNDER TURKISH CONDITIONS

Orhan Ercan *[1]

[1] International Federation of Surveyors (FIG), Ankara, Turkey
ORCID ID 0000-0001-5231-8692
drorhanercan@yahoo.com

* Corresponding Author
Received: 23/11/2019 Accepted: 30/12/2019

ABSTRACT
The Turkish planning system is lack of macro-scale spatial plans at national and regional levels as well as micro-scale land use plans at local levels for rural areas, which are to be produced pursuant to the Law No. 5403 on Soil Protection and Land Use Planning. Integration of land consolidation, irrigation and crop pattern projects with agricultural and rural development projects and land use planning initiatives is another issue which has to be associated with location decisions for agro-based industrial sites and zones in ensuring economy-ecology balance and fulfilling requirements of sustainability principle in development planning.
Although the General Directorate for Agricultural Reform (TRGM) initiated preliminary activities for agricultural land use planning based on certain workshops organized in 2011; however, an obvious progress could not be achieved. Beside various reasons, the required projects by the Law No. 5403 found no chance to be launched yet, since agriculture-based land use planning asks for a teamwork cooperation among certain professionals such as agricultural economists, soil scientists, physical planners, surveyors, sociologists, economists, ecologists, etc. Lack of such interdisciplinary organizations have regretfully hindered production and implementation of such projects in Turkey, even at pilot dimensions. This study focuses on initiatives geared towards macro-scale land use plans for rural areas, expected benefits from rural land use planning attempts, essentials of sustainable land use plans for rural areas and concludes with an application model proposal.

Keywords: *Land Use Plan, Agriculture-Based Land Use Planning, Rural Development, Macro Scale Spatial Plan, Soil Threshold Analysis*

1. INTRODUCTION

Spatial planning policies which are targeted at a balanced development in principle are influenced by society, economy and environment (EC-JRCLUP, 2006). Within these main categories, relevant objectives are defined. Among these objectives are common; trying to provide as much living conditions as possible for the population, trying to improve these living conditions by creating a balanced economy and social system structure, protecting the population and the environment from damages caused by natural or man-made extraordinary events, natural resources, especially ecosystems (plants, animals and landscaping) to protect land, water and climate, to provide housing, infrastructure, recreation opportunities for social, educational needs of the society, to secure agricultural resources to ensure the supply of society to food and related raw products, to improve land use in ecological and economic capacities and balance, to give priority to the public interest.

Land-use planning is the systematic assessment of land and water potential, alternatives for land use and economic and social conditions in order to select and adopt the best land-use options. Its purpose is to select and put into practice those land uses that will best meet the needs of the people while safeguarding resources for the future. The driving force in planning is the need for change, the need for improved management or the need for a quite different pattern of land use dictated by changing circumstances. All kinds of rural land use are involved: agriculture, pastoralism, forestry, wildlife conservation and tourism. Planning also provides guidance in cases of conflict between rural land use and urban or industrial expansion, by indicating which areas of land are most valuable under rural use (FAO, 1993).

Land use planning is an instrument of the technical co-operation used in resources management (forestry, production systems compatible with resources and agroforestry, pasture management, nature protection and erosion control), rural regional development, community support and village development, government consultation (environmental strategy planning, agricultural sector planning, development planning, assessment of land potential (B. Amler, *et al*, 1999).

The prime provisions of the Law No. 5403 envisage development of prototype projects for agricultural enterprises and micro-level settlements as well as promotion of their extensive use with appropriate applications and adjustments to local conditions. Integration of land consolidation, irrigation and crop pattern projects with agricultural and rural development projects and land use planning initiatives is another issue which has to be associated with location decisions for agro-based industrial sites and zones in ensuring economy-ecology balance and fulfilling requirements of sustainability principle in development planning. For these reasons, agricultural land use planning has become a necessity.

In this paper, a practical/applicable model has been developed in order to solve the problems encountered due to lack of agricultural land use plans. This proposed methodological approach has been developed in a fit for purpose approach and is considered to be easily applicable in all developing countries under the United Nations Sustainable Development Goals (SDG's).

2. INITIATIVES TOWARDS MICRO-SCALE LAND USE PLANS FOR RURAL AREAS

The Environs Plans prepared in Turkey at 1/100,000 scale are essential for protection of the natural and ecological assets in course of national development processes, whilst those prepared at 1/25,000 scale are for regulating functional and spatial relations between the settlement centers and their peripheral areas. Other lower scale plans prepared at 1/10,000 or 1/5,000 scales stand as Master Plans for urban development, whilst 1/1,000 scaled Implementation Plans include detailed indications for applications. These plans are produced for every urban settlement center in Turkey, which possess the characteristics of physical land use development and spatial organization plans for socio-economic activities. Although up-to-date some studies have been carried out at upper scales, neither national nor regional development plans have been prepared at 1/1,000,000; 1/500,000; 1/250,000 scales, yet. In addition to absence of such upper scale macro-plans, lower scale micro-plans are also missing in the Turkish planning practice.

In order to avail a thorough consultation on the preparation of micro-scale land use plans for rural areas in Turkey, a 2-day workshop has been organized by the Ministry of Food, Agriculture and Livestock (Restructured in 2018 as Ministry of Agriculture and Forestry) which took place between 21-22 December 2011 in Ankara, Turkey with participation of central and local ministerial staff, academicians, practitioners, consultants and NGO representatives. The focal theme of the workshop was "A Quest for Methodology of Agricultural and Rural Land Use Planning in Conformance with EU Standards", whilst the main discussions were centered around effective integration of agricultural and rural development into the spatial planning system of Turkey.

In context of intensive discussions in above mentioned workshop pertaining to controversial approaches as "top-down planning" and "bottom-up planning"; a sound "bottom-up planning" approach starting from lower scale micro plans and climbing towards upper scale macro plans could be formulated for Turkey. This approach was aimed at:

- Re-organization of the national spatial distribution system to enhance the efficiency of functions allocated to rural settlements and agricultural centers, as well as
- Incorporation of agricultural aspects into physical and urban development plans widely and amply,

in order to strengthen the instrumental basis of agricultural and rural development policies and practices.

These policies were then associated with respective strategies which envisage:

- Giving priority to diversification and extension of micro-scale and local level planning works in course of "bottom-up" initiatives,
- Devoting relevance to natural and ecological aspects in planning the man-made physical and socio-economic environment,
- Optimal raking of metropolitan, major, secondary and small urban centers, rural service centers and agro-industrial bases within the framework of agropolitan and integrated rural development models,

- Filling the spatial dimension gap of socio-economic development plans (5-year national development plans and annual investment programs) prepared by the former state planning organization (SPO) and current ministry of development on sectoral basis.

Unfortunately, there has been no noteworthy record of progress in these policy issues and connected strategies over the past six years. Notwithstanding, the following activities of the GDAR carried out in June were standing in the website of the Ministry of Food, Agriculture and Livestock as of September 2017 indicating that:

- Identification of technical specifications and their announcement in the tender document of the Land Use Planning project for the Şile District of the Istanbul Province are conducted, while
- Inspection and ex-post evaluation works pertaining to applied land consolidation and on-farm service projects are on-going along with
- Opinions and attitudes related to agricultural development which have to be taken into account in course of spatial development and physical reconstruction plans and projects are elaborated.

As a matter of fact; above mentioned activities hardly comply with appropriate decisions and rational land use intentions, where spatial dimensions of development are sufficiently emphasized and adequately incorporated to planning processes. The shortcomings in formulation of opinions and attitudes of the Ministry of Food, Agriculture and Livestock to be taken into account by the Ministry of Environment and Urbanization in preparation of Environs Plans always hampered allocation of fertile lands in favor of industrial land use and housing purposes, which led to successively diminishing agricultural areas and consequently ecological distortions.

3. EXPECTED BENEFITS FROM AGRICULTURAL AND RURAL LAND USE PLANNING

The absence of spatially disaggregated upper scale macro-plans and lower scale micro-plans create serious handicaps in elaborations on and formulation of development objectives, which have to be ultimately oriented towards providing a nation-wide urban-rural integration in functional and spatial terms. Filling the micro-plan deficit by comprising agricultural and rural land use planning in Turkey would provide an excellent basis to deal with political, regulative and operational aspects of this matter of concern with diverse benefits which could be categorized as mentioned below:

i. Political benefits

- Identification of implementation and action areas for support and subsidy policies and instruments in the light of agricultural land use and rural development planning guidelines
- Giving orientation to spatial distribution of agricultural production activities and rural development investments
- Fulfilling the requirements of natural resources management and environmental protection principle in the preparation of agricultural development and rural land use plans
- Referring to risk estimations (pollution, climate change, salination, etc.) in the preparation of agricultural and rural development and land use plans
- Encouragement of "bottom-up planning" initiatives originating from local levels and extending to national level in the Turkish planning process

ii. Technical and operational benefits

- Integration of prototype projects for agricultural enterprises, farming practices and agro-industrial facilities in land use plans with regard to local activities and rural settlement characteristics
- Integration of land consolidation and on-farm service projects in land use plans
- Identification of the crop pattern depending on agricultural marketing analyses and predictions

iii. Legislative and administrative benefits

- Cooperation with the Ministry of Environment and Urbanization for effective integration of agricultural and rural land use plans in the overall spatial planning processes
- Cooperation with the Ministry of Development to devote more emphasis to agricultural and rural development planning as well as collaboration with the Regional Development Agencies for diversification of supports oriented towards local level initiatives
- Cooperation with the Ministry of Science, Industry and Technology in location planning for agro-industrial plants and zones
- Cooperation with the Ministry of Agriculture and Forestry for integration of hydrological resources and forest management issues in agricultural and rural development and land use planning
- Cooperation with the Ministry of Energy and Natural Resources for integration of underground resources in agricultural and rural development and land use planning
- Cooperation with the Ministry of Transport, Maritime and Communications for fulfilling transportation and logistics requirements of agricultural marketing and land use planning

4. ESSENTIALS OF SUSTAINABLE LAND USE PLANS FOR RURAL AREAS

Effective integration of the natural environment including soil, water and air components with the man-made environment including socio-economic and built-up components on the basis of sustainability principle is a prerequisite for making successful development plans. (Ercan, O., Dericioğlu, K.T., October 14, 2013, and October 21, 2013)

Within this framework, it is essential to precisely analyze:

- Soil, forest, water and underground resources in the "geography based" natural environment,
- Industry, trade, service and tourism activities in the "economy based" man-made environment,
- Education, health, culture and housing activities in the "society based" man-made environment,
- technical infrastructure, transportation and logistics activities in the "physical linkage based" man-made spatial environment

.

and to adequately match them with each other. The utmost relevant issue in planning process is attaching due regard to functionality, rationality, sustainability and integrity principles throughout location decisions and implementation actions. Effectiveness in implementation of actions relies on strong substantiations for taken decisions, whereas updated and disaggregated databases are required for strong justifications.

The primary goal of harmonization and integration of natural and man-made environments is to reduce economy and ecology conflict up to the possible lowest level and to ensure a balance between these two system components. For this purpose, it is unavoidable to amply investigate the interrelations between the (man-made) settlement centers and the (natural) life support systems in their surroundings. Identification of the optimal demographic size of settlements for meeting the requirements of human activities and community needs from life support systems adequately is necessary for sake of sustainability. Urban congestions in certain areas or over-population tendencies in certain settlements have to be avoided for protection and rational use of natural resources. In this respect, the indicative characteristics of plans associated with imperative provisions and enforcement instruments are of utmost importance.

The primary provisions of the Law No. 5403 on Soil Protection and Land Use Planning envisage:

i. Development of prototype projects for agricultural enterprises and micro-level settlements as well as promotion of their extensive use with appropriate applications and adjustments to local conditions,
ii. Integration of land consolidation, irrigation and crop pattern projects with agricultural and rural development and land use planning initiatives,
iii. Focusing on agro-based industrial sites and zones in ensuring economy/ecology balance and fulfilling the requirements of sustainability principle in development planning,
iv. Referring to functionality principle and relying on swot (strengths, weaknesses, opportunities, threats) analyses in spatial re-organization and land use planning tasks.
v. Saving land by preventing the loss of its features by natural or artificial ways and developing and determining planned land use based on principles of sustainable development (Çay. T. *et al*, 2017).

In producing land use plans for rural and agricultural areas, high priority is to be devoted to:

- Inputs for agricultural production and husbandry (labor force, pesticides, insecticides, fodder, mechanical equipment, seeds, fertilizers, etc.),
- Agricultural production activities and enterprises,
- Gathering of agricultural products and their processing, packaging, warehousing, dispatching, distribution, etc.,
- Consumption norms,
- Waste disposal and sanitary landfill, refusal treatment and recycling, composting and renewable energy generation, etc.

Creation of a hierarchical scheme of production, processing and service centers in compliance with the rationality principle is a basic requirement in spatial re-organization and land use planning tasks. The followings are pertinent functions and roles which the small-sized urban centers in rural areas have to play as well as services they have to provide within the hierarchical scheme of centers:

- Input (seeds and fertilizers) supply along with mechanization and equipment maintenance and repair etc. In context of agricultural production services,
- Administration along with education and health, cultural and social amenities and facilities etc. In context of social infrastructure services,
- Transportation along with water, electricity and gas supply, waste water treatment, solid waste disposal and sanitary landfilling, etc. In context of technical infrastructure services.

5. DETERMINANTS AND DIMENSIONS, PRINCIPLES AND APPROACHES IN PLANNING PROCESS

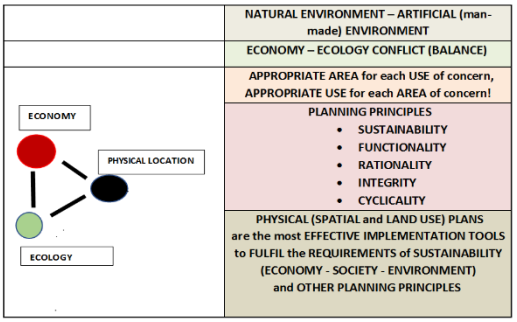

Fig. 1. Determinants and dimensions, principles and approaches in the planning process (Project on the Establishment of Macro Framework for Agricultural Land Use Plans in Thracian Provinces and Ergene Basin (2012); TR Ministry of Food, Agriculture and Livestock, General Directorate of Agricultural Reform, Ankara, Turkey)

The main determinants which have to be tackled with throughout a certain planning process are economic and socio-economic functions, physical and spatial location options as well as ecological and natural features of the area of concern.

Economy stands for functions which are related with sectoral development plans in the planning system of Turkey. Sectoral development plans are prepared by the Ministry of Development at national level and by affiliated Regional Development Agencies at regional level. The physical locations of sectors and planned functions are elaborated in and modelled by urban master and physical development plans, which are produced primarily by the Ministry of Environment and Urbanization and secondarily by the Ministry of Transport, Maritime and Communications, the Ministry of Science, Industry and Technology as well as Ministry of Culture and Tourism, etc. whenever required and wherever deemed necessary.

Ecology, on the other hand, is regulated through environs and landscape plans, which are produced by the Ministry of Environment and Urbanization. The Ministry

of Agriculture and Forestry; the Ministry of Energy and Natural Resources are other important actors with regard to the planning of ecological structures and natural assets.

Within the "economy - physical space - ecology" triangle, "natural environment - artificial environment" and "economy - ecology" balance/conflict should be regulated within the framework of "appropriate area for each use of concern versus appropriate use for each area of concern" principle with due regard to pertinent planning principles.

6. APPLICATION MODEL PROPOSAL IN REGARD OF CURRENT COUNTRY CONDITIONS

Relying on above mentioned theoretical explanations and implementation approaches in general as well as regulations and practices in particular, a certain methodology can be developed and proposed for Turkey in compliance with current conditions. The details of such a proposal for preparation of agricultural land use plans are mentioned below, which is composed of project management, data collection and processing, analysis and evaluation, decision making and planning components as a whole. The coverage of each component is briefly described under following headings.

6.1. Project Management Method

System set-up in scope of project management includes;

i. Identification of project operation framework by the GDAR,
ii. Ensuring the establishment of an organization and coordination structure with the aim of effective collaboration between the GDAR representatives and representatives from other ministries as well as launching local meetings (identifying the actors to be included in the project, indicating priority meetings at provincial level, setting an information exchange basis, etc.)
iii. Creating templates comprising;
    - Information request form for data to be obtained from related institutions,
    - Questionnaire form,
    - Analytical tables for environ plans,
    - Comparative tables for environs plans,
    - Analytical tables for regional reports,
    - Swot tables,
    - Current situation reports,
    - District information sheets,
    - Synthesis reports and information sheets,
    - Protection-use pattern,
    - Inquiry system,
    - Systems approach for identification of agricultural ecological structures,
    - Legends, and
    - Plan provisions.
iv. Setting up the reporting system by determining;
    - visual design of the report,
    - scope and contents of the legend.
v. Organization of the workshop to introduce the project to all public stakeholders and steering of the implementation by;
    - identifying the stakeholders,
    - preparing the workshop presentations and conducting visualization works.

6.2. Spatial, Institutional, Scientific and Statistical Data

4 different data sets will be used as for land use planning projects.

6.2.1. Spatial Data

Digital maps of respective institutions and organizations indicating the boundaries of demanded and permitted areas for non-agricultural land use, soil database, legend data based on Law No. 5403, topographic maps, rangeland database, forest data, landscape plans at 1:100,000 scale, master plans at 1:25,000 and 1:5,000 scales, cadaster data and village borders, climate data, LPIS data, updated transportation axes and facilities (highways, village roads, railway maps and airports, etc.), updated stream, lake, pond, dam, water surfaces and irrigation maps, contour lines, CORINE data, water basins, agricultural basins, national parks, nature conservation areas, special environmental protection areas, protected areas, tourism areas, environmental pollution and drainage data, geology data, STATIP, etc., which are digitally approved, produced by and available at different institutions and organizations across the country will constitute the main data basis of the system (Ercan. O., 2016).

6.2.2. Statistical Information

Population, health, education, general economy, agriculture, environment, industry, transportation, tourism data will be statistically collected at district, provincial, regional and national levels, and they will be used for decision making processes of planning.

6.2.3. National and regional reports

Academic studies related to agricultural sector; reports and research studies of the Ministry of Agriculture and Forestry; former State Planning Organization and current Ministry of Development reports, development plans and Regional Development Agency reports; environs plans; strategic plans of certain institutions such as Ministries and Governorates will be used as important documents throughout the planning activities.

6.2.4. National and international evaluation studies on agricultural economics

Academic studies, studies conducted, and reports prepared by the ministries as well as national and international studies will be important information sources for the planning process.

Within the scope of "Preparation of Agricultural Land Use Plans";

- The obtained data will be analyzed, standardized and uploaded to the database, in which
- They will be classified at district, provincial, regional and national levels in a way to be used as contributive elements in preparation of the fundamental basis for the plan.

Furthermore, a relevant questionnaire for preparation of the fundamental basis for the plan will be designed which enables investigation of ecological, physical and functional relations in order to obtain area-specific information. This questionnaire will be published on the GDAR website to be completed by the personnel at local units of the GDAR whereby up-dated data will be made steadily available.

Findings obtained through this activity will be holistically elaborated and associated with functional and physical linkages at regional level in order to contribute to the preparation of fundamental basis for maps and reports of national agricultural land use plan and settlement pattern at 1/25,000 scale. Thus, the emphasis devoted to spatial evaluations will be highly considered in scope of conducted works.

6.3. Approach and Method

In relation to Agricultural Sector following works will be undertaken comprising Evaluation of the National SWOT Analysis and Preparation of the Productivity Matrix. Subsequently, Macro and Meso Zoning Activities (Spatial) will be carried out, which will help to identify Integrated Clusters based on Surface Structure and Relations (e.g.: identification of Identical/Homogenous Basins) Analyses.

Through socio-economic, natural, spatial and functional analyses and evaluations carried out in this approach, rational utilization of local resources will be thoroughly interrogated, which will enable a productivity and efficiency inquiry to be undertaken at provincial level.

Productivity inquiry will be carried out by investigating whether local resources pertaining to agriculturally relevant ecological structures are rationally utilized. This investigation will be based on findings of the analyses focused on legend components of 1/25,000 scaled maps as well as discrimination and harmonization of urban and rural (agricultural, non-agricultural, settlement and production) type of land uses within the provincial borders.

By looking at the ecological structures and land use within the provincial borders;

- Weak links in the production, distribution, consumption activity chains will be assessed, and
- Issues hindering productivity and efficiency of the system which cause low-potential use and even loss of resources will be identified and listed

in scope of productivity inquiry.

In the light of the analyses and evaluations conducted above, existing problems will be defined by referring particularly to current land use practices and location decisions. Thereafter, solid proposals regarding elimination of these problems will be offered for future developments, which will include rational location selection decisions and land use plans with specific regard to local agricultural ecological structures.

These evaluations will be supplemented by Strengths, Weaknesses, Opportunities and Threats (SWOT) analysis comprising spatial diagrams pertaining to natural, social, economic and built environments.

6.4. Classification of Data at Provincial Level

On one hand, activities will be conducted to figure out the current system at district and provincial levels, and on the other hand, macro evaluations will be carried out with available data at regional and national levels in order to achieve comparative and holistic evaluations in respect of priorities of the GDAR.

In scope of these activities to be undertaken at district and provincial levels, current situation analysis will be primarily conducted. In this respect, use and formation of natural and man-made environments as well as socio-economic situation will be revealed. Agricultural resources and production potential will be stated in detail. Current hierarchical settlement system and structure within the provincial borders will be analyzed in terms of current roles and functions of urban and rural centers particularly in agricultural production areas.

This study will also briefly refer to the macro level evaluations to be carried out at a higher scale for explanation of current agricultural production activities carried out national, regional, sub-regional levels as well as relationships between agricultural sector and other sectoral activities.

6.5. Evaluation of Data and Establishment of Information Infrastructure

Synthesis and reporting will be conducted for natural environment – natural structure, built environment – physical structure, social environment – service sector, economic environment - sectoral activities within the framework of spatial (protection-use pattern, agricultural ecological structures) analyses of the data collected.

Decisions and implementations in land use planning rely heavily on the identification of local resources for mobilization and threshold analyses for location identification. Land use decisions can mainly be distinguished between (Project on the Establishment of Macro Framework for Agricultural Land Use Plans in Thracian Provinces and Ergene Basin (2012); TR Ministry of Food, Agriculture and Livestock, General Directorate of Agricultural Reform, Ankara, Turkey);

- Built Up Areas and
- Absolute Protection Areas,

whereby those lying between these two can be identified as

- Areas to be both built up and protected in a balanced manner.

In built up areas; urban expansions of settlements will take place along with land requirement for industrial production as well as social and technical infrastructure services. Absolute protection areas; on the other hand, will comprise ecological production areas, particular vegetation areas, absolute agricultural production areas, irrigated agricultural production areas, natural conservation areas, etc., which have to be officially registered and legally restricted.

Preparation of criteria list for particular land use types, identification of specifications for protection in built up land use types as well as mechanisms for control and enforcement (plan provisions) are the necessary studies which have to be undertaken in order to be respectively applied for

(i) Pre-dominantly built up and subsidiary protected areas,

(ii) Equivalently protected and built up areas, and lastly

(iii) Pre-dominantly protected and subsidiary built up areas.

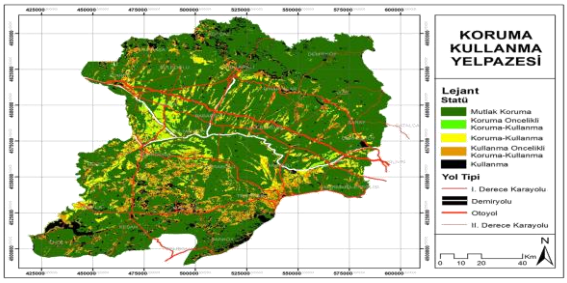

Fig. 2 Identification of absolute soil protection areas and built up areas

Areas where ecologically compliant agricultural activities are currently carried out will be identified in scope of surveys pertaining to agricultural-ecological structures. In the next step, impacts of natural structure components on each other and their interaction processes will be handled to the possible widest extent which the study allows.

Accordingly, 1/25,000 scaled maps and reports will be produced related to identification of agricultural-ecological structures and a set of activities will be prepared to provide firstly inputs for the protection of soil and agricultural resources; and secondly to define agricultural policies and develop connected planning activities (Landscape Plans, Master Plans, and Implementation Plans). This is of significant importance in terms of relying on integrity, functionality and sustainability principles in planning processes, which will constitute an important basis for preparation of potential land utilization maps.

After describing the protection-use pattern and identifying agricultural-ecological structures, functional relationship inquiries mainly including socio-economic evaluations will be conducted at district level. With the natural, built up, social and economic environment analyses, the following works will be accomplished:

- Identifying problems in production, distribution and consumption activity chains based on agricultural-ecological structures and current land use practices,
- Assessing agricultural - ecological potentialities and evaluation of rational use of resources,
- Undertaking macro evaluations on current agricultural production activities and clarification of relationships between agriculture and other sectoral activities,
- Investigating whether provided urban services increase production performances,
- Setting up a contextual framework for urban-rural integrated relations system (hierarchically positioned activity units in the reciprocal relations system).

Conducted studies and surveys as well as investigations and evaluations will be utilized for further assessments, which will be carried out within the framework of Strengths, Weaknesses, Opportunities and Threats (SWOT) analyses including spatial diagrams pertaining to natural, social, economic and built up environments.

6.6. Interpretations and Creation of a Model as Fundamental Basis for Land Use Plans

Land use plan basis will be completed upon definition of agricultural status of the concerned land (classification of the area based on resource features), identification of agricultural functions (classification of the area based on activities) and finalization of legends (contents, colors and symbols) as planning aids.

After describing the protection-use pattern and identifying agricultural-ecological structures, functional relationship inquiries including mainly socio-economic evaluations will be conducted at district level.

"Potential Land Use Maps" at 1/25,000 scale will be prepared at district and provincial levels by using all analyses carried out for natural and built up environments and all data layers included in the "Spatial Data Model" which constitute the fundamental basis of the land use plan. Thereupon, the "Model Proposal" on the development of agricultural sector and its integration with other economic and social activity sectors will be developed at provincial level.

The “Model Proposal” will be developed in a way to include all basic contents for agricultural production policies related to local agricultural-ecological structures as well as measures and incentive packages for local activities along with location selection decisions to be made in this regard. In the reports to be prepared at provincial level, current situation analyses will be carried out focused on;

- Natural structure,
- Physical structure,
- Spatial structure,
- Population and demographic characteristics,
- General economic situation,
- Socio-economic structure,
- Land existence in the districts,
- Agricultural products and production processes,
- Animal products and production processes,
- Water resources and irrigation systems,
- Mechanization in agriculture,
- Agricultural problems and risks,
- Agricultural investment projects and subsidies,
- Agricultural holdings,
- Agricultural organizations, and
- Agricultural structure assessments, etc.

In light of syntheses of above-mentioned analyses as well as evaluations and interpretations, pertinent specifications will be set forth for;

- Landscape plans,
- Non-agricultural requirements, and

- Protection - use pattern,

which are essential for agricultural land use planning. Thereupon, the relationships between agricultural subventions and agricultural production processes will be evaluated and formation of a fundamental basis for preparation of the agricultural land use plans will be achieved.

6.7. Iterative Compliance Investigation of Proposed Model for Land Use Plan Basis

The proposed model will be iteratively evaluated by the experts from the ministries, local interest groups and academicians who are effective in regional evaluations and their feedbacks will be obtained.

Furthermore, the proposed model will be compared with National Plans, Environ Plans, Basin Plans, Regional Plans, Sectoral / Development Plans and its suitability will be steadily investigated.

Contributions regarding land use and location selection decisions will include features pertaining to activating the processes related to utilization of local agricultural resources and ecological structures as well as to establishing and strengthening regional functional and physical (production-added value-transfer-marketing-consumption) linkages.

6.8. Identification of Compliant and Conflicting Parts of the Model with Current Plans

Conflicting elements will be identified as a result of comparison of the proposed model with National Plans, Environ Plans, Basin Plans, Regional Plans and Sectoral / Development Plans. Based on the outputs of comparative studies, thematic research proposals will be made in order to identify institutional mechanisms to be established in connection with management and governance operations for harmonization purposes. These efforts are for firstly for assessment of conflicts and secondly for their elimination with aid of adequate measures and actions.

6.9. Preparation of the Model Related LUP Basis at National and Regional Levels

Land Use Planning basis will be produced at national and regional levels which relies on;

- Identifying the protection - use pattern through Absolute Protection, Use, Conditions and Significance Rating (Usage with Protection Priority, Protection-Use Balance, Protection with Usage Priority) decisions,
- Integrating the functional and physical linkages (Production - Added Value-Marketing-Consumption) for creating macro, meso and micro level agricultural ecological zoning and relations system, and
- Ensuring the connection among ecologically, statistically and administratively defined spatial clusters.

Thus, the processes of producing a well elaborated Agricultural Land Use Plan at 1/25,000 scale in accordance with its priorities and implementation tools (political, legal, administrative, financial, technical, educational, etc.) will be identified.

6.10. Description of Macro Agricultural Policies and Tools in line with LUP Basis Prepared at National and Regional Levels

Upon preparation of the fundamental basis of the Land Use Plan, agricultural policies will be identified with due regard to ecological, economic and social sustainability principles. Subsequently, macro agricultural preferences and policy tools such as support and subsidy mechanisms; research studies, extension and training programs; as well as export and import regulations will be described in the final synthesis of accomplished works.

7. CONCLUSION

The mission line required by the duty of producing agricultural land use plans, which are assigned to the Ministry of Agriculture and Forestry by the Soil Protection and Land Use Law No. 5403; Drawing on the basis of internal and inter-institutional cooperation, communication, sharing and governance will be an important step towards fulfilling the requirements of planning, functionality, rationality, sustainability and integrity. It is deemed necessary to base the agricultural land use planning process on such a mission, to be among the actors currently active in planning in the country, and to play an active role in filling the gaps in the planning studies being carried out.

The physical plan (1/25,000 scaled Settlement Pattern and Land Use Plan) model proposal for land use planning is summarized in stages below. Operation steps of the proposed model are composed of;

1) Collection of spatial, institutional, scientific and statistical data and their transfer to a database,
2) Identification of main structural indicators (natural structure, settlement pattern demography, socio-economic structure),
3) Identification of functional indicators (agricultural product profiles, specialization),
4) Selection of indicators (technical infrastructure and thresholds),
5) Identification characters and types (spatial and functional clusters),
6) Definition of pre-planning proposals (links between clusters),
7) Undertaking suitability analysis in location selection,
8) Definition of final planning proposals,
9) Establishing links between clusters and action areas (local coherences – functional associations),
10) Undertaking location selection decisions (protection-use pattern), and
11) Preparing the physical plan (land use plan and settlement pattern at 1:25,000 scale).

Continuing the Land Use Planning project development activities initiated by the GDAR in 2011 is an indispensable task in terms of protecting economy-ecology balance, saving absolute agricultural areas from occupation and achieving sustainable environment as well as fulfilling the legal obligations entrusted to the GDAR.

The proposed fit for purpose agricultural land use planning model can be easily implemented within the framework of the United Nations Sustainable Development Goals, especially in developing countries.

ACKNOWLEDGEMENTS

I would like to thank to Assoc. Prof. Dr. K. Taylan DERİCİOĞLU for reviewing the manuscript and valuable contributions. I also thank to General Directorate for Agricultural Reform for allow me to use the necessary data and document which made this paper more concrete and meaningful.

REFERENCES

B. Amler, D. Betke, H. Eger, C.Ehrich,A. Kohler, A. Kutter, A. von Lossau,U. Müller,S. Seidemann, R. Steurer,W. Zimmermann (1999), Land Use Planning Methods, Strategies and Tools, Deutsche Gesellschaft für Technische Zusammenarbeit (GTZ) GmbH, Eschborn, Germany

Ceyhan, M. (2011) Provincial Director of Environment and Urbanization, Coordinator of Ergene Basin. Ergene Havzası Koruma Eylem Planı ve Yürütülen Çalışmalar, I. Kıyı Bölgelerinde Çevre Kirliliği ve Kontrolü Sempozyumu [Ergene Basin Conservation Action Plan and Activities, I. Environmental Pollution and Control in Coastal Areas Symposium],

Cay. T, Toklu. N, Esen.O., (2017), Evaluation of Land Reform Policies In Turkey *International Journal of Engineering and Geosciences 2* (2017): 61-67

EC-JRCLUP Guidance, Land Use Planning Guidelines (2006), in the Context of Article 12 of the Seveso II Directive 96/82/EC as Amended by Directive 105/2003/EC, FAO, Guidelines for Land-Use Planning, FAO Development Series 1, ISSN 1020-0819, (1993), Rome, Italy

Edirne Special Provincial Administration, (2011). 1/25 000 Scale Edirne İl ÇevreDüzeni Planı [Edirne Provincial Environmental Plan].

Ercan, O. (2015). Towards Effective Integration of Agricultural and Rural Development In Spatial Planning System Of Turkey As Based On Extended And Diversified "Bottom-Up" Initiatives; "Management of Agricultural Zones – Survey Engineer in the Centre of Sustainable Development and Distribution of Responsibility" Symposium, September 7, 2016, Beirut, Lebanon

Ercan, O., Dericioğlu, K.T. TRGM'ne Yapilan Sunumlar [presentations delivered for the GDAR] Ankara, (2013),

a) Essentials of Land Use Planning, October 14, 2013.
b) Agricultural Land Use Planning Methodological Approach and Explanations, October 21, 2013

Ercan, O. TRGM Toplantı Sunumları [presentations delivered for the GDAR] Ankara, (2016)

a) Tarımsal Arazi Kullanım Planlaması Veri ve Metodolojisi [Agricultural Land Use Planning Data and Method], July 26, 2016.
b) Tarımsal Arazi Kullanım Planlaması Uygulama Sistemi [Agricultural Land Use Planning Operation System], July 27, 2016.

Kırklareli Special Provincial Administration, (2011). 1/25 000 Scale Kırklareli İl Çevre Düzeni Planı [Kırklareli Provincial Environmental Plan]..

Leppert, G., Hohfeld, H., Lech, M., Wencker. T., (2018), Impact, diffusion and scaling up of a comprehensive land-use planning approach in the Philippines, From Development Cooperation to National Policies, Evaluation Report, German Institute for Development Evaluation (DEval).

Ministry of Environment and Forestry, General Directorate of Environmental Management. (2008). Meriç – Ergene Havzası Koruma Eylem Planı, [Meriç - Ergene Basin Conservation Action Plan],

Ministry of Environment and Forestry, General Directorate of Environmental Management, Department of Water and Soil Management; Meriç-Ergene Havzası - Havza Koruma Eylem Planı [Meriç-Ergene Basin - Basin Protection Action Plan], accesed May 2012 at www.cygm.gov.tr, Ankara.

Ministry of Environment and Forestry, (2009). 1/100 000 Scale Trakya Alt Bölgesi Ergene Havzası Revizyon Çevre Planı [Thrace Subregion Ergene Basin Revision Environmental Plan).

Ministry of Forestry and Water Affairs, General Directorate of State Hydraulic Works, (2011). Ergene Havzası Koruma Eylem Planı kapsamında DSİ tarafından yapılacak çalışmalar [Works to be carried out by DSI within the scope of Ergene Basin Conservation Action Plan], 11th Regional Directorate, Edirne.

Ministry of Agriculture and Rural Affairs, (2005). Edirne Tarım Master Planı. Edirne Tarım İl Müdürlüğü, İl Tarım ve Kırsal Kalkınma Master Planlarının Hazırlanmasına Destek. [Edirne Agricultural Master Plan. Edirne Agriculture Provincial Directorate, Support to the Preparation of Provincial Agricultural and Rural Development Master Plans].

Ministry of Agriculture and Rural Affairs, (2004). Tekirdağ Tarım Master Planı. Tekirdağ Tarım İl Müdürlüğü, İl Tarım ve Kırsal Kalkınma Master Planlarının Hazırlanmasına Destek.[Tekirdag Agricultural Master Plan. Support to the Preparation of Provincial Agricultural and Rural Development Master Plans],

Ministry of Agriculture and Rural Affairs, (2010) Kırsal Kalkınma Planı [Rural Development Plan] 2010 - 2013, Ankara.

Ministry of Agriculture and Rural Affairs, (2007), TR 2 Batı Marmara Bölgesi Tarım Master Planı [Batı Marmara Bölgesi Tarım Master Planı [Agricultural Master Plan of West Marmara Region],

Ministry of Agriculture and Rural Affairs, (2007), TR 4 Doğu Marmara Bölgesi Tarım Master Planı [Agricultural Master Plan of Eastern Marmara Region]

Project on the Establishment of Macro Framework for Agricultural Land Use Plans in Thracian Provinces and Ergene Basin (2012); TR Ministry of Food, Agriculture and Livestock, General Directorate of Agricultural Reform, Ankara, Turkey

Tarım Reformu Genel Müdürlüğümde Arazi Kullanım Planlaması Çalışmaları [Agricultural Land Use Planning Works at GDAR] http://www.tarim.gov.tr/sgb/Belgeler/SagMenuVeriler/TRGM.pdf [accessed May 2017],

Tekirdag Special Provincial Administration, (2011), 1/25 000 Ölçekli Tekirdag İli Çevre Düzeni Planı,

Thrace Development Agency, (2010), TR21 Trakya Bölgesel Planı 2010-2013.

Turkish Journal of Engineering

Turkish Journal of Engineering (TUJE)
Vol. 4, Issue 3, pp. 164-168, July 2020
ISSN 2587-1366, Turkey
DOI: 10.31127/tuje.650989
Research Article

THREE-DIMENSIONAL EARTH MODELLING PERFORMANCE ANALYSIS OF GOKTURK-2 SATELLITE

Aycan Murat Marangoz *[1], Umut Güneş Sefercik [2] and Damla Yüce [3]

[1] Zonguldak Bulent Ecevit University, Faculty of Eng., Department of Geomatics Engineering, Zonguldak, Turkey
ORCID ID 0000 – 0003 – 4409 – 6000
aycanmarangoz@hotmail.com

[2] Zonguldak Bulent Ecevit University, Faculty of Eng., Department of Geomatics Engineering, Zonguldak, Turkey
ORCID ID 0000 – 0003 – 2403 – 5956
ugsefercik@hotmail.com

[3] General Directorate of Mapping, Department of Photogrammetry, Tıp Fakültesi Cad. Ankara, Turkey
ORCID ID 0000 – 0002 – 3343 – 4775
damlay1990@hotmail.com

* Corresponding Author
Received: 26/11/2019 Accepted: 01/01/2020

ABSTRACT
Following RASAT, Göktürk-2, placed into its orbit as Turkey's second domestic production of earth observation, has three times higher spatial resolution (2.5 m) than RASAT and has much more advanced stereo vision capability. However, like all-optical imaging satellites, Göktürk-2 has problems in data quality due to reasons such as sensor geometry, contrast, dense forest cover in the field of view and topographic slope. In this study, it is aimed to evaluate the horizontal and vertical geolocation accuracy performance of three-dimensional Digital Surface Models (DSM) derived from Göktürk-2 stereo images in comparison with a reference DSM obtained by traditional photogrammetry method in Derik district of Mardin province with high slope and variable topographic conditions. The results demonstrated that the three dimensional topographic representation capability of Göktürk-2 is quite successful despite offering a medium spatial resolution. The Göktürk-2 DSM has an absolute horizontal geolocation accuracy of ≤0.1 pixels (25 cm) both for X and Y directions. On the height, it provides accuracy as standard deviation of 7.3 m and normalized median absolute deviation of about 5.7 m.

Keywords: *Göktürk-2, Digital Surface Model, Performance, Quality*

1. INTRODUCTION

Remote Sensing (RS), the technology of acquiring airborne or space-borne information from target objects on earth without making direct contact with them, has become a modern method that is increasingly used worldwide with rapidly developing optical, radar and lidar technologies. Countries have been working hard for many years to integrate this technology.

In Turkey, space-borne RS activities started in the 1990s under the leadership of Scientific and Technological Research Council of Turkey (TUBITAK), and BILSAT, which emerged as a product of collaboration with Surrey University in the UK, was orbit in September 2003 as the first Turkish satellite mission. Through BILSAT, Turkey had the chance to acquire 12.6 m panchromatic and 26.7 m multispectral own satellite imageries (Yüksel *et al*., 2016). BILSAT mission, which worked until 2006, was terminated in August 2006 as a result of technical failures in communication links. After BILSAT, Turkey's first domestic production of earth observation satellite RASAT was successfully placed into orbit in August, 2011. RASAT is a satellite mission with an optical principle capable of 7.5 m panchromatic and 15 m multispectral image acquisition. Despite some technical failures in the positioning systems immediately after its launch, RASAT continues its duty successfully. RASAT, which does not have infrared vision, could not provide the expected performance in stereo imaging due to the very slow stereo-vision camera. Turkey, learning more from each mission and developing, planned a new developed domestic satellite mission which corrected all deficiencies and the third earth observation satellite Göktürk-2 was placed into the orbit in December 2012. Göktürk-2, which is the first high-resolution earth observation satellite developed by our country, was not only designed, produced, but also the engineering activities in the test stages were utterly national.

In optical satellite missions, because of solar dependence, high-altitude imaging geometry, contrast and sensor characteristics, some limitations exist in product quality. Due to this fact, it is an indispensable requirement to determine the quality loss experienced by each satellite mission and determine the quality level of the satellite data and the resulting products (Aguilar *et al*. 2010; Zhao *et al*. 2011; Hladik and Alber 2012; Hobby and Ginzler 2012). Likewise, it is revealed that the satellite data whose quality is determined may be the reason of choice in such studies. In this study, it is aimed to evaluate the planimetric and vertical quality of three dimensional Digital Surface Models (DSM) obtained from Göktürk-2 stereo images. As it is known, DSMs, which represent the earth in three dimensions including all natural and man-made objects, are indispensable products for many disciplines such as forestry, archeology, hydrology and city planning (Fraser, 2003; Navalgund *et al*., 2007; Font *et al*., 2010; Sterenczak and Kozak, 2011; Sefercik *et al*. 2013; Yılmaz and Uysal, 2017).

The study is divided into five sections. In the second section, the study area and the properties of the materials used are presented. In the third section, the methodology of the study is given. In the fourth section, the results are presented, and in the fifth and final section, the conclusions and future targets are given.

2. STUDY AREA AND MATERIALS USED

Derik District is located in South-eastern Anatolia Region and is 42 km from Mardin City centre. The district is located between 40º 16 '5' 'East longitude and 37º 21' 53 " North parallel and has a surface area of 1,381 km2. An area of 1.35 × 3.45 km including Derik District Centre and its surrounding area was determined as the study area. Fig. 1 presents the location of the study area in Turkey and shows a close-up image. Derik was selected as the study area because of its variable and steep topography which enables a better interpretation of Göktürk-2 DSM performance.

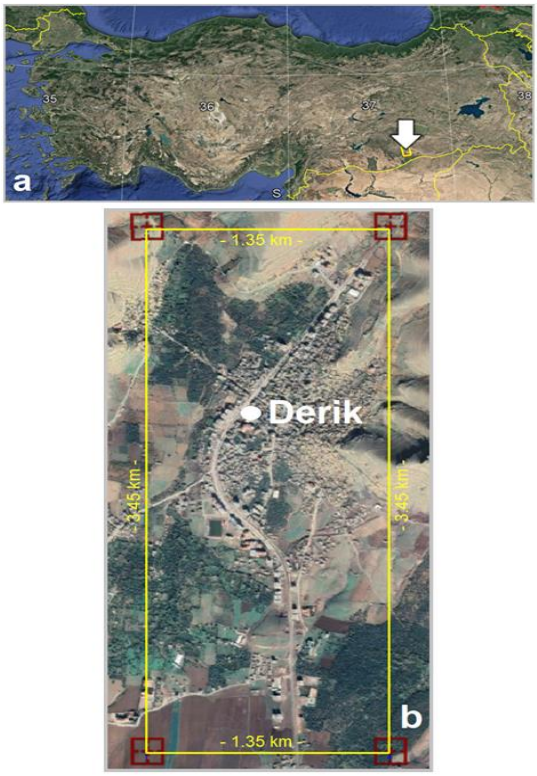

Fig. 1. Study area: (a) the location on the map of Turkey, (b) Derik district study area boundaries

The three-dimensional coverage and characteristics of the Göktürk-2 satellite images used in the study are presented in Fig. 2 and Table 1. As shown in Fig. 2, the study area is located in a steep region in the approximate middle portion of the stereo images.

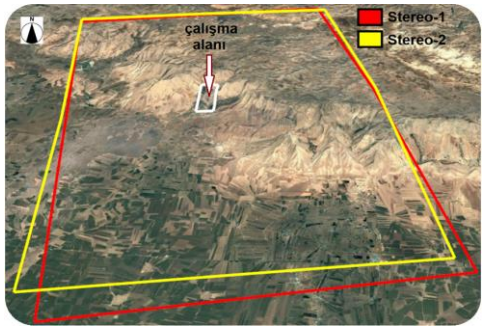

Fig. 2. Göktürk-2 stereo image boundaries

Table 1. Characteristics of Göktürk-2 stereo images

Characteristics	Göktürk-2 Stereo-1	Göktürk-2 Stereo-2
Reception Date (y/m/d)	2018-09-16	2018-09-16
Reception Time (h/m/s)	07:15:17.63	07:17:10.21
Stereo reception mode	Along-track	
Spatial resolution (m)	2.5 PAN / 5 MS	
Sun azimuth angle (°)	134.80406	135.36513
Sun height angle (°)	45.90185	46.15824
Coordinate reference system	WGS84	
Dimensions (width × length) (km)	~24×40	

3. METHODOLOGY

In this study, Göktürk-2 images were oriented by three-dimensional affine transformation. In the process, 18 Ground Control Points (GCP) collected from Google Earth images with a resolution higher than the spatial resolution of 2.5 m PAN of Göktürk-2 satellite were used. All of them were utilized for the orientation of stereo image 1 and 16 of them were used for the orientation of stereo image 2. The distribution of the GCPs used in the orientation process is shown in Fig. 3.

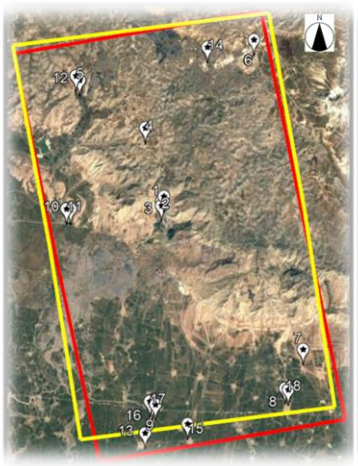

Fig. 3. GCP distribution

After the completion of the orientation process, 5 m grid DSM was produced from Göktürk-2 stereo images with DPLX software. The performance of the produced DSM is demonstrated visually and statistically using a reference photogrammetric DSM which have ~8 cm horizontal and ~12 cm absolute vertical accuracy. The 0.5 m grid reference DSM was derived from aerial photos taken by a Phase One 80 megapixel digital aerial camera at 800 m flight altitude. In the visual evaluations, the height error map produced from the differential model of Göktürk-2 DSM with reference photogrammetric DSM was interpreted. In height error map generation, the grid intervals of the DSMs were balanced by re-sampling. In statistical analyses, Göktürk-2 DSM geolocation accuracy was calculated using standard deviation (SZ) (equation 1) and normalized median absolute deviation (NMAD) (equation 2) metrics.

$$SZ = \sqrt{\frac{\sum_{i=1}^{n}(\Delta Z_i - \mu)^2}{n-1}} \quad (1)$$

$$\boldsymbol{NMAD = 1.4826 \times \widetilde{X_i}\left[\left|\Delta Z_i - \widetilde{X_j}(\Delta Z_j)\right|\right]} \quad (2)$$

In Equation 1, n is the number of pixels compared, ΔZ is the height difference of the compared pixels, and μ is the arithmetic mean of these differences. In Equation 2, $\widetilde{X_j}$ is the median of the univariate data set of height differences, and $\widetilde{X_i}$ is the median value of the height differences from $\widetilde{X_j}$. While NMAD stands out as a value very close to SZ in normal error distribution, if there is a structure that causes random error distribution in DSM, NMAD value is higher than SZ which is an undesirable situation indicating that DSM tested in absolute vertical accuracy analysis is in structural difficulty. Although NMAD is a robust accuracy metric for detecting significant structural errors, it does not perform as well as SZ in terms of revealing minor height differences (Hellerstein, 2008).

After the Göktürk-2 horizontal geolocation accuracy determination, the error amounts occurring in X and Y directions were eliminated by horizontal shifting by area-based cross-correlation method and Göktürk-2 DSM and reference DSM were fully overlapped horizontally before vertical geolocation accuracy analysis. Likewise, the basic condition of correct vertical accuracy evaluations is %100 horizontal overlap of analyzed DSMs. If horizontal overlap is not achieved, it is indisputable that vertical error detection in different parts of the models will lead to misleading results.

4. RESULTS

The horizontal geolocation accuracy of Göktürk-2 DSM obtained based on the standard deviation metric according to the reference photogrammetric DSM, as well as the horizontal offset amounts performed before the vertical accuracy are presented in Table 2. As can be seen from the Table 2, Göktürk-2 DSM's horizontal geolocation accuracy is 0.1 pixels in the X direction and 0.01 pixels in the Y direction. This also clearly demonstrates the performance of the GCPs used in the image orientation process.

Table 2. Absolute horizontal accuracy of Göktürk-2 stereo images

Reference DSM	Tested DSM	ΔX (m)	ΔY (m)
Photogrammetric (0.5m)	Göktürk-2 (5m)	0.26	-0.03

DSMs obtained from photogrammetric reference data, and Göktürk-2 stereo images are shown in Fig. 4. When DSMs are examined, it can be mentioned that the topographic description performance of the 5 m grid DSM obtained from Göktürk-2 images with 2.5 m medium spatial resolution is quite successful. When the coloured height scale is considered, it can be seen that the correlation of topographic elevation zones with photogrammetric reference is quite high and even some narrow linear lines can be represented. Besides, the

minimum and maximum elevation values appear to be equal on the colour elevation scales, which is not typical for DSMs from medium resolution satellite data.

Table 3 shows the absolute vertical geolocation accuracy results of Göktürk-2 DSM. In the Table, the performances of DSM in the whole area and only the uninclined topography are presented separately. Inclination expression was used for plots with slope $<\tan^{-1}0.1$ (~6°) as usual in DSM quality researches (Jacobsen, 2016).

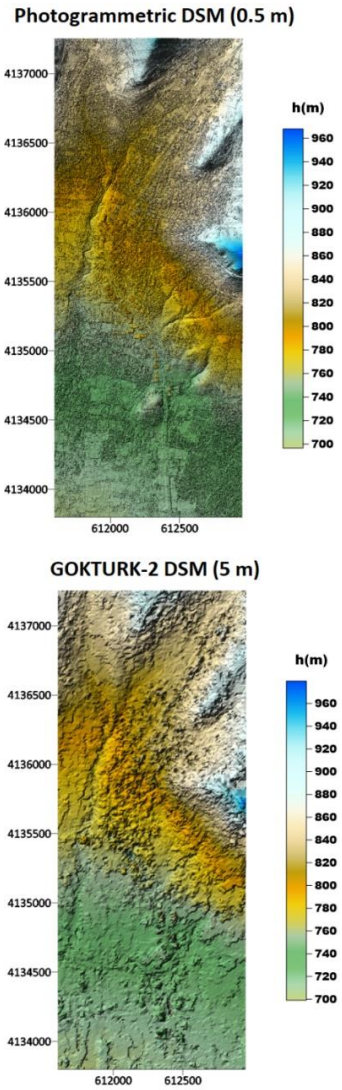

Fig. 4. Göktürk-2 and reference photogrammetric DSM

Table 3. Absolute vertical geolocation accuracy of Göktürk-2 DSM

Reference DSM	Tested DSM	Class	SZ (m)	NMAD (m)
Photogrammetric (0.5m)	Göktürk-2 (5m)	All terrain	7.37	5.77
		Slope	5.88	4.32

As seen in Table 3, it is determined that Göktürk-2 has higher performance in uninclined areas as in all DSMs obtained from space-borne optical RS data. In the analyses made on the whole area; The absolute vertical geolocation accuracy of Göktürk-2 is around 7.3 m as SZ and around 5.7 m as NMAD. In uninclined areas, both values are about 1.5 m higher. The height error maps reflecting the grid-by-grid height differences between Göktürk-2 and reference photogrammetric DSM are shown in Fig. 5. To facilitate visual interpretation, the maps were prepared in different versions to reflect height errors of ± 20 m, ± 10 m, ± 5 m and ± 1 m. It was evident from the height error maps that the biggest problem of Göktürk-2 DSM is the topographical slope. In regions where the topographic slope is high, the correlation with photogrammetric DSM decreases significantly. Another problem stands out in the narrow streets of Derik town centre. Some of narrow streets could not be represented at the required level. However, considering the spatial resolution of Göktürk-2, this is a natural result. On the other hand, it was concluded that the performance of Göktürk-2 was quite successful in areas other than over-sloping topography. Particularly, the performance of Göktürk-2 stereo images at an altitude of 684 km is admirable when examining the bounded zones with an error of ± 1 m. In these zones, the photogrammetric reference obtained at an altitude of 800 m, the vertical topographic difference between DSM and Göktürk-2 is ≤1 m.

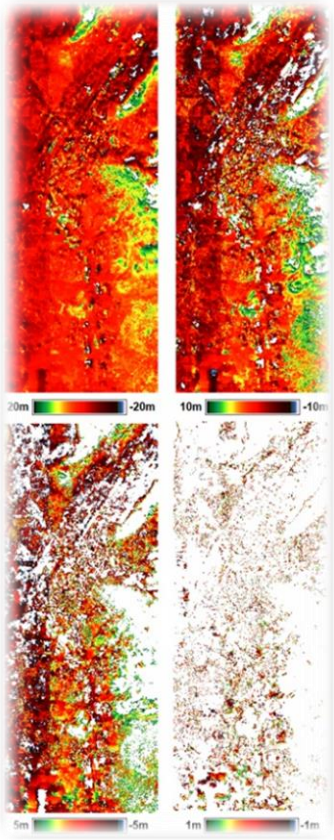

Fig. 5. Height error maps at different scales

5. CONCLUSIONS

The study carried out by Turkey's second domestic production Göktürk-2 earth observation satellite was evaluated with its horizontal and vertical absolute

geolocation accuracy performance of 5 m grid DSM produced from 2.5 m spatial resolution stereo satellite images. Evaluations were conducted by using visual and statistical methods with reference to photogrammetric DSM in Derik District of Mardin Province, where topographic slope is highly variable.

As a result of statistical accuracy, the analysis was performed based on standard deviation — also, normalized median absolute deviation metrics. Besides, visual interpretations in the light of height error maps, it was concluded that despite the medium spatial resolution of Göktürk-2 satellite at 2.5 m levels, the three-dimensional topographic representation capability was quite successful. The Göktürk-2 DSM has an absolute geolocation accuracy of ≤0.1 pixels in both directions horizontally. On the vertical, it provides accuracy as standard deviation of 7.3 m and normalized median absolute deviation of about 5.7 m. The biggest problem of the satellite is in the regions where the topographic slope is hardened. Likewise, the vertical accuracy level in the uninclined areas was found as 1.5 m better in both standard deviation and normalized median absolute deviation. Influence of the slope was clearly visualized in the generated height error maps. Height error maps revealed that Göktürk-2 satellite data also had problems in narrow streets in the town centres. The next target of our study team will be to find the primary sources of these problems detected in the narrow streets and improve image performance by filtering algorithms and improve the topographic description performance of the satellite.

ACKNOWLEDGEMENTS

We would like to express our gratitude to the Air Force Command Intelligence Department and all its military personnel who assisted in obtaining the Göktürk-2 stereo satellite images used in the study and to all MAS Aviation Solutions Inc. personnel who also assisted in obtaining the photogrammetric DSM with the aerial photographs used in the study.

REFERENCES

Aguilar F. J., Mills J. P., Delgado J., Aguilar M. A., Negreiros J. G., Perez J. L. (2010), "Modelling vertical error in Lidar-derived digital elevation models", *ISPRS Journal of Photogrammetry and Remote Sensing*, 65(1):103–110.

Fraser C. S. (2003), "Prospects for mapping from high-resolution satellite imagery", *Asian Journal of Geoinformatics*, 4(1): 3–10.

Font M., Amorese D., Lagarde J. L. (2010), "DEM and GIS analysis of the stream gradient index to evaluate effects of tectonics: the Normandy intraplate area (NW France)", *Geomorphology*, 119(3–4): 172–180.

Hellerstein J. M. (2008), "Quantitative Data Cleaning for Large Databases", Technical Report Presented at United Nations Economic Commission for Europe (UNECE), p. 42.

Hladik C., Alber M. (2012), "Accuracy assessment and correction of a LIDAR-derived salt marsh digital elevation model", *Remote Sensing of Environment*, 121:224–235.

Hobi M. L., Ginzler C. (2012), "Accuracy assessment of digital surface models based on WorldView-2 and ADS80 stereo remote sensing data", *Sensors*, 12(5): 6347–6368.

Jacobsen K. (2016), "Analysis and Correction Of Systematic Height Model Errors", The International Archives of the Photogrammetry, Remote Sensing and Spatial Information Sciences, Volume XLI-B1, 2016 XXIII ISPRS Congress, 12–19 July 2016, Prague, Czech Republic.

Navalgund R. R, Jayaraman V., Roy P. S. (2007), "Remote sensing applications: an overview", *Current Science*, 93(12): 1747–1766.

Sefercik U. G., Alkan M., Büyüksalih G., Jacobsen K. (2013), "Generation and Validation of High-Resolution DEMs from Worldview-2 Stereo Data", *The Photogrammetric Record*, Wiley Blackwell (ISI), 28(144): 362-374.

Sterenczak K., Kozak J. (2011), "Evaluation of digital terrain models generated in forest conditions from airborne laser scanning data acquired in two seasons", *Scandinavian Journal of Forest Research*, 26(4): 374–384.

Şasi, A., Yakar M. (2018) "Photogrammetric Modelling of Hasbey Dar'ülhuffaz (Masjid) Using an Unmanned Aerial Vehicle", *International Journal of Engineering and Geosciences (IJEG)*, Vol; 3; , Issue; 1, pp. 006-011, February, 2018, ISSN 2548-0960.

Yakar, M., Doğan, Y. (2018), "GIS and Three-Dimensional Modeling for Cultural Heritages", *International Journal of Engineering and Geosciences (IJEG)*, Vol; 3; Issue; 2, pp. 050-055, June, 2018, ISSN 2548-0960.

Yemenicioglu, C., Kaya, S., Seker, D.Z. (2016), "Accuracy ff 3D (Three-Dimensional) Terrain Models In Simulations", *International Journal of Engineering and Geosciences (IJEG)*, Vol; 1, Issue; 01, pp. 34-38,Decemberh, 2016, ISSN 2548-0960.

Yilmaz, M., Uysal, M. (2017), "Comparing Uniform and Random Data Reduction Methods For DTM Accuracy", *International Journal of Engineering and Geosciences (IJEG)*, Vol;2, Issue;01, pp. 9-16, February, 2017, ISSN 2548-0960.

Yüksel G., Tunalı E., Gürol S., Leloğlu U. M. (2016), TÜBİTAK-UZAY yer gözlem uydusu çalışmaları ve görüntü temin politikaları, UZAL-CBS 2016 Sempozyumu, Adana

Zhao S. M., Cheng W. M., Zhou C. H., Chen X., Zhang S., Zhou Z., Liu H., Chai H. (2011), "Accuracy assessment of the ASTER GDEM and SRTM3 DEM: An example in the Loess Plateau and North China Plain of China", *International Journal of Remote Sensing*, 32(23): 8081–8093.

CONTENTS

ISSN 2587-1366

TURKISH JOURNAL OF ENGINEERING

VOLUME 4 ISSUE 3 JULY 2020